A COMPARISON OF RESOLUTION ENHANCEMENT METHODS AS PRE-PROCESSING FOR CLASSIFICATION OF HYPERSPECTRAL IMAGES

by

Shirley Morillo Contreras

A thesis submitted in partial fulfillment of the requirements for the degree of
MASTER OF SCIENCE IN COMPUTER ENGINEERING
in
Department of Electrical and Computer Engineering
University of Puerto Rico
2004

Approved by:

Shawn Hunt, Ph.D. Member, Graduate Committee	Date
Manuel Rodríguez-Martínez Ph.D. Member, Graduate Committee	Date
Miguel Velez-Reyes, Ph.D. President, Graduate Committee	Date
Paul Castillo, Ph.D. Representative of Graduate Studies	Date
Isidoro Couvertier, Ph.D. Chairperson of the Department	Date

Abstract

The increasing use of Hyperspectral data is causing many data analysis problems; one of these problems is to reduce noise in Hyperspectral images. One approach is resolution enhancement technique based on oversampling theory. The oversampled spectrum in a Hyperspectral image implies that the information is redundant which can be exploited to reduce noise. Another approach is Truncated Singular Value Decomposition (TSVD), a method for noise reduction. The main idea of this method is to let the Hyperspectral image represent the noisy signal, compute the Singular Values Decomposition, discard small singular values that represent the noise, and then reconstruct the filtered image. This research work compares the use of resolution enhancement versus TSVD filtering as image enhancement pre-processor on classification accuracy and class separability of Hyperspectral imagery. Hyperspectral imagery from different sensors showing different scenarios were use for the study. Overall results show that resolution enhancement pre-processing does a better job improving the classification accuracy than TSVD and at much lower computational cost, making it an attractive technique for Hyperspectral Image Processing.

Resumen

El crecimiento en el uso de datos hiperespectrales esta causando problemas para analizar estos datos. Uno de estos problemas es reducir el ruido en imágenes hiperespectrales. Una solución a esto es el aumento de resolución en imágenes hiperespectrales basado en la teoría de sobre-muestreo. El espectro sobre-muestreado en una imagen hyperspectral implica que la información es redundante y esta información puede ser utilizada para reducir ruido. Otra solución es truncar la descomposición de valores singulares (TSVD) como método para reducir ruido. La idea principal de este método es que la imagen hyperspectral represente la señal con ruido, calcular los valores singulares y descartar los valores singulares más pequeños que representan el ruido y luego reconstruir la imagen filtrada. En esta tesis se comparo el uso del aumento de resolución basado en la teoría de sobre-muestreo versus truncar la descomposición de valores singulares como pre-procesadores en el realce de imágenes hiperespectrales sobre la clasificación y la separabilidad entre clases. Se utilizaron imágenes hiperespectrales tomadas con diferentes sensores e ilustrando diferentes escenarios. Resultados generales muestran que el aumento de resolución como pre-procesamiento realiza un mejor trabajo mejorando la clasificación que truncar los valores singulares y con menor costo computacional, haciéndolo una técnica atractiva para el procesamiento de imágenes hiperespectrales.

TABLE OF CONTENTS

LIST OF FIGURES

Page

LIST OF TABLES

LIST OF APPENDICES

ACKNOWLEDGMENTS

I would like to thank my thesis advisor, Dr. Miguel Vélez Réyes, for all his integral support, guide and patience during all my research work. Thanks also to the Center for Subsurface Sensing and Imaging (CENSSIS) team for their financial support and interaction with other academic institutions.

I also want to thank specially my mother, because her support in my live is a motivation in everything I do. I want to thank my husband for his guidance during my research work, thanks to my sister and to my family in Cartagena, Colombia.

The TRWISS III data sets are GRSS_DFC_0008 of the benchmark image database of the Data Fusion Committee (DFC) of the IEEE Geosciences and Remote Sensing Society (http://www.dfc-grss.org). GRSS_DFC_0008 was contributed by the Remote Sensing Technologies Center at Mississippi State University through an MOU with the DFC and the hyperspectral imaging system used for the collection of the data set was TRWIS III, developed by TRW Inc.

This work was supported in part by CenSSIS, the Center for Subsurface Sensing and Imaging Systems, under the Engineering Research Centers Program of the National Science Foundation (Award Number EEC-9986821).

CHAPTER 1

1. INTRODUCTION

1.1 Motivation

Recently, there has been a growing interest in hyperspectral image analysis with applications ranging from remote environmental monitoring, atmospheric correction, and cancer detection, among others. Hyperspectral imagery has been used for remote sensing. This monitoring is dependent on the spectral coverage, spectral resolution, and signal-to-noise ratio of the spectrometer, the abundance of material and the strength of absorption features for that material in the wavelength region measured. Hyperspectral data sets are composed of about 100 to 200 spectral bands of relatively small bandwidths of 5-10 nm, for example, the Airborne Visible/Infrared Spectrometer (AVIRIS) collects data in 224 spectral bands covering 0.4-2.5 μm wavelength region with 20 m spatial resolution. Figure 1 illustrates the hyperspectral image concept, where each pixel represents many samples of the object spectral signature.

Noise is produced by numerous factors including thermal effects, sensor saturation, quantization errors and transmission errors. Noise added to the data in an optical remote sensing system is typically independent of the data, and is generally additive in nature. Therefore, filtering of noise is particularly important because noise present in a hyperspectral image is the main limiting factor for successful image classification.

The signal-to-noise ratio is of prime importance in hyperspectral remote sensing, since it is closely related to our capability to retrieve information about the spatial process of interest. The noise associated with any spectral measurement reduces the ability to

discriminate among different spectral features. Noise can be dealt by methods such as amplitude resolution spectral enhancement and truncated singular value decomposition.

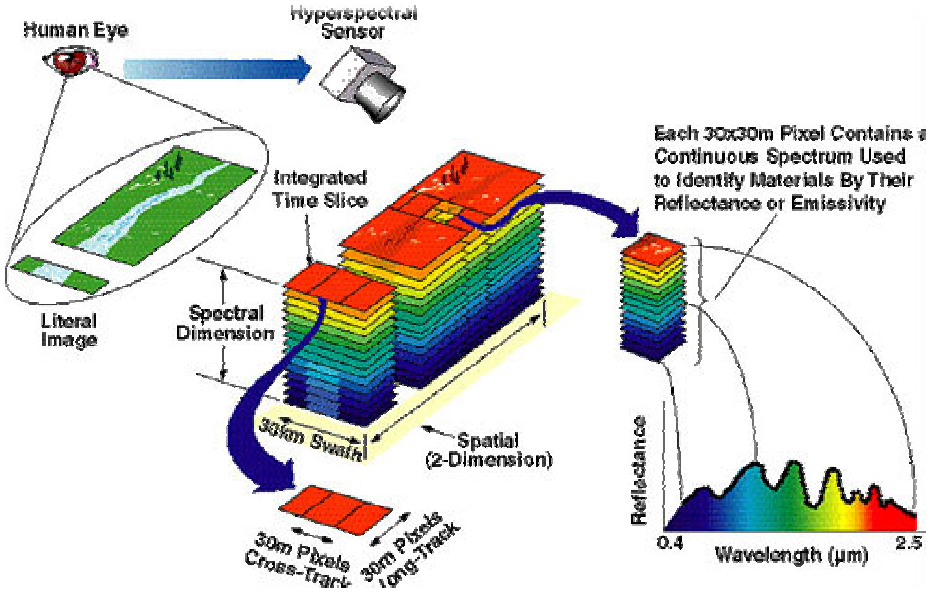

Figure 1 – Hyperspectral Image Concept (CSIRO)

1.2 Problem Statement

This research work compares the impact of amplitude resolution spectral enhancement based on oversampling theory versus Truncated Singular Value Decomposition in the classification accuracy and class separability of Hyperspectral imagery.

1.3 Objectives

The objectives of this work are

To compare the impact of amplitude resolution spectral enhancement based on oversampling versus Truncated Singular Value Decomposition in the classification accuracy and separability among classes in Hyperspectral imagery.

To determine the effect of amplitude resolution spectral enhancement based on oversampling and Truncated Singular Value Decomposition over atmospheric correction.

To compare the computational efficiency of amplitude resolution spectral enhancement based on oversampling versus Truncated Singular Value Decomposition

1.4 Literature Review

In (Wei et al., 2001), the method for truncated singular value decomposition is proposed for electrocardiogram (ECG) data compression. The signal decomposition capability of SVD is exploited to extract the significant feature components of the ECG by decomposing the ECG into a set of basic patterns with associated scaling factors. The signal information is mostly concentrated within a certain number of singular values with their related singular vectors due to the strong interbeat correlation among ECG cycles (Wei, et al. 2001). The insignificant overhead can be truncated to eliminate the redundancy of ECG data compression. Moreover, Herries (1996) applies singular value decomposition to optical airborne data at different resolutions. The use of SVD as a tool in remote sensing is demonstrates in many applications. In particular, SVD is applied to characterize agricultural species covering a highly dynamic terrain in Bavaria, Germany. A novel use of SVD for extracting mixed pixel quantities is also shown. Also, Hansen (1998) shows that the reduced-rank output signal computed via truncated singular value decomposition is identical to that from an array of parallel connected analysis-synthesis finite impulse response (FIR) filter pairs. Finally, Migliacco (2003) performed a sensitivity study the truncated singular value decomposition (TSVD) for spatial resolution enhancement of radiometric data.

Hunt et al. (2002) investigated the use of oversampling techniques applied to hyperspectral imagery and whether oversampling actually occurs in hyperspectral signals also study the use of resolution enhancement based on oversampling to increase classification performance. Hunt et al. (2004) also proposed an algorithm to exploit the

fact that the system is supervised to determine the oversampling rate, using the training samples for this purpose. The oversampling rate is used to determine the cutoff frequency for each class, and the highest of these is used to filter the image.

Vélez-Reyes et al. (2004) investigated the effect of resolution enhancement as a pre-processing technique in a classification system. Also, they studied the effect on classification accuracy of resolution enhancement with and without atmospheric correction. The main result is that resolution enhancement does improve classification accuracy with and without atmospheric correction. Furthermore, classification accuracy using radiance data enhanced by resolution enhancement techniques was higher than accuracies obtained by atmospherically corrected data even when it was enhanced.

1.5 Contribution

Hunt et al. 2003 proposed a new method to improve signal to noise ratio in hyperspectral imagery using oversampling theory. In order to incorporate this method into the Hyperspectral classification system, it is necessary to compare its performance against a benchmark method, such as Truncated Singular Value Decomposition (TSVD).

A key question can be stated: "Does resolution enhancement, based on oversampling theory result in equal or better classification results than TSVD?" The answer, according to the experiments performed in this research work, is that resolution enhancement improves classification accuracy in comparison with truncated SVD. In addition, the resolution enhancement complexity is smaller than the complexity of Truncated SVD since on is based on the fast Fourier transform (FFT), making it more attractive as a pre-processing enhancement step on a Hyperspectral classification system.

1.5 Thesis Overview

Chapter 2 presents a literature review of the remote sensing concepts, oversampling and amplitude resolution approach, singular value decomposition theory and the fundamentals of atmospheric correction.

Chapter 3 shows the details of the hyperspectral images and the sensors used, the characteristics of the Hyperspectral Matlab Toolbox, truncated singular value decomposition algorithm and the resolution enhancement algorithm used.

Chapter 4 presents the experimental results of the classifications accuracy and class separability for the hyperspectral images studied in Chapter 3

Chapter 5 presents the conclusions of this work and propose some possible alternatives to continue this work.

The appendices present the Matlab code for the amplitude resolution spectral enhancement based on oversampling and the truncated singular value decomposition algorithms.

CHAPTER 2

2. BACKGROUND AND LITERATURE REVIEW

This Chapter presents a literature review of the remote sensing concepts, oversampling and amplitude resolution approach, singular value decomposition theory, and the fundamentals of atmospheric correction.

2.1 Hyperspectral Image Classification System

Hyperspectral Image classification system is the process of creating an informational representation of an image which shows the spatial distribution of a particular area as vegetation, crops, benthic habitat, among others from satellite imagery.

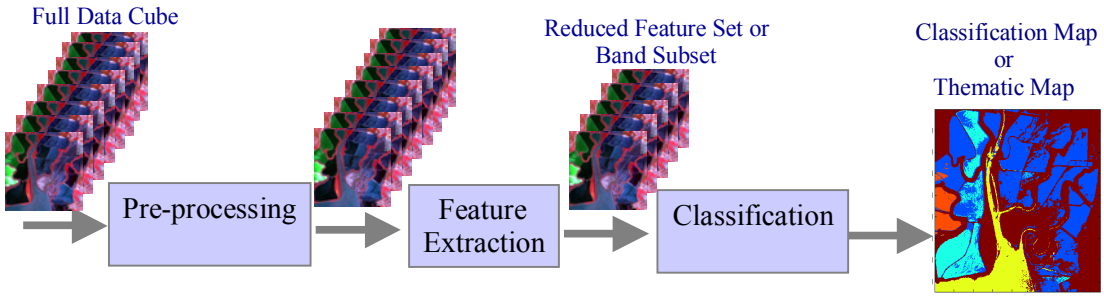

Figure 2 - Typical Hyperspectral Image Classification System

Figure 2 illustrates the organization of a Hyperspectral classification system. As the figure shows, the system may be divided into three basic parts: Pre-processing, Feature Extraction, and Classification.

Pre-processing generally precedes data analysis or information extraction. Its goal is the reduction of distortion or the enhancement of some aspect of the data. There

are a variety of types of pre-processing that are sometimes applied on the data. Some examples are: Radiometric Calibrations, Atmospheric Correction, Contrast Enhancements, and Image Registration. This chapter will cover the atmospheric correction and two enhancements algorithms resolution enhancement based on oversampling theory and truncated singular value decomposition.

Feature extraction is an optional step on the classification process which serves as a pre-processing of the image to reduce its spectral or spatial dimensionality. It can be accomplished by selecting the optimum subset of channels (bands) in order to avoid the estimation problems due to interband correlation. In this stage, the Hyperspectral image is transformed into a feature image. The feature extraction algorithm must be designed to preserve the information of interest for a special problem such as classification.

Classification of Hyperspectral data is used to identify and classify pixels in the data and this process assigns each pixel in an image to a particular class or theme based on statistical characteristics of the pixel values. There are two generic approaches which are used most often taken to perform classification, namely supervised and unsupervised classification. The classified results should be checked and verified for their accuracy and reliability.

In the following sections will be described each of these stages of Hyperspectral image classification system in more detail.

2.2 Spectroscopy

Spectroscopy is the science of measuring the emission and absorption at different wavelengths of visible and non-visible light; anything that produces light or radiates energy, whether a light bulb, is telling us about itself and anything between us and the source. This is possible because each element has a unique signature, emitting or absorbing radiation at specific wavelengths.

2.3 Remote Sensing

The following definition will be use: "Remote sensing is the science of deriving information about an object from measurements made at a distance from an object, i.e., without actually coming in contact with it. The quantity most frequently measured in present-day remote sensing systems is the electromagnetic energy emanating from objects of interest, and although there are other possibilities (e.g., seismic waves, sonic waves, and gravitational force)." (Landgrebe et al. 1978)

The process of remote sensing involves an interaction between incident radiation and the targets of interest (Figure 3). This is exemplified by the use of imaging systems where the following seven elements are involved:

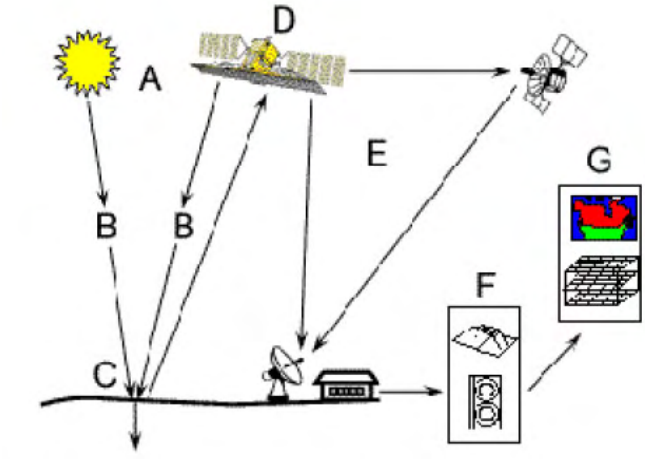

Figure 3 - Remote Sensing Process (CCRS 2004)

- Energy Source or Illumination (A)
- Radiation and the Atmosphere (B)
- Interaction with the Target (C)
- Collect the electromagnetic radiation (D)
- Transmission, Reception, and Processing (E)

- Interpretation and Analysis (F)
- Application (G)

2.4 Hyperspectral Remote Sensing

Hyperspectral remote sensing, also known as imaging spectroscopy, is a relatively new technology that is currently being investigated with regard to the detection and identification of minerals, vegetation, backgrounds and benthic habitats. Spectroscopy can be used to detect individual spectral features due to specific chemical bonds in a solid, liquid, or gas. Recently, with advancing technology, imaging spectroscopy has begun to focus on Earth. Remote sensing of the Hyperspectral at this point has been used most widely by geologists for the mapping of minerals. Actual detection of materials is dependent on the spectral coverage, spectral resolution, and signal-to-noise ratio of the spectrometer, the abundance of the material and the strength of absorption features for that material in the wavelength region measured. Hyperspectral remote sensing combines imaging and spectroscopy in a single system which often includes large data sets and requires new processing methods. Hyperspectral imagery is typically collected and represented as a data cube with spatial information collected in the x-y plane, and spectral information represented in the z-direction.

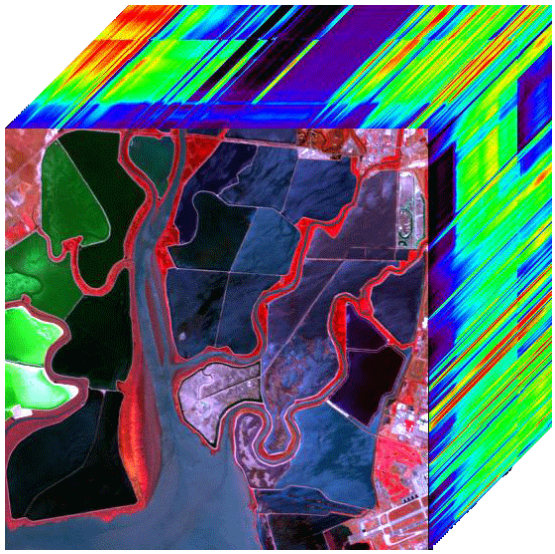

Figure 4 – AVIRIS hyperspectral data cube over Moffett Field, CA (Generated using ENVI)

2.5 The Electromagnetic Spectrum

The electromagnetic spectrum ranges from the shorter wavelengths (including gamma and x-rays) to the longer wavelengths (including microwaves and broadcast radio waves) (Figure 5). There are several regions of the electromagnetic spectrum which are useful for remote sensing. For most purposes, the ultraviolet or UV portion of the spectrum has the shortest wavelengths which are practical for remote sensing. This radiation is just beyond the violet portion of the visible wavelengths. Some Earth surface materials, primarily rocks and minerals, fluoresce or emit visible light when illuminated by UV radiation. The visible wavelengths cover a range from approximately 0.4 to 0.7 μm. The longest visible wavelength is red and the shortest is violet. Common wavelengths of what we perceive as particular colors from the visible portion of spectrum are listed below.

Color	**Wavelength**
Violet	0.400 - 0.446 μm
Blue	0.446 - 0.500 μm
Green	0.500 – 0.578 μm
Yellow	0.578 – 0.592 μm
Orange	0.592 – 0.620 μm
Red	0.620 – 0.700 μm

The next portion of the spectrum of interest is the infrared (IR) region which covers the wavelength range from approximately 0.7 μm to 100 μm. The infrared region can be divided into two categories based on their radiation properties. The reflected IR, and the emitted or thermal IR. Radiation in the reflected IR region is used for remote sensing purposes in ways very similar to radiation in the visible portion. The thermal IR region is quite different than the visible and reflected IR portions, as this energy is essentially the radiation that is emitted from the Earth's surface in the form of heat. Other portion of the spectrum is the microwave region; this covers the longest wavelengths used for remote sensing. The shorter wavelengths have properties similar to

the thermal infrared region while the longer wavelengths approach the wavelengths used for radio broadcasts.

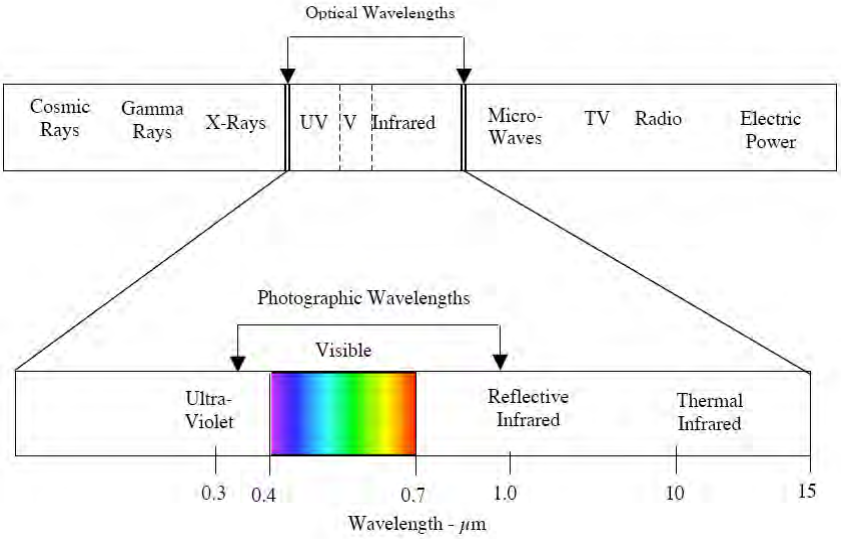

Figure 5 - The Electromagnetic Spectrum (Landgrebe 2003)

2.6 The Atmosphere

Before radiation used for remote sensing reaches the Earth's surface it has to travel through some distance in the Earth's atmosphere. Particles and gases in the atmosphere can affect the incoming light and radiation. These effects are caused by mechanisms of scattering and absorption. (Landgrebe 2003)

Scattering occurs when particles or large gas molecules present in the atmosphere interact with and cause the electromagnetic radiation to be redirected from its original path. How much scattering takes place depends on several factors including the wavelength of the radiation, the abundance of particles or gases, and the distance the radiation travels through the atmosphere. There are three types of scattering which take place.

- **Rayleigh scattering** occurs when particles are very small compared to the wavelength of the radiation. These could be particles such as small specks of dust or nitrogen and oxygen molecules.

- **Mie scattering** occurs when the particles are just about the same size as the wavelength of the radiation. Dust, pollen, smoke and water vapour are common causes of Mie scattering.
- **Nonselective scattering** occurs when the particles are much larger than the wavelength of the radiation. Water droplets and large dust particles can cause this type of scattering.

Absorption is the other main mechanism at work when electromagnetic radiation interacts with the atmosphere. In contrast to scattering, this phenomenon causes molecules in the atmosphere to absorb energy at various wavelengths. Ozone, carbon dioxide, and water vapor are the three main atmospheric constituents which absorb radiation.

Path radiance is radiation entering the sensor aperture that did not arrive directly from the scene pixel under view. Its origin is scattering from the atmosphere and radiance from adjacent scene pixels.

Transmittance is related to Visibility or Meteorological Range, a quantity often available in a generalized sense from meteorological sources for a given area.

In addition to direct solar rays, the surface target is illuminated by the diffuse light from the rest of the sky. This light emanates from direct rays scattered by the atmosphere. This illumination is not spectrally similar to the direct rays. Rather, it tends to be blue on a clear day since its origin is primarily Rayleigh scattering, but it varies significantly depending on the clarity or optical depth of the atmosphere. As result the total irradiance falling on a given area can vary quite significantly both in magnitude and spectral distribution depending on the atmosphere. It is also varies depending on how much of the sky is visible from the ground surface element under consideration.

A significant problem arises due to the scattering of the response from nearby objects that have different reflectance characteristics than the object being viewed. Due

to the atmospheric scattering, the spectral response at a given point on the Earth's surface can be significantly affected by what is present on the Earth's surface at nearby points. This is referred to as the adjacency effect.

Clouds pose a significant limitation to passive optical remote sensing systems. They affect both the illumination and the view of the surface; they vary in this effect spatially, spectrally, and temporally, and these variations are of high frequency.

2.7 Satellites and Sensors

In order for a sensor to collect and record energy reflected or emitted from a target or surface, it must reside on a stable platform removed from the target or surface being observed. Platforms for remote sensors may be situated on the ground, on an aircraft or some other platform within the Earth's atmosphere, or on a spacecraft or satellite outside of the Earth's atmosphere. Ground-based sensors are often used to record detailed information about the surface which is compared with information collected from aircraft or satellite sensors. In some cases, this can be used to better characterize the target which is being imaged by these other sensors, making it possible to better understand the information in the imagery. Aircraft are often used to collect very detailed images and facilitate the collection of data over virtually any portion of the Earth's surface at any time. In space, remote sensing is conducted from satellites. Satellites are objects which revolve around another object in this case, the Earth.

2.8 Spatial Resolution

For some remote sensing instruments, the distance between the target being imaged and the platform, plays a large role in determining the detail of information obtained and the total area imaged by the sensor. Sensors onboard platforms far away from their targets, typically view a larger area, but cannot provide great detail. The detail discernible in an image is dependent on the spatial resolution of the sensor and refers to

the size of the smallest possible feature that can be detected. Spatial resolution of sensors depends primarily on their Instantaneous Field of View (IFOV). The IFOV is the angular cone of visibility of the sensor and determines the area on the Earth's surface which is "seen" from a given altitude at one particular moment in time. The size of the area viewed is determined by multiplying the IFOV by the distance from the ground to the sensor. This area on the ground is called the resolution cell and determines a sensor's maximum spatial resolution. (CCRS 2004)

2.9 Spectral Resolution

Spectral resolution describes the ability of a sensor to define fine wavelength intervals. The finer the spectral resolution, the narrower the wavelengths range for a particular channel or band. Black and white film records wavelengths extending over much, or the entire visible portion of the electromagnetic spectrum. Its spectral resolution is fairly coarse, as the various wavelengths of the visible spectrum are not individually distinguished and the overall reflectance in the entire visible portion is recorded. Colors film is also sensitive to the reflected energy over the visible portion of the spectrum, but has higher spectral resolution, as it is individually sensitive to the reflected energy at the blue, green, and red wavelengths of the spectrum. Thus, it can represent features of various colors based on their reflectance in each of these distinct wavelength features of various colors based on their reflectance in each of these distinct wavelength ranges. (CCRS 2004)

2.10 Hyperspectral Imagery

Hyperspectral imagery is in essence a picture that contains both spatially and spectrally continuous data. The term "hyper" means more than enough. By having a hyperspectral image, there are more than enough spectra, or spectral bands, than absolutely necessary to resolve whatever component is looking for within the image. Hyperspectral imagery often times consists of hundreds of bands.

Hyperspectral imagery is spectrally over determined; they provide ample spectral information to identify and distinguish between spectrally similar but unique materials. Consequently, hyperspectral imagery provides the potential for more accurate and detailed information extraction than is possible with other types of remotely sensed data.

Most multispectral imagers (e.g. Landsat, IKONOS, and AVHRR) measure reflectance and/or emission of Earth's surface at few wide bandwidth bands separated by spectral segments where no measurements are taken. In contrast, most hyperspectral sensors measure reflected radiation as a series of narrow and contiguous wavelength bands. This type of detailed pixel spectrum can provide much more information about a surface than is available in a traditional multispectral pixel. See Figure 6.

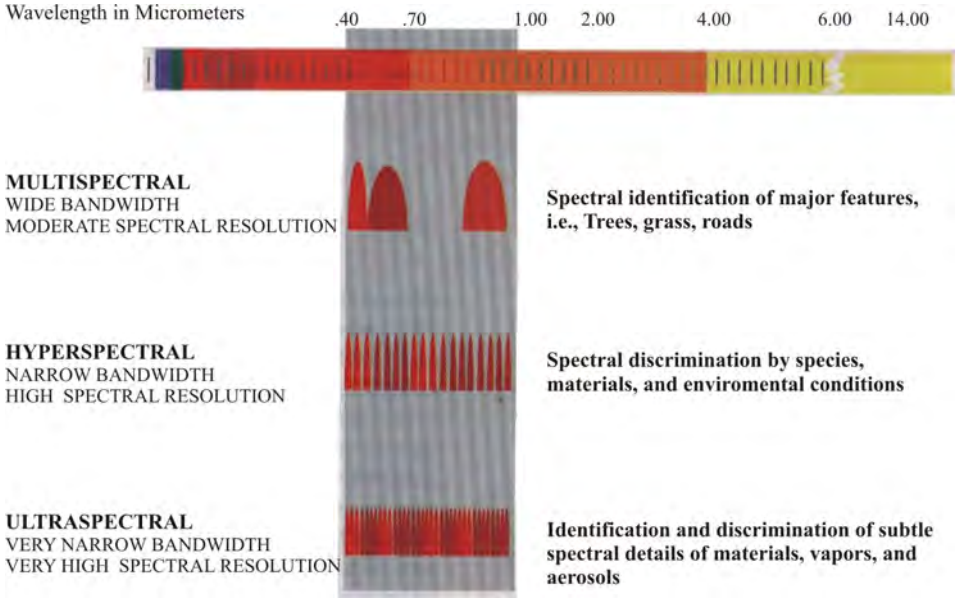

Figure 6 – Types of Spectral Imaging

2.11 Dimension Reduction

Dimension reduction is a process designed to reduce data volumes by filtering out specific redundant information. With hundreds of channels, hyperspectral imagery possesses much richer spectral information than multispectral imagery. However, realizing the full potential of hyperspectral technology remains a challenge. It is clear that more effective data processing techniques are needed to deal with hyperspectral images (Umaña et al, 2003). One example is land image classification with sensors such

as HYPERION. For this application, it is necessary to have a minimum number of training pixels to the number of spectral bands in order to ensure a reliable estimate of class statistics, and as a consequence, dimension reduction has become a significant part of hyperspectral land classification.

2.12 Atmospheric Correction

The nature of remote sensing requires that the solar radiation pass through the atmosphere before it is collected by the sensor. Remotely sensed images therefore include not only the information about the surface but also about the atmosphere. For those interested in quantitative analysis of surface reflectance, removing the influence of the atmosphere is a critical pre-processing step. To compensate for atmospheric effects, properties such as the amount of water vapor, distribution of aerosols, and scene visibility must be known. Because direct measurements of these atmospheric properties are rarely available, techniques have been developed to infer them from their imprint on hyperspectral radiance data. These properties are then used to constrain highly accurate models of atmospheric radiation transfer to produce an estimate of the true surface reflectance. Moreover, atmospheric corrections of this type can be applied on a pixel-by-pixel basis because each pixel in a hyperspectral image contains an independent measurement of atmospheric water vapor absorption bands. (Adler-Golden 98)

Some atmospheric correction methods are FLAASH and ACORN, based on ENVI, here an introduction of this methods.

2.12.1 Fast Line-of-sight Atmospheric Analysis of Spectral Hypercubes (FLAASH)

ENVI's atmospheric correction module, called FLAASH is a first-principles atmospheric correction modeling tool for retrieving spectral reflectance from hyperspectral radiance images. With the FLAASH module for ENVI, you can compensate for atmospheric effects accurately. FLAASH module incorporates the

MODTRAN4 radiation transfer code. You may choose any of the standard MODTRAN model atmospheres and aerosol types to represent the scene, and a unique MODTRAN solution is computed for each image. FLAASH also includes a correction for the "adjacency affect" (pixel mixing due to scattering of surface reflected radiance), provides an option to compute a scene-average visibility, and utilizes techniques for handling particularly stressing atmospheric conditions (such as the presence of clouds). Other features include a cirrus and opaque cloud classification map and adjustable spectral "polishing" for artifact suppression. (Research Systems, 2001)

FLAASH supports most high spectral resolution instrument that covers the reflective spectra (0.4 to 2.5μm), including the following sensors: HyMAP (Keeling et al, 98), AVIRIS (Adler-Golden 98), HYDICE (Kappus et al, 96) and HYPERION (EO-1 Webpage). In addition, FLAASH can correct images collected in either vertical (nadir) or slant viewing geometries. FLAASH was developed by Spectral Sciences, Inc., a world leader in optical phenomenology research, under the sponsorship of the U.S. Air Force Research Laboratory. (Research Systems, 2001)

2.12.2 Atmospheric Correction Now (ACORN)

ACORN uses look-up-tables calculated with the MODTRAN4 (Adler-Golden 98), radiative transfer code to model atmospheric gas absorption as well as molecular and aerosol scattering effects. These modeled atmospheric characteristics are used to convert the calibrated sensor radiance measurements to apparent surface reflectance. The technique uses a fast and accurate look-up-table approach to calculate water vapor amounts on a pixel-by-pixel basis. The user may choose to use the water vapor absorption bands at 940 or 1150nm or both for the water vapor derivations. Additionally the user may input a visibility or ask ACORN to attempt to estimate the visibility from the data. A set of artifact suppression options are included in the ACORN software. (ImSpec LLC, 2002)

The Atmospheric CORrection Now (ACORN) software package provides an atmospheric correction of Hyperspectral and Multispectral data measured in the spectral range from 350 to 2500 nm. ACORN is designed to work with all airborne and spaceborne calibrated hyperspectral and multispectral data types including HYPERION, ASTER, LANDSAT, AVIRIS, IKONOS, among others. (ImSpec LLC, 2002)

ACORN provides the following specific modes of Atmospheric Correction**:**

- Mode 1 Radiative transfer atmospheric correction of calibrated hyperspectral data.
- Mode 1.5 Radiative transfer atmospheric correction of calibrated hyperspectral data with water vapor and liquid water spectral fitting
- Mode 2 Single spectrum enhancement of a hyperspectral atmospheric correction.
- Mode 3 Atmospheric correction using the empirical line method for hyperspectral data.
- Mode 4 User specified convolution of hyperspectral data to multispectral data.
- Mode 5 Radiative transfer atmospheric correction of calibrated multispectral data.
- Mode 5.5 Radiative transfer atmospheric correction of calibrated multispectral data with independently know water vapor image for spatially varying water vapor correction
- Mode 6 Single spectrum enhancement of a multispectral atmospheric correction.
- Mode 7 Atmospheric correction by the empirical line method for multispectral data.

2.13 Singular Value Decomposition Noise Filtering

Signal Model

Let us model the Hyperspectral pixel as a combination of a random spectral signature, **s**, (pure or mixed) with additive noise, **n**, given by:

$$\boldsymbol{x} = \boldsymbol{s} + \boldsymbol{n} .$$

where **s** is the spectral signature with covariance Σ_s, **n** is white noise with covariance $\mu^2 I$ and s and n are uncorrelated. The nxn covariance matrix for x, Σ_x, given by

$$\Sigma_x = \Sigma_s + \mu^2 I$$

where Σ_s is of rank $p<n$ which is equal to the dimension of the signal subspace. The eigenvalues of Σ_x, λ_{xi}, are given by:

$$\lambda_{xi} = \lambda_{si} + \mu^2, \; i= 1, 2, ..., n$$

where λ_{si} is the i–th eigenvalue of Σ_s and the eigenvalues are ordered in descending order of magnitude. Since Σ_s is rank p, $\lambda_{si} = 0$ for $i > p$, so that:

$$\lambda_{xi} = \lambda_{si} + \mu^2, \;\; i = 1, 2, ..., p \text{ (signal and noise)}$$

and

$$\lambda_{xi} = \mu^2, \qquad i = p+1, ..., n \text{ (only noise contribution)}$$

If we have a good signal to noise ratio, we should expect that $\lambda_{si} >> \mu^2$ for all i.

Of the measured signal **x**, only the first *p* principal components carry signal information and a filtered **x** is constructed using the first *p* eigenvectors of the $\mathbf{\Sigma}_x$

$$\mathbf{x}_p = \mathbf{V}_p \mathbf{V}_p^T \mathbf{x} \qquad (2.1)$$

Where x_p is the filtering version of x, $\mathbf{V}_p$ is the matrix of the first p eigenvectors of the covariance matrix. Notice that 2.1 is a projection of x onto the space spawned by the signal eigenvectors. This reconstruction is optimal in a mean squared sense; and it is used in many multivariable statistical applications.

Computing the filtered image

Let $A = [x_1, x_2, \ldots, x_N]$ (pixels of the Hyperspectral cube) be a set of independent measurement of the random variable x (mean subtracted).

The singular Value Decomposition (SVD) of a matrix *A* of size *mxn* is a decomposition of the form (Trefethen et al, 1997):

$$A = USV^T \qquad (2.2)$$

where U and V are orthogonal, square matrices of sizes *mxm* and *nxn* respectively, and S is a diagonal matrix of size *mxn*. The columns u_i ($1 \le i \le m$) and v_j ($1 \le j \le n$) of U and V are called the left and right singular vectors, respectively, and the diagonal elements s_{kk} ($1 \le k \le min\{m,n\}$) of S are called the singular values of A. The left (u_i) and right (v_j) singular vectors of A form orthonormal bases, and are related by the following relation:

$$Av_i = s_i u_i \tag{2.3}$$

showing that each right singular vector is mapped onto the corresponding left singular vector, and the "magnification factor" is the corresponding singular value.

Since $\Sigma_x = \frac{A^t A}{N}$, we get that $\lambda_{xi} = \frac{\sigma_i^2}{N}$, where σ_i is the i-th singular value of A. So we can use the SVD of A to compute the filtered mode. The desired approximation is the rank p approximation to A. Given by $A_p = U_p \Sigma_p V_p^T$ where U_p is the matrix of the first p left singular vectors, Σ_p is a diagonal matrix with the first p singular values, and V_p is the matrix of the first p right vectors. Notice that the right singular vectors of A are equal to the eigenvalues of Σ_x.

SVD has a variety of applications in scientific computing, signal processing, automatic control, and many other areas. In signal processing, the SVD decomposition, followed by the truncation of the lower singular values has been traditionally used for noise reduction, in voice and image signals (Hansen et al, 98). The central idea can be summarized as follows: let A be the matrix that represents the discretized noisy signal, compute the SVD decomposition of A (2.1), and then discard the smaller singular values of A and their corresponding singular vectors. It can be shown that the small singular values of A, mainly represent the noise, and thus the rank-p matrix A_p ($p < n$) represents a filtered signal with less noise (A key problem is to determine the dimension of the signal space *p*). This application of the SVD is called Truncated SVD (TSVD) or Reduced-Rank Noise Reduction. (Hansen 1998)

2.14 Oversampling and Amplitude Resolution

Shannon's sampling theorem states that a band-limited signal needs to be sampled at least at a frequency that is twice its bandwidth in order to reconstruct it from its samples. There are, however, advantages to sampling at higher rates. The theory relating the sampling rate to precision assuming additive white noise will be presented first, with the results generalized later (Hunt et al., 2004).

A hyperspectral image can be viewed as a three dimensional data cube, where two dimensions are spatial, and one spectral. Only the spectral dimension is considered in oversampling analysis, so for simplicity, we will write each pixel as a function of the spectral dimension only,

$$x[\lambda] = x[x, y, \lambda]\,|_{x=x_o, y=y_o} \tag{2.4}$$

where x[λ] is the pixel at location (x_o, y_o) in the image, and λ is the spectral index. Let $2f_m$ be the signal bandwidth and f_s be the sampling frequency. The oversampling rate is defined as:

$$OSR = \frac{f_s}{2f_m} \tag{2.5}$$

In the case where the signal has an oversampling rate of 1, x[λ] cannot be filtered without loosing signal, given that the signal spectrum ranges from –π to π and it is periodical with period 2π. Otherwise, if the signal is oversampled say by two, the signal spectrum ranges between –π/2 to π/2 and hence can be filtered with a Lowpass filter with cut off frequency also between –π/2 to π/2 without changing the signal but eliminating the noise located between π/2 and π, as can be seen in Figure 7, leading to an increase in the signal to noise ratio.

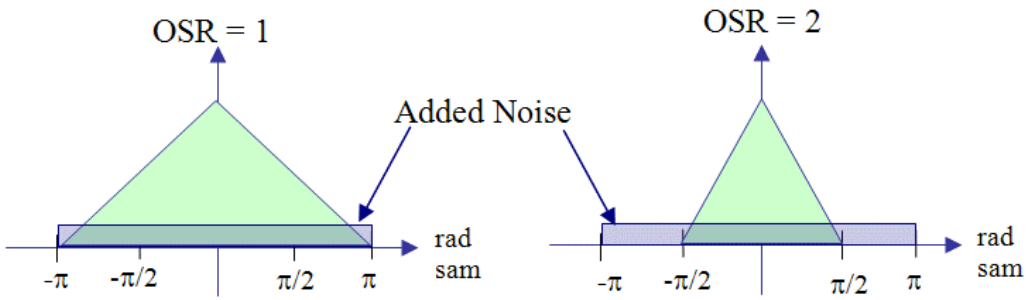

Figure 7 - Oversampling

Where the added noise is assumed to be additive white noise with power spectral density, given by:

$$S_v(\omega) = \sigma_v^2 \qquad |\omega| < \pi \tag{2.6}$$

where σ_v^2 is the variance of the noise. Hence, its power will be uniformly distributed over all frequencies from - π to π. Filtering a signal that has been oversampled by a factor of two using a Lowpass filter with cut off frequency at π/2 rad will eliminates the noise in the interval [-π, π/2] and [π/2, π], as the Figure 7 shows. This represents a reduction of the noise by exactly a half, without changing the signal, which means an increase in SNR of $10\log_{10}(2)$ = 3dB. This can be related to the increase in precision or amplitude resolution as follows: for B number of bits and maximum amplitude of ±A, the amplitude resolution, or distance between one rounding level and the next is

$$\Delta = \frac{2A}{2^B}. \tag{2.7}$$

Thus, the number of bits determines its precision, and the amount of quantization noise. Quantization noise is typically modeled as additive white noise that is independent of the signal of interest. Using the results above, oversampling by 4 and filtering at π/4 rad/sam will lead to an increase in the SNR of 6 dB or one bit. This formula works in general, so that

$$w = \frac{\log(OSR)}{\log(4)} \tag{2.8}$$

where w is the additional number of bits of precision.

The additive noise was assumed white in the above examples, but this is not necessary. The only thing necessary to obtain an increase in precision is to have an oversampling of the desired signal. If we do not assume white noise, then we will not have the simple relation between the oversampling rates to the increase in precision shown in the previous equation. The performance, however, may even be better than this case. If the power of the noise is mainly concentrated at high frequencies, then there will be a greater SNR increase than with white noise.

2.15 Pattern Recognition

Pattern recognition is the scientific discipline whose goal is the classification of objects into a number of categories or classes. These objects can be images, acoustic signal, seismographic signals and tomographic data.

The general scheme of a pattern recognition system is shown in the following figure. A natural pattern is viewed or measured with some type of a receptor containing a sensor. The receptor reports out the measurements as an asset of numbers. This set of numbers $X=[x_1,x_2 \ldots x_n]$, usually represented as a vector, (e.g Multi/Hyperspectral pixel), is then fed to a classifier which makes a decision as to what pattern the set of numbers of each pixel represent. (Landgrebe 2003)

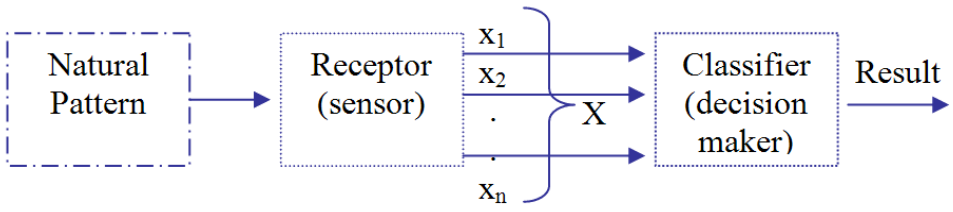

Figure 8 - Diagram of a Pattern Recognition System

2.15.1 Feature Extraction

Feature extraction is the identification of real world objects or features from spatial datasets especially remotely sensed data. The traditional goal of the feature extractor is to characterize an object by making numerical measurements. Good features are those whose values are similar for objects belonging to the same category and distinct for objects in different categories. Usually one feature is not enough to differentiate between objects from different categories.

Feature extraction is an optional step on the classification process which serves only as a low level pre-processing of the image to reduce its spectral, or spatial, dimensionality. It can be accomplished by using any type of spatial filters or spectral transforms to reduce the data and/or enhance its hyperspectral features, or even by simply selecting a subset of bands. In this stage, the hyperspectral image is transformed into a feature image.

2.15.2 Classification Concept

The task of the classifier component is to use the features to assign the object to a category. Essentially the classifier divides the feature space into regions corresponding to different categories. The degree of difficulty of the classification problem depends on the variability in the feature values for objects in the same category relative to the feature value variation between the categories. Variability is natural or is due to noise.

Image classification is the process of creating an informational representation of an image which shows the spatial distribution of a particular theme (thematic maps) from satellite imagery. Themes can be as diversified as their areas of interest. Examples of themes are soil, vegetation, water depth, and coral among others. Inside a theme, there can be defined sub-themes, and thus the process of classification needs to become more refined.

2.15.2.1 Classification Process

The image classification process can be summarized in 3 steps, as it is shown in the schematics bellow.

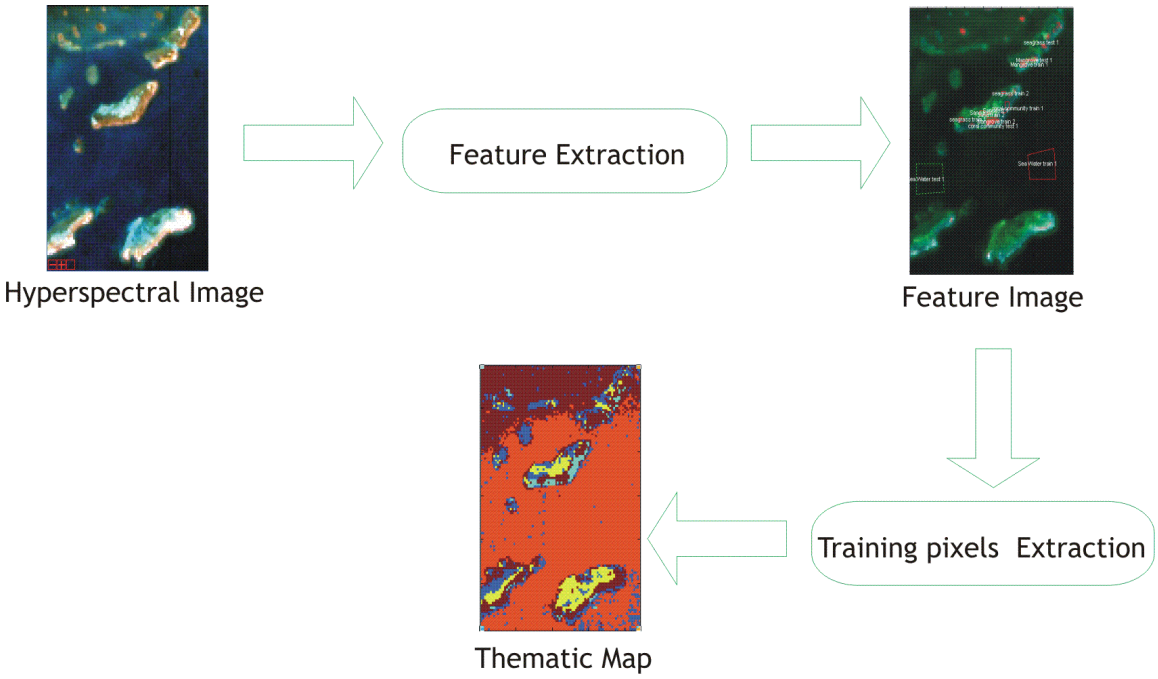

Figure 9 - Image Classification Process

2.15.2.2 Supervised and Unsupervised Classification

Pixels from the hyperspectral image are extracted to train the classifier to recognize patterns which help differentiate the classes. Based on these patterns, the classifier creates discriminant functions to assign each pixel to a class in the feature space (Landgrebe 2003).

The training of the classifier can be either *Supervised* or *Unsupervised*.

In **Supervised classification,** some pre-determined knowledge about the spatial distribution of the classes on the image is assumed. The training points for each site are

selected prior to the application of discriminant functions. Themes are known at the time that the classes are labeled.

In **Unsupervised classification**, the data is clustered according to its natural groups. Those groups then become the classes.

2.15.2.3 Classification Algorithm: Maximum Likelihood Classifier

During the process of training the pixels, the classes are separated using classification algorithms. One of these algorithms is Maximum Likelihood that uses a probability model to determine the decision boundaries; it also assumes that the training data for each class in each band are normally distributed. Makes use of the mean measurement vector *Mc* for each class and the covariance matrix of class *c* for all bands V_c; to classify the measurement vector *X* of a pixel into a class, the maximum likelihood decision rule computes the value *pc* for each class, then it assigns the pixel to the class that has the largest value assign the pixels class *c* if $i \neq c$

$$p_c > p_i (i = 1,2,3,...,m)$$

$$\text{Where } p_c = \ln(a_c) - 0.5\ln[\det(V_c)] - [0.5(X - M_c)^T V_c^{-1}(X - M_c)] \quad (2.9)$$

here Det(V_c) is the determinant of the covariance matrix V_c, a_c is the apriori probability for a pixel to be in class *c*. A probability threshold can exclude outliers, pixels with a low probability of belonging to any class. The a posteriori probability of a pixel belonging to class *c* can be computed as:

$$p(c \mid X) = \frac{a_c p(X \mid c)}{\sum_{k=1}^{m} a_k p(X \mid k)} \quad (2.10)$$

$$p(c \mid X) = \frac{a_c p(X \mid c)}{|V_c|^{1/2}(2\pi)^m} e^{-(X-M_c)^T V_c^{-1}(X-M_c)/2} \quad (2.11)$$

where $p(X \mid c)$ is the probability density function for a pixel X as a member of class c, ac is the priori probability of membership of class c, and m is the total number of classes. The a posteriori probabilities sum to 1.0 for each pixel. The posteriori information may be used to assess how much confidence should be placed on the classification of each pixel. It may be interpreted as the relative proportions of each category within the spatially and spectrally integrated multispectral vector of the pixel.

When the number of training samples is relatively small compared to the dimensionality, maximum likelihood estimates of parameters have large variances, leading to a large classification error (Fukunaga et al., 89)

2.15.2.4 Bhattacharyya Distance

The Bhattacharyya distance is a theoretical distance measure between two Gaussian distributions, this technique measures the statistical separability of spectral classes, giving an estimate of the probability of correct classification.

To relate the effect of the resolution enhancement algorithms to class separability, we use the Bhattacharyya distance between normaly distributed classes. The Bhattacharyya distance is widely used as a measure of class separability because of its analytical form and its relation to the Bayes error.

$$B = \frac{1}{8}[\mu_i - \mu_j]^T \left[\frac{\sum_i + \sum_j}{2}\right]^{-1} [\mu_i - \mu_j] + \frac{1}{2}\ln \frac{\left|\frac{1}{2}\left[\sum_i + \sum_j\right]\right|}{\sqrt{\left|\sum_i\right|\left|\sum_j\right|}} \qquad (2.12)$$

where, B is the Bhattacharya distance, i and j are sub-indices that corresponds to the i^{th} and j^{th} classes, Σ stands for the covariance matrix, and μ for the mean. The first term and the second term represent the class separability due to the mean difference and covariance difference, respectively.

2.16 Summary

In this chapter, the basic concepts of Hyperspectral remote sensing were introduced. Also, the fundamentals of atmospheric correction, the basis of truncated singular value decomposition and the theory of oversampling were described in conceptual form as the pattern recognition method.

CHAPTER 3

3. METHODOLOGY

This chapter presents the methodology used in this research work, shows the details of the Hyperspectral images and the sensors used, the characteristics of the Hyperspectral Matlab Toolbox, the truncated singular value decomposition algorithm and the resolution enhancement based on the oversampling theory algorithm used.

3.1 Methodology used for comparison

The Methodology used for the comparison of the resolution enhancement based on the oversampling theory and the truncated singular values is described as follow.

For this study several Hyperspectral images from different types of sensors, under different environmental conditions, and the availability of ground truth were used. These images were taken from the Hyperion sensor over the benthic habitat of Enrique Reef in Puerto Rico, the Aviris sensor over the crops in the Indian Pine test site, North West of Indiana and the Moffet field in California, the TRWISS III sensor over the crops of the GRS site in Brooksville, MS, and a test image using the Hyperspectral SOC-700 camera available at the Laboratory of Remote Sensing and Image Processing (LARSIP) in the UPRM.

In the pre-processing stage of the Hyperspectral Image classification system, resolution enhancement based on the oversampling theory and truncated SVD methods for enhancement were applied to the images. In the feature extraction stage, we used band subset selection based on matrix factorization, this algorithm requires as input the number of bands to select, which in turn depends on the dimensionality of the data. The dimensionality of the images was determined as the number of principal components

needed to explain at least 99.5% of the total variability. The classification method employed was the supervised Maximum Likelihood. The training and testing samples of each class were manually selected over the images with the aid of the graphical tool provided by the Hyperspectral image analysis Matlab Toolbox. The results of these classifications are the accuracy (the ratio of the number of correctly classified samples to the total number of samples) and the Bhattacharya distance, which helps to compute the effect of each algorithm used in the pre-processing stage.

In all the experiments the feature extraction and classification methods were fixed. Only the pre-processing stage was changed. Samples for training and testing came from the same location.

The methodology explain before is illustrated in the following figure

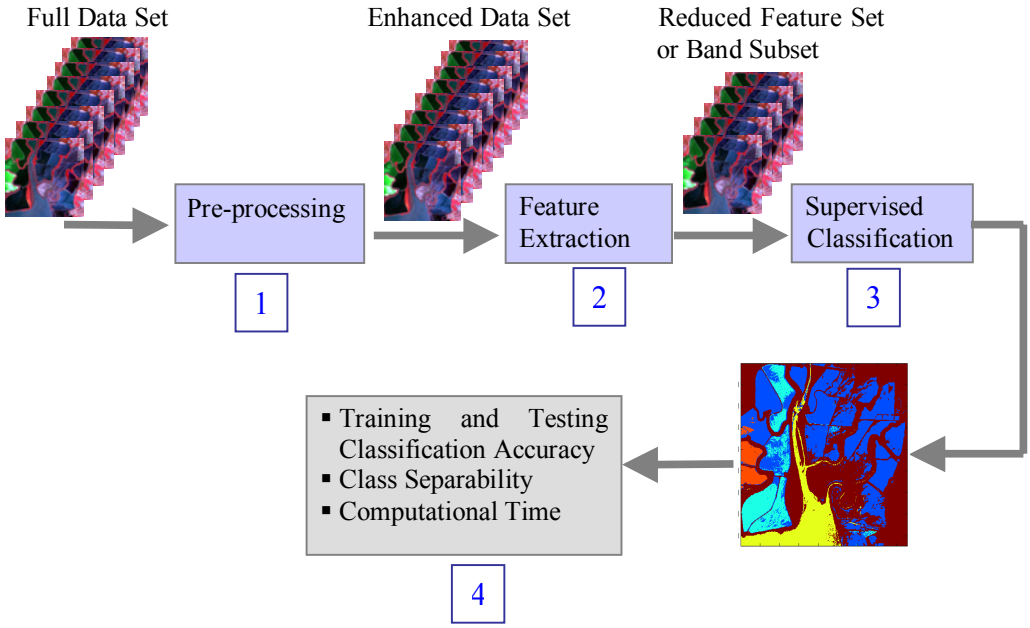

Figure 10 - Methodology used for Comparison

3.2 Hyperspectral Sensors Description

This section presents a brief description of the Hyperspectral sensors used in this work.

3.2.1 Airborne Visible/Infrared Imaging Spectrometer (AVIRIS)

AVIRIS is an acronym for the Airborne Visible InfraRed Imaging Spectrometer. AVIRIS is a world class instrument in the realm of Earth Remote Sensing. It is a unique optical sensor that delivers calibrated images of the upwelling spectral radiance in 224 contiguous spectral channels (also called bands) with wavelengths from 400 to 2500 nanometers (nm). AVIRIS has been flown on two aircraft platforms: a NASA ER-2 jet and the Twin Otter turboprop. The ER-2 is a U2 aircraft modified for increased performance which flies at approximately 20 km above sea level, at about 730 km/hr. The Twin Otter aircraft flies at 4km above ground level at 130km/hr.

Figure 11 - AVIRIS Instrument (EarthSat, 2004)

AVIRIS uses a scanning mirror to sweep back and forth ("whisk broom" fashion), producing 614 pixels for the 224 detectors each scan. The pixel size and swath width of the AVIRIS data depend on the altitude from which the data is collected. When collected by the ER-2 20km above the ground each pixel produced by the instrument covers an area approximately 20 meters square on the ground with some overlap between pixels, thus yielding a ground swath about 11 kilometers wide. When collected by the Twin

Otter (4km above the ground), each ground pixel is 4m square, and the swath is 2km wide.

3.2.2 HYPERION

Hyperion provides a high spectral resolution hyperspectral imager capable of resolve 220 spectral bands (from 0.4 to 2.5 μm) with a 30 meter spatial resolution (EO-1 webpage). The instrument images a 7.5 km by 100 km land area per image and provides detailed spectral mapping across all 220 channels.

Figure 12 - Hyperion Instrument (Taken from NASA EO-1 Webpage)

The major components of the instrument include the following:

- System fore-optics design based on the KOMPSAT EOC mission. The telescope provides for two separate grating image spectrometers to improve signal-to-noise ratio (SNR).
- A focal plane array which provides separate short wave infrared (SWIR) and visible/near infrared (VNIR) detectors based on spare hardware from the LEWIS HSI program.
- A cryocooler identical to that fabricated for the LEWIS HSI mission for cooling of the SWIR focal plane.

Hyperion Specifications

Instantaneous FOV (Field of View)	0.043 mrad
Sensor Altitude	705 km
Spectral bands	242
Swath	7.5 Km
Spectral Coverage	VNIR: 355 – 1000 nm SWIR: 900 – 2577 nm

3.2.3 TRW Imaging Spectrometer III (TRWIS III)

The latest generation of TRWIS hyperspectral instruments, TRWIS III shown in Figure 13, provides broader spectral coverage (0.3 to 2.5 microns) and improved signal/noise (Sandor-Leahy et al, 2000). It has 384 channels with the VNIR segment covering 0.3 to 1.0 microns in 5nm channels and the SWIR segment covering from 0.9 to 2.5 microns in 6.25 nm channels. The sensor operates in a pushbroom mode with 256 spatial channels. Although it is designed to operate up to 240 Hz frame rate, most operations will be between 15 and 60 Hz depending on altitude and aircraft velocity. The IFOV (or resolution) is 0.9 milliradians, which corresponds to a resolution of better than 1 meter from an altitude of 1000 meters. The total field of view is 230 milliradians.

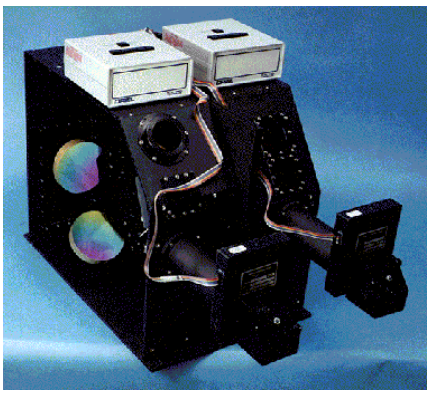

Figure 13 - The TRWIS 3 Hyperspectral Imager (Pearlman et al, 1999)

TRWIS III was designed to satisfy the requirements of a wide variety of earth observing missions such as geological surveying, natural resource management, and environmental monitoring. It can fly on many different aircraft platforms and can also mimic the capability of the TRW-built Lewis hyperspectral imager (HSI), the primary payload on the Lewis satellite which was also built by TRW for NASA. In its first flight season, TRWIS III was used to gather data for applications including remote classification of desert vegetation, forest species, and man-made materials. Along with its first season of operational demonstrations, the instrument underwent laboratory performance validation and radiometric calibration.

3.2.4 SOC-700 Visible Spectral Imaging System

The SOC700 Hyperspectral Imager (shown in Figure 14) is a high quality, portable and easy-to-use spectral imaging instrument that is radiometrically calibrated with software for analysis and viewing. The imager acquires a 640 pixel by 640 pixel images that are 120 bands deep in as little as four seconds.

Figure 14 - SOC-700 Visible Spectral Imaging System (taken from SOC) Webpage)

Highlights

- Spectral Band: 0.43 – 0.9 microns
- Number of Bands: 120, 240 or 480 (configurable)
- Dynamic Range: 12-bit

- Line Rate: Up to 100 lines/second (120 bands)
- Pixels per line: 640
- Exposure Time: 10 - > 10^7 microsecond

3.3 Hyperspectral Data Description

3.3.1 Indiana Pine

The Indiana Image was acquired over Indian Pines test site in NW Indiana on June 12, 1992 by the AVIRIS sensor, (see Figure 15). The image is 145 lines, 145 samples and has 220 bands from 400nm to 2500nm at a spectral resolution of 10nm. It contains 16 classes (Landgrebe 2003). For this study, six classes were selected, see Figure 16. The classes selected were Corn no-till, Grass/Pasture, Woods, Hay Windrowed, Corn Min and Soybean min-till.

The original data has 220 bands, but, for classification, the water adsorption bands and band 220 have to be eliminating, because they are noisy (Tadjudin et al 1998). Additionally, bands 1-5, 77-80, 102-112, and 147-219 were eliminate because, the atmospherically corrected spectrum has strong artifacts in these bands.

Figure 15 - AVIRIS 1992 NW Indiana Indian Pines Image

Figure 16 – Indian Pine Image Ground Truth for the 6 Selected Classes

The data values in the scene are proportional to radiance, 1000 has been added to the calibrated data so that all data values in this scene are positive, to convert the scene data values (SDV) to radiance values (RV), one must first subtract 1000 and then divide by a gain factor of 500 provided by NASA Jet Propulsion Laboratory (JPL)[1].

$$RV = \frac{(SDV - 1000)}{500} \text{ , The RV units are } \frac{W}{cm^2 * nm * sr} \qquad (3.1)$$

3.3.2 Moffet Field

The Moffet Field image was taken from the JPL's Airborne Visible/Infrared Imaging Spectrometer (AVIRIS). AVIRIS acquired the data on August 20, 1992 when it was flown on a NASA ER-2 plane at an altitude of 20,000 meters (65,000 feet) over Moffett Field, California, at the southern end of the San Francisco Bay.

[1] This data is from the AVIRIS (Airborne Visible/Infrared Imaging Spectrometer) built by JPL and flown by NASA/Ames on June 12, 1992

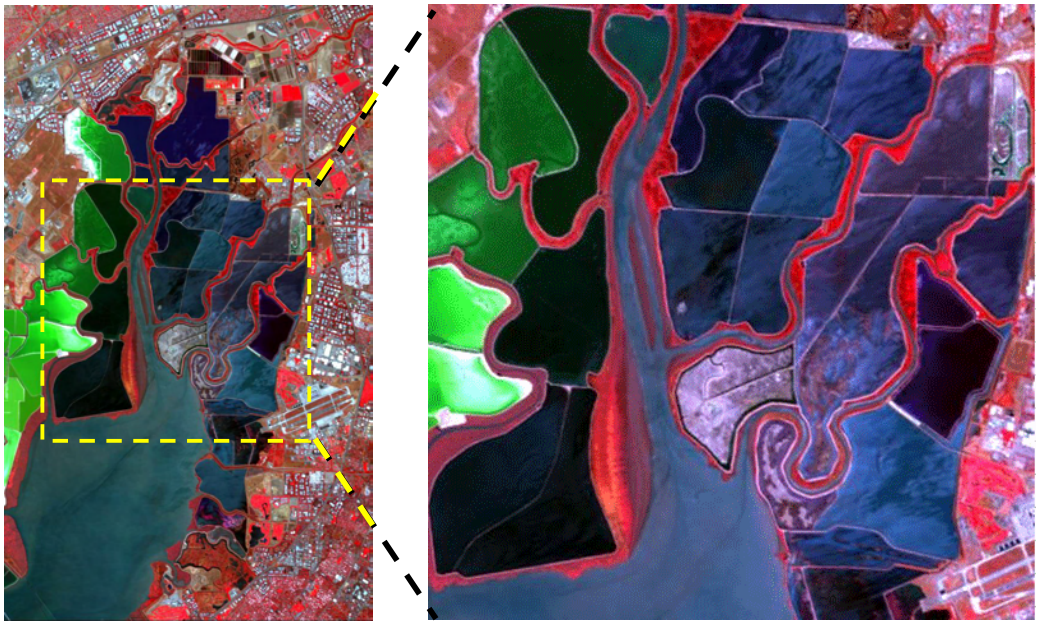

Figure 17 - Moffet Field data from AVIRIS. RGB created using 53, 29, 19 bands.

Figure 17 shows an image of the Moffett field data recorded using the AVIRIS sensor in 224 bands (0.4 µm to 2.4 µm spectral range). This data are 12 bit digital numbers without any atmospheric corrections for absorption and scattering. Five regions of interest are marked in the image for classification (Figure 18). Four of these regions are different water bodies ranging from clear water to an evaporation pond. The water bodies in between have different levels of clarity due to different amounts of particle suspension. Another region is sparse vegetation. The entire image was classified to identify pixels belonging to these 5 regions (classes). The same bands of the Indiana Pine image were eliminated in Moffet Field image. The ground truth was taken from (Subramanian et al, 1997)

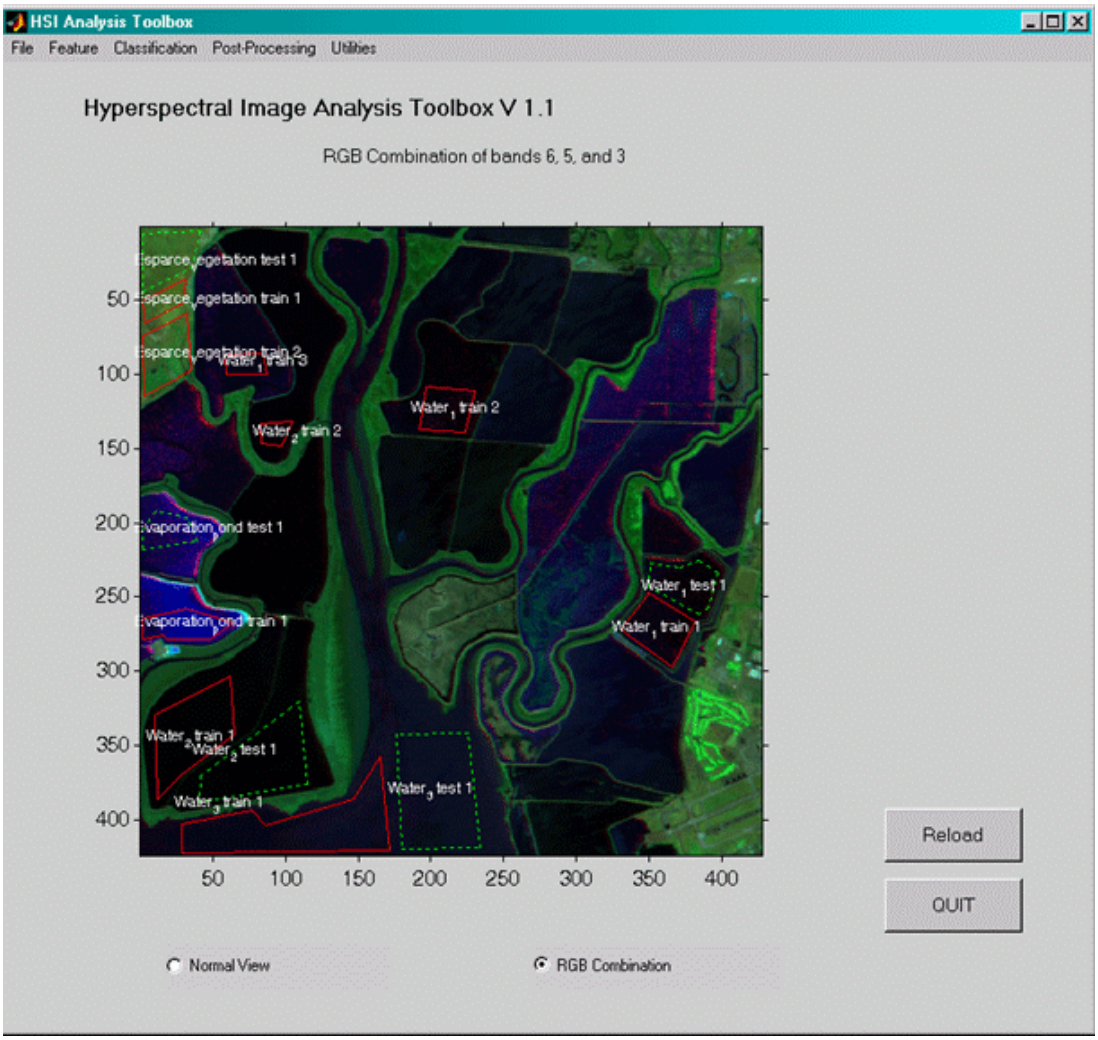

Figure 18 – Moffet field data. The polygons are the 5 classes

3.3.3 GRS-S Data Fusion Committee Data Set

The Geoscience and Remote Sensing Society (GRS-S) Data Fusion Committee benchmark data set GRSS_DFC_0008 was acquired over Brooksville in MS on June 25, 2000 by the TRWISS III sensor (see Figure 19). The image is 1515 lines, 256 samples and has 384 bands from 367nm to 2500nm at a spectral resolution of 2m. It contains 3 classes Corn, Cotton and Soybean. The original data set was already atmospheric corrected using ACORN in mode 1.

Image Description

Elevation of Target:	82 meters
Altitude of Sensor:	1800 meters (MSL)
Image Length:	2337 meters
Spatial Resolution (GSD)	2 meters
Time:	17:37 UTC
Visibility	7 miles
Visual Description:	Slight overcast

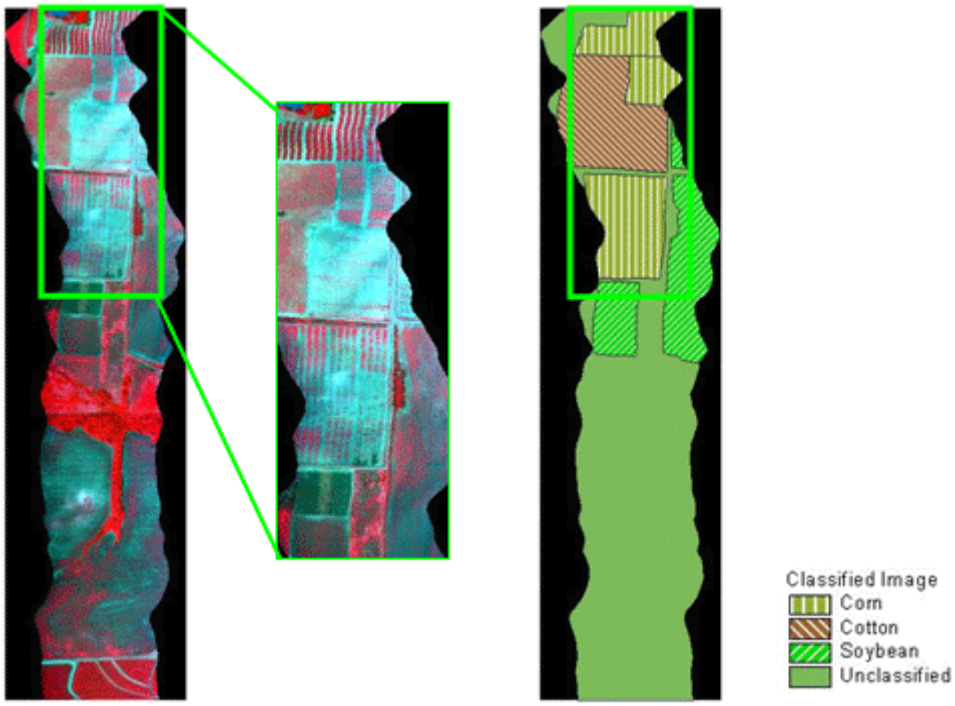

Figure 19 - GRS-S Data Fusion Committee benchmark data set GRSS_DFC_0008

3.3.4 Benthic Habitat of La Parguera in Puerto Rico

This image was acquired over "La Parguera" in Southwestern Puerto Rico on February 21, 2003 by the HYPERION satellite hyperspectral sensor (see Figure 20) at 17:05:50. The original image is 3128 lines, 256 samples and has 242 bands from 355.6 nm to 2577nm at a spectral resolution of 30m. Five classes were selected: Mangrove,

Seagrass, Coral Community, Sand, and Seawater (see Figure 22). The HYPERION data set was atmospheric corrected using ACORN in mode 1 (see section 3.4 for details).

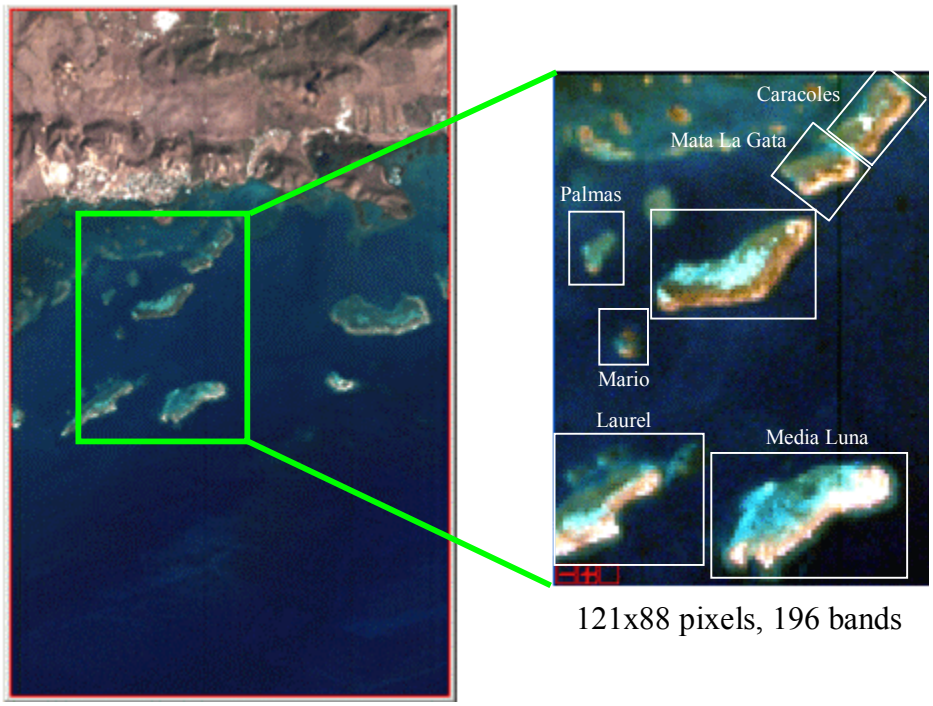

Figure 20 – La Parguera in Southwestern Puerto Rico. (HYPERION)

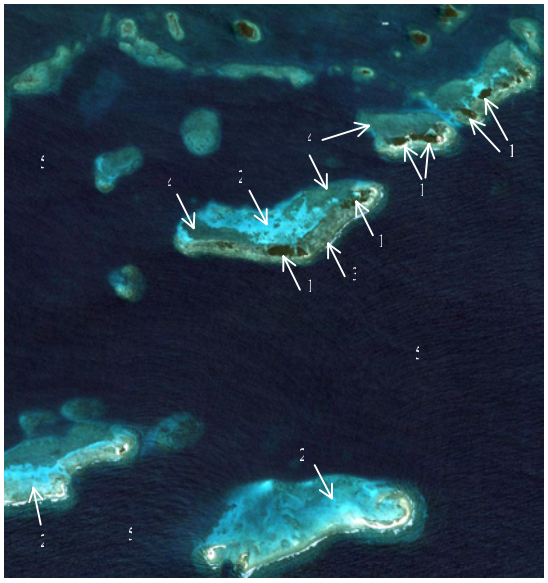

1. Mangrove
2. Carbonate Sand
3. Coral Community
4. Sea grass
5. Sea Water

Figure 21 - "La Parguera" image from IKONOS (Grount truth)

The image processed is 121 lines, 88 samples, 196 bands, starting at column 48, line 1914 as can be seen in the Figure 20. Hyperion data always is delivered at level 1, where the data have been calibrated in radiance units (W/m^2-sr-µm). The SWIR bands have a scaling factor of 80 and the VNIR bands have a scaling factor of 40. Level 1 Radiometric product has 242 channels but only 196 of them are calibrated because the overlap that exists between the VNIR (426-925 nm) and SWIR (912-2395 nm) bands. The reason for not calibrating all 242 channels is due to the detectors low responsivity in the 1-7, 58-76 channels. It is necessary to eliminate these channels because are set to zero.

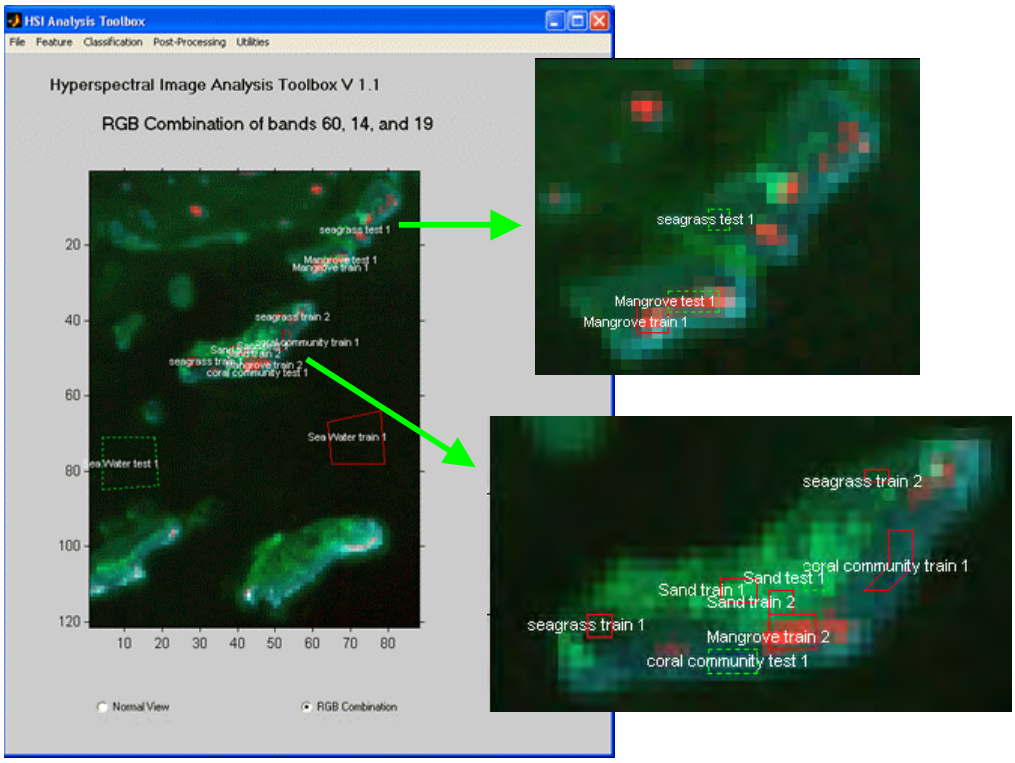

Figure 22 – HYPERION Image. Training and Testing Samples

Five regions of interest are marked in the HYPERION image for classification Figure 22. These regions are Seagrass, Sand, Mangrove, Coral Community and Seawater. The ground truth was provided by Dr. Fernando Gilbes and Jeannette Arce from the Department of Geology in the University of Puerto Rico at Mayagüez.

3.3.5 Hyperspectral SOC700 Camera Test Image

This image was acquired over grass on August 13, 2004 by the Hyperspectral SOC700 Camera (see Figure 23). The original image is 640 lines, 640 samples and has 120 bands from 430 nm to 900nm. Three regions of interest are marked in the SOC700 Test Image for classification Figure 24. These regions are Grass (Background), Coin1 (Quarter Dollar) and Coin2 (Half dime).

Figure 23 - SOC700 Test Image. Grass and Coins

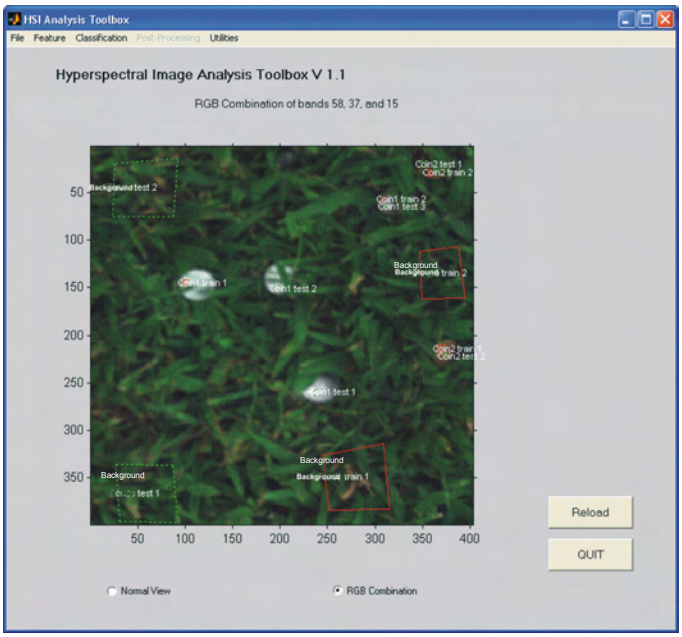

Figure 24 - SOC700 Test Image. Training and Testing Samples

3.4 The MATLAB Toolbox for Hyperspectral Image Analysis

The Hyperspectral Image Analysis Toolbox (Arzuaga et al, 2004) is an application being developed at the UPRM Laboratory for Applied Remote Sensing and Image Processing (LARSIP). This toolbox has a graphical user interface (GUI) (Figure 25) in MATLAB offering several options to manipulate and analyze the Hyperspectral Image data

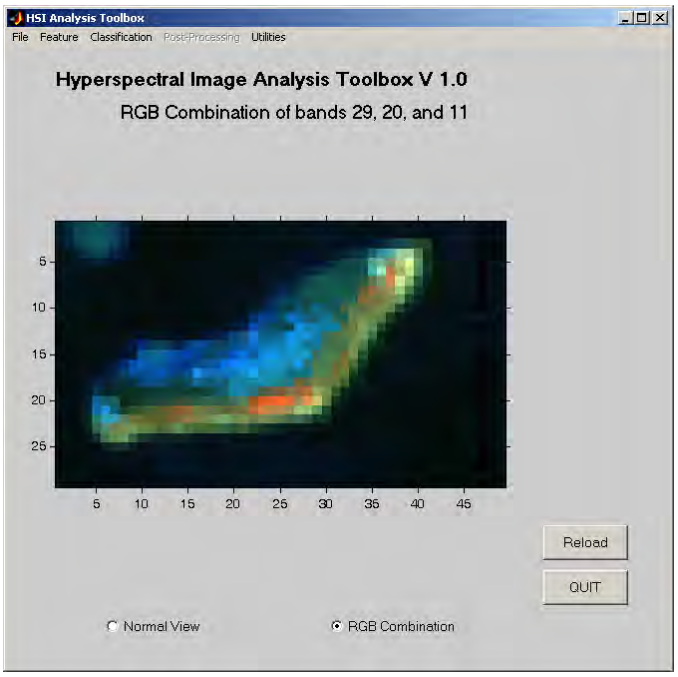

Figure 25 - MATLAB Toolbox for Hyperspectral Image Analysis

MATLAB Toolbox features.

- Load and Save between different image formats as MATLAB (.mat), Remote Sensing binary (bil, bis, bsq), JPG and TIFF.
- Visualization of the image, band by band presented in grayscale or in a RGB composite color using three selected bands.
- Select from one of the available feature extraction/selection routines:
    - Principal Components Analysis (Fukunaga 1990)
    - Discriminant Analysis (Fukunaga 1990)

- Singular Value Decomposition (SVD) (Vélez 1998)
- Band Subset Selection (Lacouture 2002)
- Projection Pursuit (Ifarraguerr 2000)
- Optimized Information Divergence Projection Pursuit (Arzuaga 2003)

- Visualization of the spectral response in each pixel.
- Supervised and unsupervised classification, using one of the following classifiers:

  - Euclidean Distance
  - Fisher's Linear Discriminant Analysis
  - Mahalanobis Distance
  - Maximum Likelihood
  - Angle Detection

  The supervised classification module allows the selection of areas of the image as training and testing samples for the spectral classes present in the image. It is also possible to load a previously saved set of samples to for training.

  The unsupervised classification module enables the user to select the stopping criteria to minimize the change of certain metric between iterations. The metrics used in the toolbox as stopping criteria are:

  - Bhattacharyya Distance
  - Covariance matrix
  - Pixel quantity of variation
  - Sum of squared error
    - Sum of squared error with covariance matrix information

- Post-processing techniques that allows integrate contextual information of the scene to the resulting spectral classification map (Rivera-Medina 2003). The available routines are:

    - Supervised & Unsupervised ECHO classifier
    - Spatial Information Integration based on Markov Random Fields

    The result of applying post-processing techniques is an enhanced classification map. After a set of classes have been defined by supervised or unsupervised classification methods the toolbox allows visualize the class/cluster statistics. The statistics available are the graphical representation of the mean vector and correlation matrix for each class/cluster.

3.5 Atmospheric Correction over Hyperion Image

The Hyperion Image product was distributed with a Hyperion level 1 radiometrically corrected (L1R) data product.

Table 1- Hyperion L1R product

File Name	Contains
EO1H0050482003015110KZ.MET	Metadata file
EO1H0050482003015110KZ.L1R	HDF datasets (image data, spectral center wavelengths, spectral bandwidths, gain coefficients, and a flag mask)
EO1H0050482003015110KZ.hdr	ENVI formatted header

ID Naming convention:

EO1 Satellite

H Hyperion Sensor

005 Target WRS path

048 Target WRS row

2003	Year of acquisition
015	Julian day of acquisition
1	Hyperion 0=off; 1=on
1	ALI 0=off; 1=on
0	AC 0=off; 1=on
K	Pointing mode
Z	Scene length
L1R	Hyperion Level 1 product

3.5.1 Input Data Requirements

ACORN only works with image files that are stored as 16 bit integers in either BIP or BIL format. The format of the integers may be big endian (NETWORK) or little endian (HOST or INTEL). The image data must be 16-bit integer format. The integer format little endian or big endian must be known and specified by the user at runtime. Data written by PCs are often little endian integer format. Hence, Level 1 product has to be converted to this format first. This operation should be done in ENVI before trying to use the FLAASH or ACORN atmospheric correction tools. The image interleave must be Band Interleaved by Pixel (BIP) or Band Interleaved by Line (BIL) and known. If the input radiance image has an ENVI header, ACORN copies the ENVI header information to an output ENVI header to allow easy use of the reflectance corrected output file in ENVI. Also, for better results in the atmospheric correction, is due to work with the calibrated channels. Calibrated channels are 8-57 for the VNIR, and 77-224 for the SWIR, these channels are set to zero.

3.5.2 Data Files

The atmospheric correction methods used is ACORN, based on ENVI. The ACORN software is designed to be simple and straight forward, however the atmosphere correction modes of ACORN requires a number of parameters and input files in specific formats. For atmospheric correction these include a calibrated radiance image file, a spectral calibration file (wavelength and FWHM), a gain file, and an offset file

(Appendix A). These files must be prepared in advance of the ACORN run and must be obtained from the hyperspectral instrument data provider, built from scratch, or developed from existing ACORN files.

3.4.2.1 Spectral Calibration file

The ACORN spectral calibration file must be an ASCII files. Spectral calibration files describe how the electromagnetic radiation is measured spectrally by the instrument of interest. Different modes of ACORN require different spectral calibration input. For example, for hyperspectral, the first column is the wavelength position of each band in units of nanometers. The second column is the full-width-half-maximum (FWHM) of the image that describes the spectral response of each band. The spectral calibration files or information to create them must come from the data provider.

3.5.2.2 Gain File

Several of the modes of ACORN require input gain files that convert the stored integer numbers of the image data to units of radiance (W/m^2 /μm/sr). To make the appropriate input gain file it is necessary to know the units of the image integers stored on disk. Then produce the ASCII input gain file that has a value for each image band that converts that band to radiance (W/m^2/μm/sr).

3.5.2.3 Offset File

The ACORN offset file is an ASCII file with one column with a value for each image band. The values in this offset file are the real numbers that are added to the image radiance values after the gain file has been applied. The units of the offset file are (W/m^2/μm/sr). For most data sets the offset file values will be 0.0.

3.5.3 The ACORN requirements to perform the atmospheric correction

Table 2- Hyperion Sensor Specifications

Instantaneous FOV (Field of View)	0.043 mrad
Sensor Altitude	705 km
Spectral bands	242
Swath	7.5 Km
Spectral Coverage	VNIR: 355 – 1000 nm SWIR: 900 – 2577 nm

Table 3 - ACORN Software Requirements

Data Required	**Assumed Value**
Image Mean Elevation (m)	0
Flight Date, Time	Taken from the metadata file
Scene Center Location (Lat, Lon)	Taken from the metadata file
Atmospheric Model	Tropic
Image Atmosphere Visibility (Km)	40
Derive Water Vapor	940 and 1140 nm
Image Spectral Calibration	Taken from the header file
Gain File	40 for VNIR, 80 for SWIR
Offset File	0 for all wavelength

ACORN offers three options of artifact removal and all can be selected simultaneously:

1. Correct by mismatch between the spectral calibration and the radiative transfer calculations.
2. Suppress small artifacts across the spectral range.
3. Suppress noisy values from low signal data.

ACORN allows to select the bands where the water vapor would be retrieved (820, 940, 1140, and 940-1140 nm). Best results were obtained using both bands at 940 and 1140 nm. This result agrees with the recommended water vapor channels in coastal water by (Gao et al 2000).

For the application to the HYPERION image considered in this study, the algorithm was run in mode 1 (Radiative transfer atmospheric correction of calibrated hyperspectral data) using a Tropic atmospheric model. The 940-1140nm bands were used to derive water vapor, and atmospheric visibility was estimated based on image characteristics. Results of ACORN using the mode 1 in Figure 26

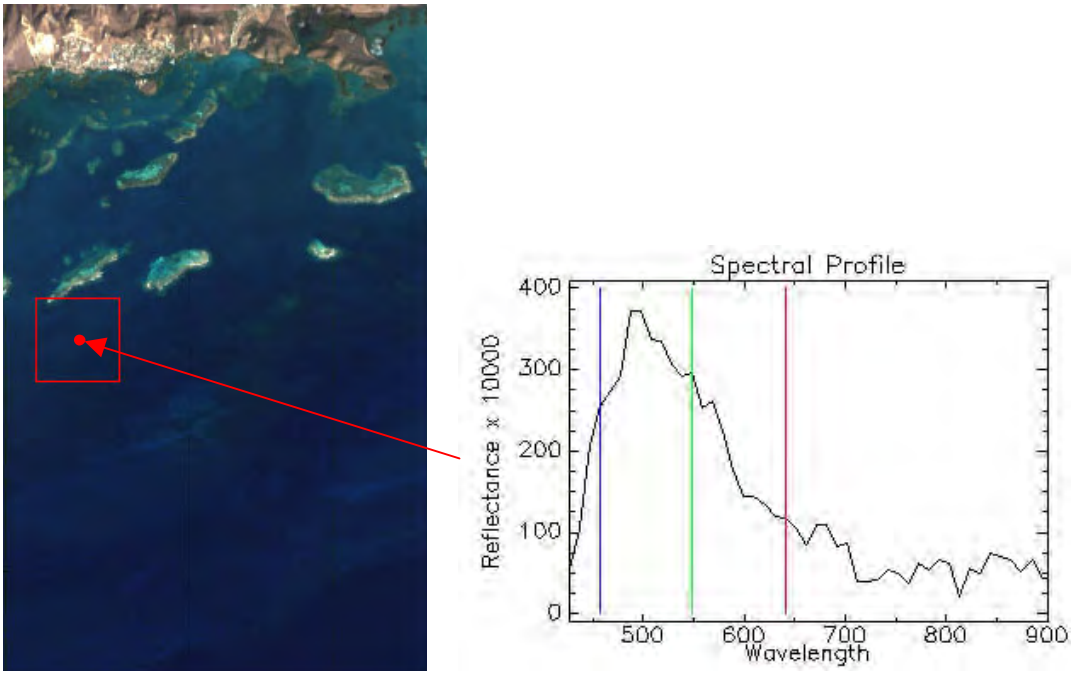

Figure 26 - Result of ACORN over Sea-Water pixels using 940-1140nm bands to retrieve water vapor

3.6 Truncated Singular Value Decomposition (TSVD)

The Singular Value Decomposition (SVD) of a rectangular matrix A of size *mxn* is a decomposition of the form: $A = USV^T$. The SVD followed by the truncation of the lower singular values has been used for noise reduction. This application of the SVD is called Truncated SVD (TSVD) or Reduced-Rank Noise Reduction. (Hansen 1998).

The algorithm can be summarized as follows:

1. Let A be the matrix representation of the Hyperspectral cube

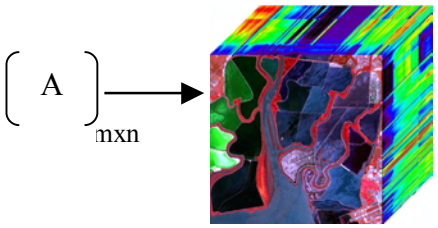

2. Compute the SVD decomposition of A

$$[A] = [u_1 u_2 u_3 \ldots u_n] \begin{bmatrix} \sigma_1 & & & & \\ & \sigma_2 & & & \\ & & \sigma_3 & & \\ & & & \ddots & \\ & & & & \sigma_n \end{bmatrix} [v_1 v_2 v_3 \ldots v_n]^T$$

3. Discard the smaller singular values of A and their corresponding singular vectors.

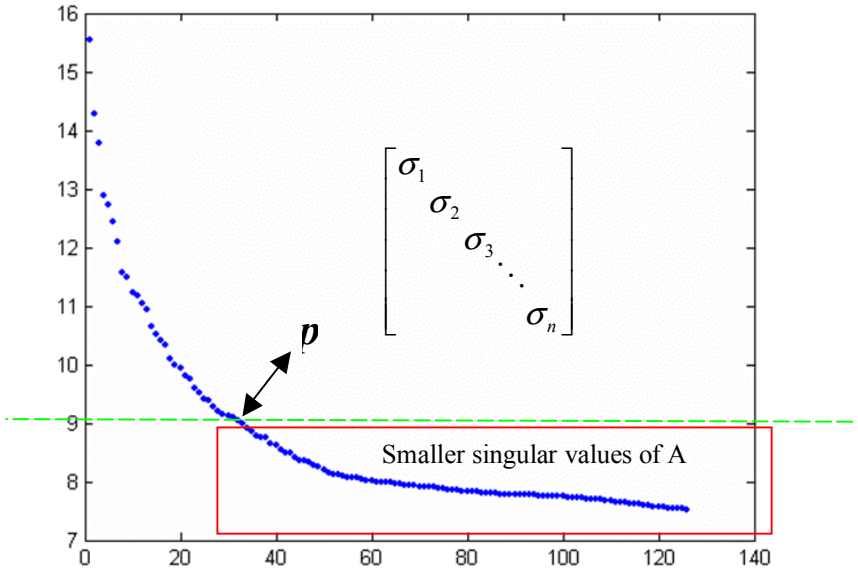

Figure 27 – Singular Values of A (Moffet Image)

The number of singular values ***p*** (See Figure 27), taken from the SVD decomposition to form the TSVD is given by:

$$\max_p \left\{ \frac{\sum_{i=1}^{p} \sigma_i^2}{\sum_{i=1}^{N} \sigma_i^2} * 100 \right\} \leq th$$

where, N is the total number of singular values and $0 < th < 100$ is a threshold that correspond to the percentage of singular taken with respect to the total, which is chosen according to the data itself.

The new SVD decomposition it is as follows:

$$[A] = \underbrace{[u_1 u_2 \ldots u_p}_{U_p} u_{p+1} \ldots u_n] \begin{bmatrix} \underbrace{\sigma_1 \; \sigma_2 \; \ddots \; \sigma_p}_{\Sigma_p} & & \\ & \sigma_{p+1} \; \ddots & \\ & & \sigma_n \end{bmatrix} \underbrace{[v_1 v_2 \ldots v_p}_{V_p} v_{p+1} \ldots v_n]^T$$

4. Finally, the filtered image is obtained by $A_p = U_p \Sigma_p V_p^T$

The small singular values of A, represent the noise, and thus the rank-p matrix A_p (p<n) approximations of A represents a filtered signal with less noise.

3.7 Amplitude Resolution Spectral Enhancement Based on Oversampling

Hyperspectral imagery is characterized by its high spectral resolution and a large number of spectral samples which results in oversampling in the spectral domain. Resolution enhancement takes advantage of the additional information provided by the oversampling to improve the signal to noise ratio of the image and class separability (Hunt et al, 2003). The resolution enhancement based on Oversampling algorithm can be summarized as follows:

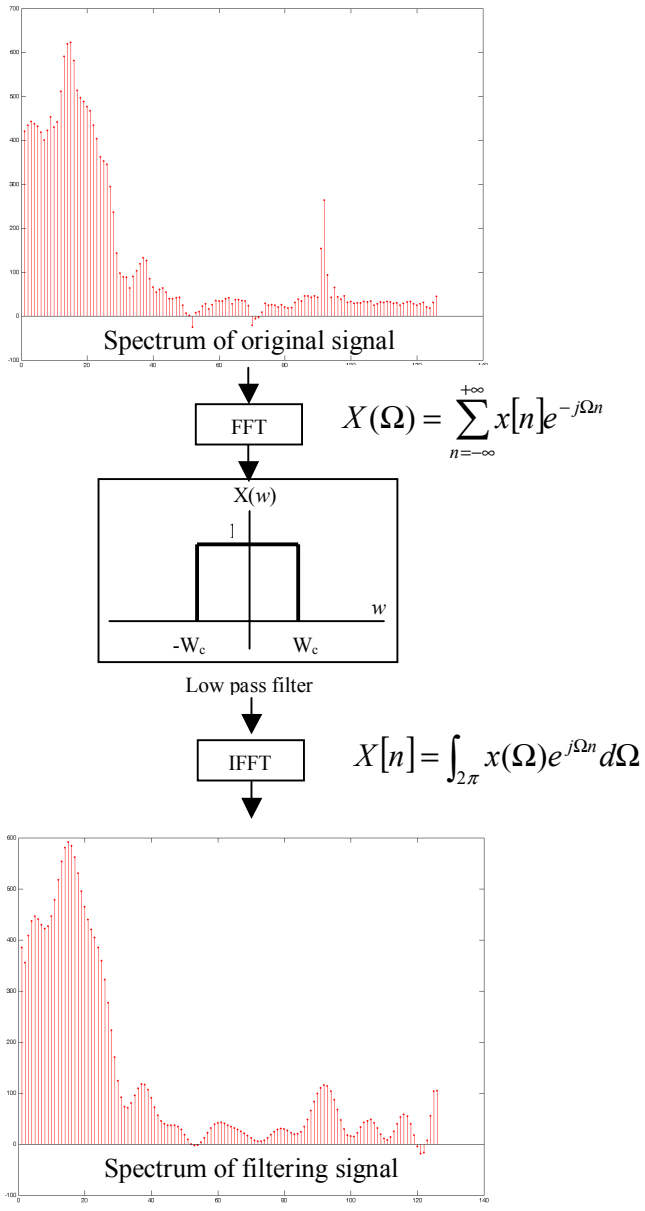

Figure 28 - Amplitude Resolution Spectral Enhancement based on Oversampling Process

3.7.1 Cutoff Frequency Selection

The amplitude resolution spectral enhancement algorithm was run using 10 cutoff frequencies in the range [0.1π, 1π], at intervals of 0.1π. The cutoff frequency that produced the highest classification accuracy was selected

3.8 Computational Complexity

A complexity analysis is performed to demonstrate the lower computational complexity of resolution enhancement over Truncated SVD.

3.8.1 Computational Complexity of Truncated Singular Value Decomposition

Let A_{mxn} be the matrix that represents the Hyperspectral image, where ***m*** are the pixels in the image and ***n*** the number of bands.

Step 1: Compute the SVD of matrix A. $A_{mn} = U_{mn}\Sigma_{nn}V_{nn}^{T}$.

$$[A] = [u_1 u_2 u_3 \dots u_n] \begin{bmatrix} \sigma_1 & & & & \\ & \sigma_2 & & & \\ & & \sigma_3 & & \\ & & & \ddots & \\ & & & & \sigma_n \end{bmatrix} [v_1 v_2 v_3 \dots v_n]^T$$

The computational complexity of this step is O (mn^2) (Van-Loan et al, 97).

Step 2: Perform Principal Component Analysis (Karhunen-Loeve method) (Te-Ming Tu, et al 2001), to reduce the dimensionality of the data, that is, compute the first *p* first singular values such that:

$$\max_p \left\{ \frac{\sum_{i=1}^{p} \sigma_i^2}{\sum_{i=1}^{n} \sigma_i^2} * 100 \right\} \leq threshold\,(\%)$$

where, threshold (%) is the percentage of contribution to the total variability of the data of the first p-singular values, which is usually taken above 90%. In this work, the threshold used was 99.5%, selected as the minimum value that does not affect the classification accuracy of the data retrieved after dimension reduction and the original data.

The computational complexity of this step is O(n), since it requires at most 2n + 2 computations of order O(1).

Step 3: Define U_p, Σ_p and V_p as

$$U_p = \lfloor u_1\ u_2 \cdots u_p \rfloor$$

$$V_p = \lfloor v_1\ v_2 \cdots v_p \rfloor$$

$$\Sigma_p = \begin{bmatrix} \sigma_1 & & \\ & \sigma_2 & \\ & & \ddots \\ & & & \sigma_p \end{bmatrix}$$

which requires O(mp) to copy the corresponding p-eigenvectors of size at most m on to the matrix $U_{p,}$ meanwhile V_p and Σ_p only requires $O(p^2) = O(mp)$ time, since $m > p$. Hence, the step requires O(mn) time.

Step 4: Compute $A_p = U_p \Sigma_p V_p^T$. The $U_p \Sigma_p$ product requires $O(mp^2)$ time and the product $(U_p \Sigma_p) V_p^T$ requires O(mpn). Since n>p, then this step requires O(mpn) time.

The computational complexity of the truncated SVD transform is $O(mn^2)$ + O(n) + O(mn) + O(mpn) = $O(mn^2)$

3.8.2 Computational Complexity of Resolution Enhancement based on oversampling

Let A_{mxn} be the matrix that represent the Hyperspectral image, where ***m*** are the pixels in the image and ***n*** are the number of bands.

Step 1: Obtain the Fast Fourier Transform (FFT) of every pixel. Here, the FFT of a vector of length n, requires O(nlogn) time (Cormen et al, 2001). Since, there are m pixels in the image, then the computational complexity of this step is O(mnlogn)

Step 2: Multiply the image with a predefined Lowpass filter. This step involves the multiplication in the domain frequency of two vectors of size n, that is O(n) steps; and since there are m pixels in the image this step takes O(mn) time.

Step3: Obtain the inverse FFT of the filtered pixels, obtained in the prior step. Here, the computational complexity is O(mnlogn) since the inverse Fourier Transform requires O(nlogn) time for each pixel.

The computational complexity of the resolution enhancement algorithm, based on oversampling theory is O(mnlogn) + O(mn) + O(mnlogn) = O(mnlogn).

3.8.3 Complexity Comparison

Since the computational complexity of the truncated SVD algorithm is $O(mn^2)$ we can see that resolution enhancement is asymptotically faster, by replacing an n factor by logn.

For comparison purposes the algorithms were run on a Dell Optiplex operating under Microsoft Windows XP, Professional. The machine specifications were: an Intel Pentium 4 processor of 2.20GHz, 1 GB of RAM.

Figure 29 present the computational cost of the amplitude resolution enhancement based on oversampling and truncated singular value algorithms in seconds. It is noteworthy that in all cases the amplitude resolution spectral enhancement runtime is better than truncated SVD. As can be revealed by the Figure 29 the Truncated SVD elapsed time is approximately twice the elapsed time of resolution enhancement in most of the cases.

Comparing the experimental results of the algorithms in terms of running time with their theoretical complexities these results agree with the complexity of the algorithms.

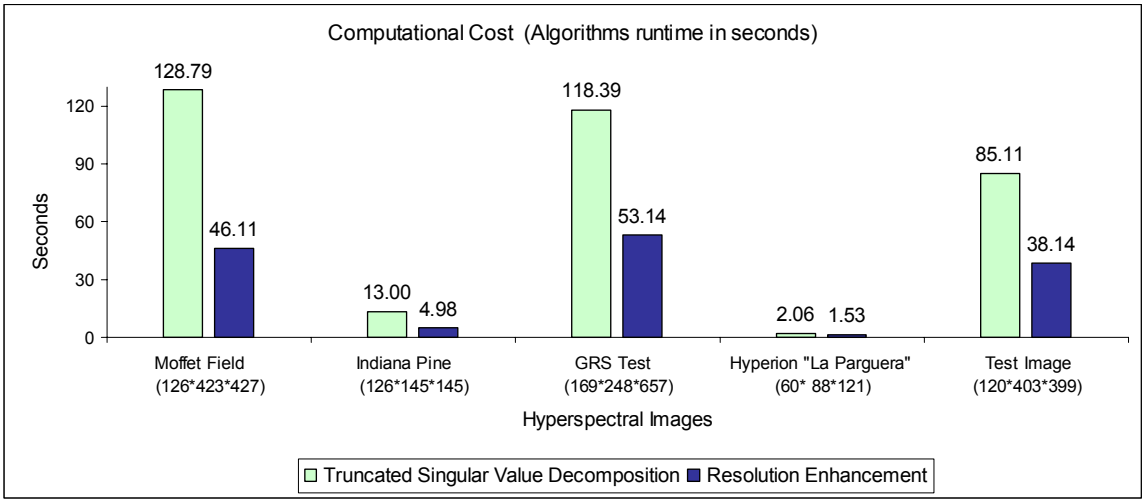

Figure 29 - Computational Cost (Algorithms run time in seconds)

3.9 Summary

The methodology for comparison of the two algorithms Truncated SVD and Resolution Enhancement based on the oversampling theory presented in this chapter were

intended to explain how the algorithms were validated, besides a brief description of the different characteristics of the Hyperspectral images used in this work, also the characteristic's of the Hyperspectral Matlab toolbox used to perform the classification of the images, additionally this chapter present the algorithms used for comparison, and finally, the algorithms computational cost.

CHAPTER 4

4. EXPERIMENTAL RESULTS

In order to evaluate the effect of amplitude resolution spectral enhancement based on oversampling, truncated singular value decomposition and atmospheric correction over classification accuracy and class separability, several experiments were conducted using the Indian Pines image in the North west of Indiana, Moffet Field image in California, Enrique Reef in Puerto Rico, GRS site in Brooksville, and a test image collected using the Hyperspectral SOC-700 camera. These experiments combined amplitude resolution spectral enhancement truncated singular value decomposition and Atmospheric correction in preprocessing before image classification. Figure 30 shows all pre-processing schemes studied.

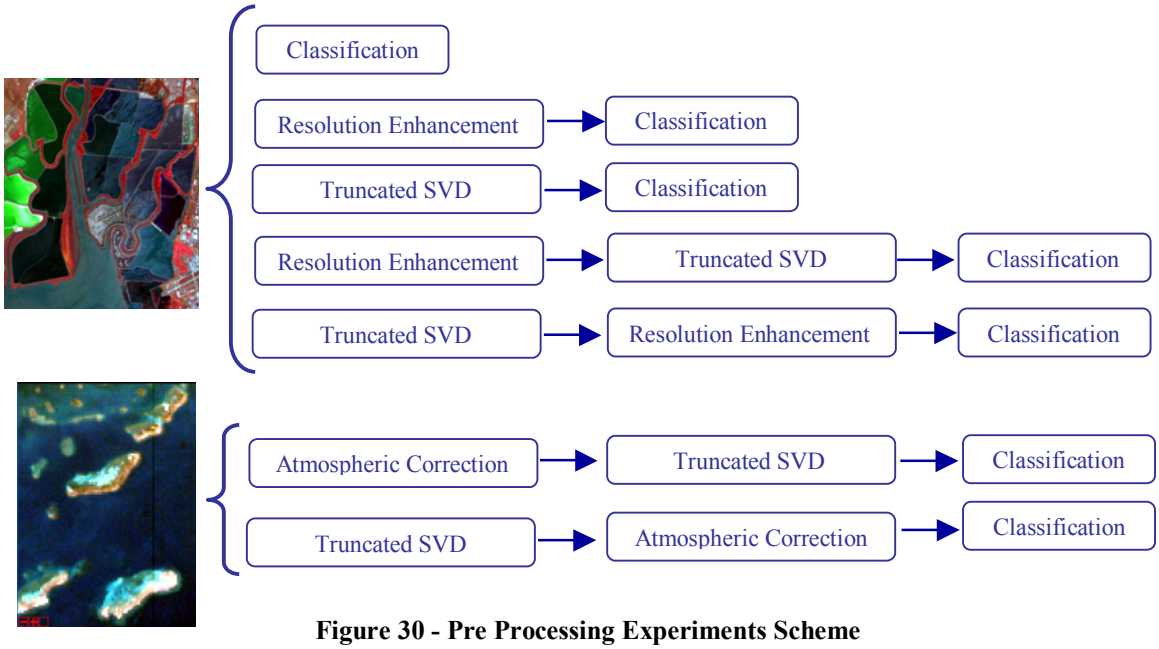

Figure 30 - Pre Processing Experiments Scheme

The classification method employed was the supervised Maximum Likelihood method (Landgrebe 2003). The training and testing samples of each class were manually selected over the image with the aid of the graphical tool provided by the hyperspectral

image analysis Matlab Toolbox (Arzuaga et al, 2004). The classification accuracy (the ratio of the number of correctly classified samples to the total number of samples) and the Bhattacharya distance were computed to asses the effect of each pre-processing scheme on the classification accuracy and on class separability.

As a feature extraction process for classification, we used band subset selection based on matrix factorizations (Velez et al, 1998). The subset band selection algorithm requires as input the number of bands to select, which in turn depends on the dimensionality of the data. We determined dimensionality of the image input to the band subset selection procedure as the number of principal components needed to explain at least 99.5% of the total variability (Umaña et al, 2003). The dimensionality estimation results are shown in Table 5.

List of Acronyms used for tables and figures

Table 4 - Nomenclature for Tables and Figures

TSVD	Truncated Singular Value Decomposition
RE	Amplitude resolution spectral enhancement
TSVD_RE	Truncated Singular Value Decomposition first, then Amplitude resolution spectral enhancement
RE_TSVD	Amplitude resolution spectral enhancement first, then Truncated Singular Value Decomposition
ATM	Atmospheric Correction
ATM_TSVD	Atmospheric Correction first, then Truncated Singular Value Decomposition
ATM_RE	Atmospheric Correction first, then Amplitude resolution spectral enhancement

Table 5 - Dimensionality of the Data after each experiment

	Bands selected by the SVDSS algorithm				
Preprocessing Method	Indiana	Moffet	GRS	Hyperion	Test Image
Original	2,24,31,35,36,65,81,102	11,23,27,35,59,91,99	46,61,114,117,118,146,148	12,19,36,51,58	8,33,62,71,79,80,81,82,85,106
TSVD	1,24,31,35,36,65,81,103	11,23,27,32,68,91,100	46, 77, 114, 116, 147	12,19,36,51,58	8,33,62,71,79,80,81,82,85,106
RE	8, 21, 36, 65, 81	11,23,27,38,58,91,99	43, 64, 117, 133, 149	6,14,22,35,57	8,21,32,44,52,61,72,82,92,109
TSVD_RE	7,21,33,43,60,82,104,114	8,21,34,63,94,108	46, 77, 114, 116, 147	4,13,22,35,57	7,20,31,40,50,61,72,82,92,107
RE_TSVD	3,13,23,34,44,62,84,106	11,22,28,65,91,114	42, 79, 149	6,14,22,35,57	8,21,32,44,52,61,72,82,92,109
ATM	N/A	N/A	N/A	13,28,48,51,53	N/A
ATM_TSVD	N/A	N/A	N/A	13,28,48,51,53	N/A
ATM_RE	N/A	N/A	N/A	13,28,49,51,53	N/A

4.1 Classification accuracy, Class Separability and Noise Reduction Effect

4.1.1 Indiana Pine

Figure 31 and Figure 32 show the classification accuracy of the training and testing samples using the maximum likelihood classifier, per class of the each combination preprocessing scheme for the Indiana Image. As can be seen in Figure 31 resolution enhancement increments the accuracy of Corn_Notill, Woods and Corn_min classes, but decrements the accuracy of the Soybeans and Grass classes, meanwhile the Hay_windrowed class remains the same. Whereas, truncated SVD increments the accuracy of the Corn_Notill and Woods classes, but decrements the accuracy of Grass and Hay_windrowed classes, meanwhile the Soybeans class remains with the same accuracy.

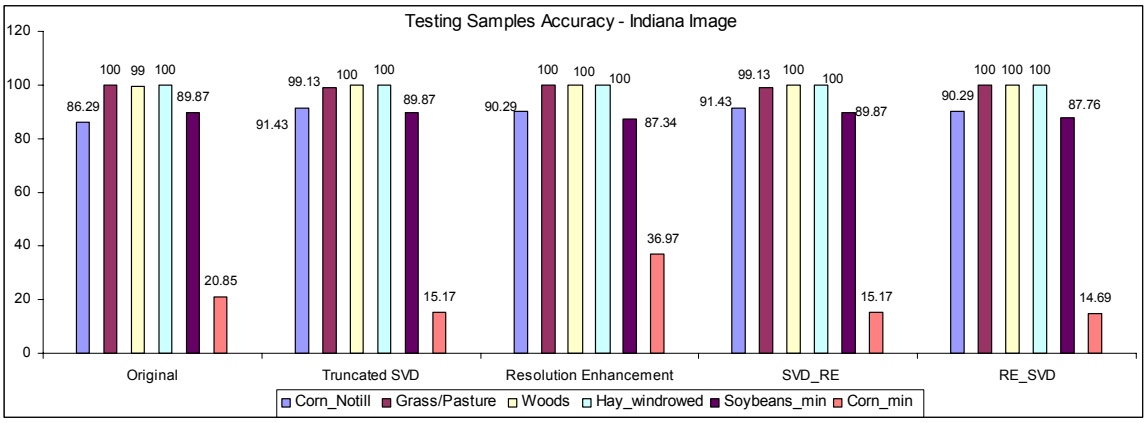

Figure 31 - Classification Accuracy of the testing samples per class in the Indiana Image

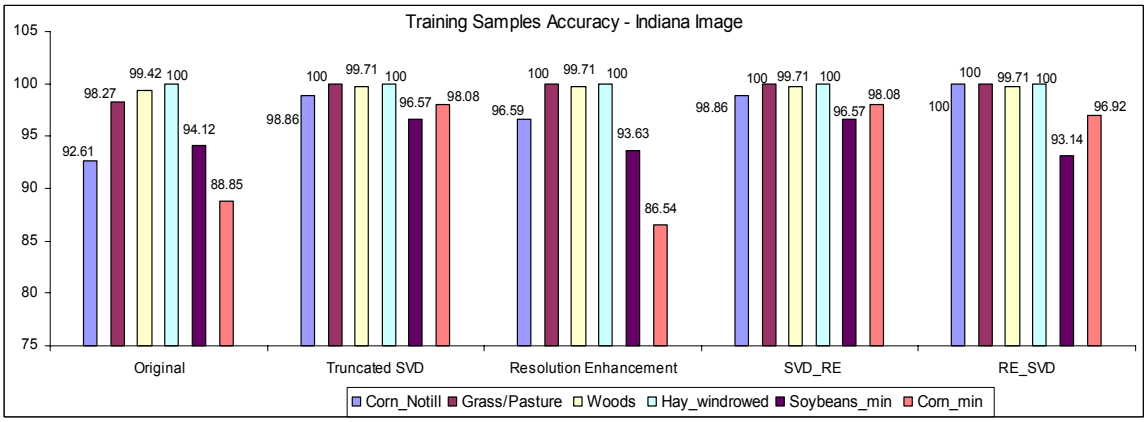

Figure 32 - Classification Accuracy of the training samples per class in the Indiana Image

The overall classification accuracy and the improvement over classification of the image without pre-processing (None) are shown in Table 6 and Table 7. For information purposes, the frequency of the low pass filter used for resolution enhancement is 0.1π and the number of singular values taken was 8. As shown in Table 7, resolution enhancement increments the overall accuracy in 3.082% in comparison with the accuracy on the image without preprocessing (None).

Table 6 - Overall Classification Accuracy per each Preprocessing Scheme (Training Samples)

Image Preprocessing Scheme	Overall Classification Accuracy (%)	Increase in accuracy from None
None	95.5772	N/A
Truncated SVD	98.8756	3.2984
Resolution Enhancement	95.8771	0.2999
TSVD_RE	98.8696	3.2924
RE_TSVD	98.2948	2.7176

Table 7 – Overall Classification Accuracy per each Preprocessing Scheme (Testing Samples)

Image Preprocessing Scheme	Overall Classification Accuracy (%)	Increase in accuracy from None
None	81.5068	N/A
Truncated SVD	81.6023	0.0955
Resolution Enhancement	84.589	3.0822
TSVD_RE	82.5994	1.0926
RE_TSVD	82.1236	0.6168

Figure 33 shows the minimum Bhattacharya distance among classes for each preprocessing scheme. As can be seen, amplitude resolution spectral enhancement based on oversampling and Truncated SVD increase class separability in the majority of cases; these results correlate with the classification accuracy results described previously and give some insight in what is the effect of each preprocessing scheme used. Figure 34 shows the maximum Bhattacharya distance per class for each preprocessing scheme. In this case, resolution enhancement reduces the maximum Bhattacharya distance between classes, meanwhile truncated SVD increases them.

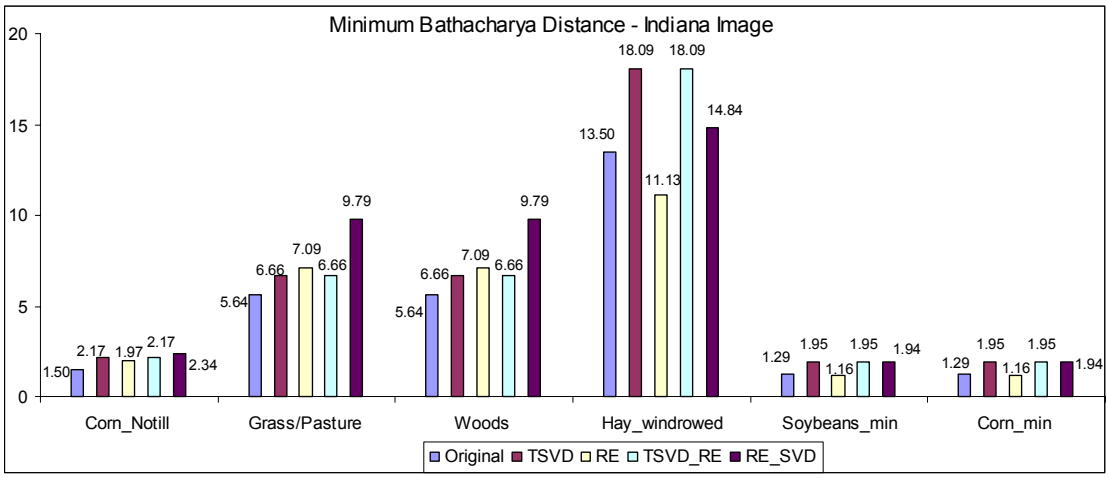

Figure 33 - Minimum Bhattacharya Distance of the Indiana image

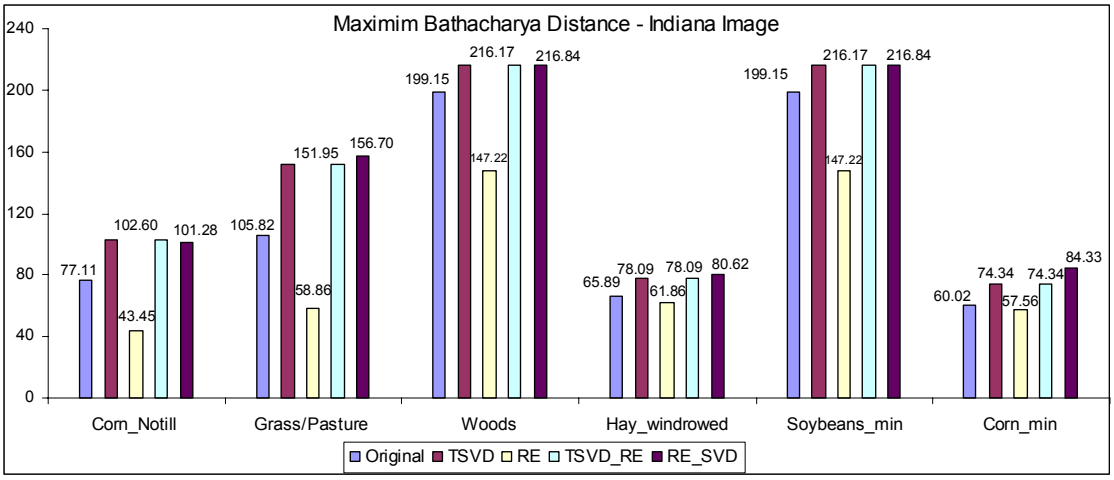

Figure 34 - Maximum Bhattacharya Distance of the Indiana image

Noise Reduction Effect

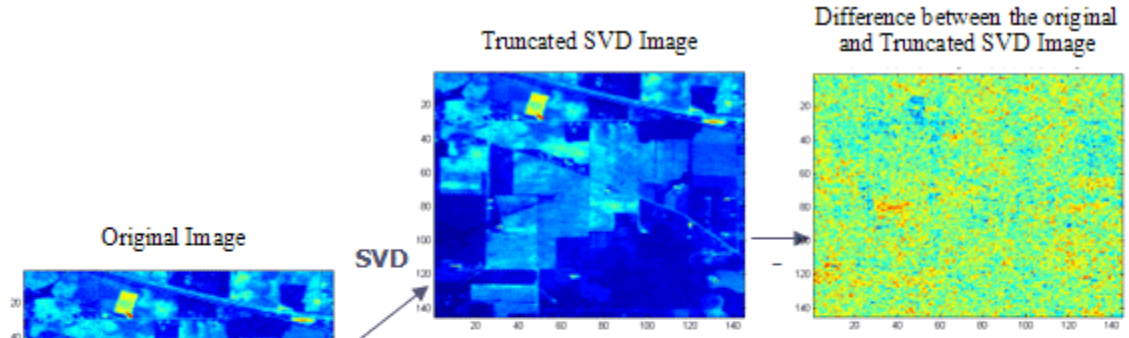

Figure 31a – Difference between Original and TSVD images

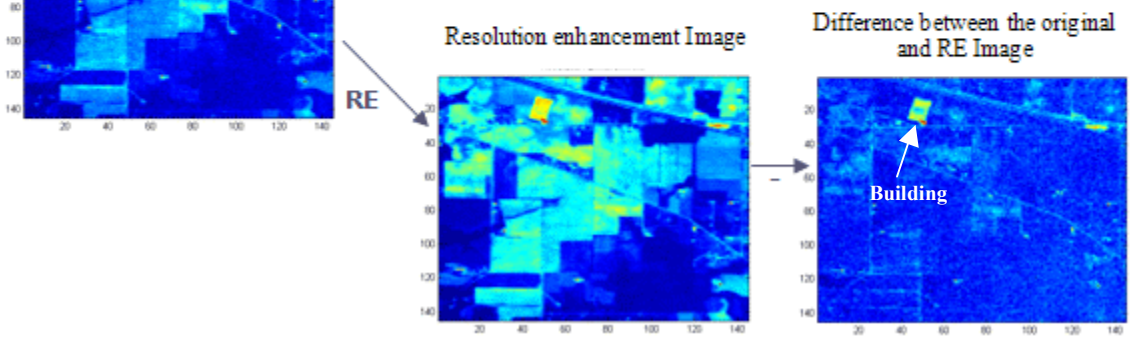

Figure 31b – Difference between Original and RE images

Figure 35 - Noise reduction effect on Indiana Pine Image

Figure 35a shows the image difference between the original and truncated SVD images, Figure 35b shows the image difference between the original and resolution

enhancement images. It is clear from this figure that truncated SVD is removing noise meanwhile; resolution enhancement is removing some information as can be appreciated on the image difference that shows clearly some features of the original image: the road, the building and part of the crops.

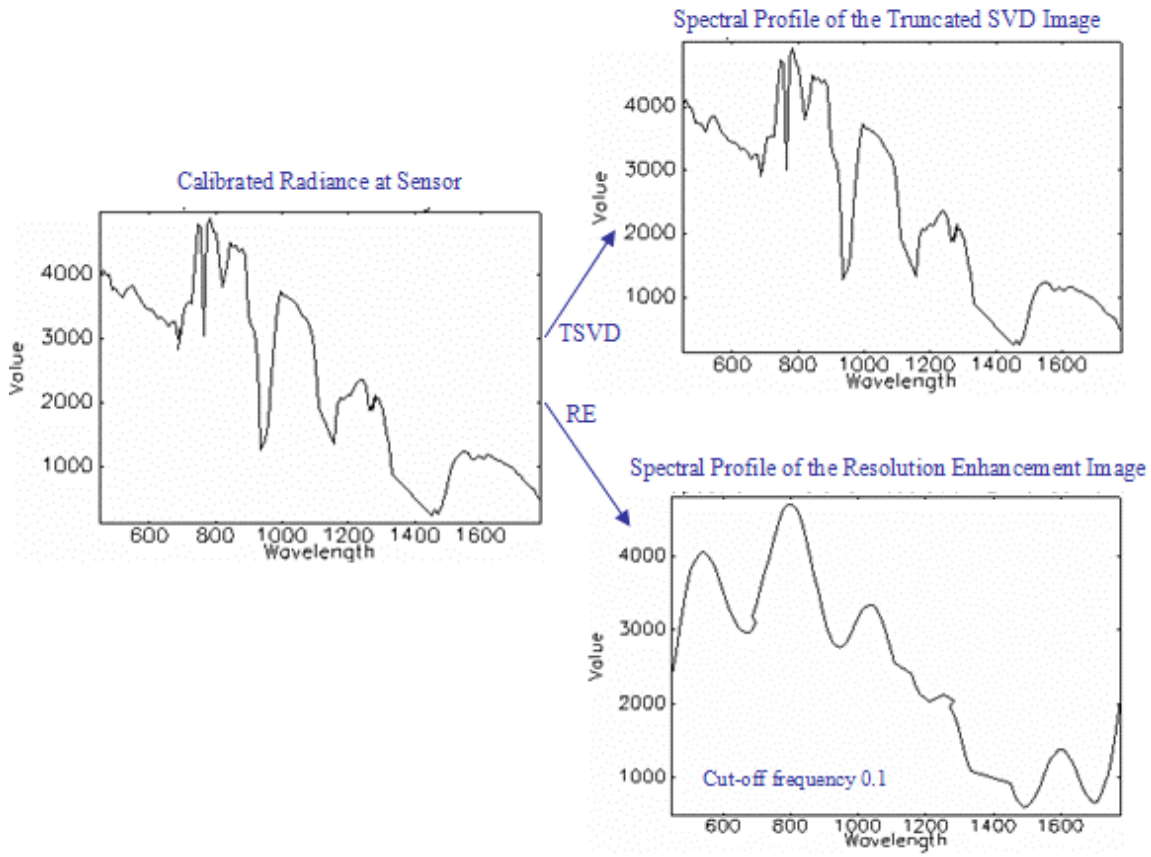

Figure 36 - Effect of Image Pre-Processing on the spectral signature (Indiana Pine)

Figure 36 shows the effect of truncated SVD and resolution enhancement on the spectral signature of the original image. It can be seen that truncated SVD does not affect sensibly the spectral signature of the original image, meanwhile resolution enhancement extract only the low frequency components of the spectral signature and modifies it sensibly.

Even though truncated SVD seems to remove noise and increase class separability better than resolution enhancement, the classification accuracy is improved more by

resolution enhancement. Maybe because resolution enhancement increased the minimum Bhattacharya distance which is a more effective measure of class separability than the maximum Bhattacharya distance; also classification by clustering do not necessarily improve by using all the information available.

4.1.2 Moffet Field

Figure 37 and Figure 38 show the classification accuracy of the testing and training samples using the maximum likelihood classifier, per class of the each combination preprocessing scheme for the Moffet Field Image. As can be seen in Figure 37 resolution enhancement increments the accuracy of Water_2 and Water_3 classes, but decrements the accuracy of the Evaporation_Pond class, meanwhile the Water_1 and Sparse_Vegetation classes remains the same. Whereas, truncated SVD decrements the accuracy of Water_2, Water_3 and Evaporation_Pond classes, meanwhile the Water_1 and Sparse_Vegetation class remains with the same accuracy.

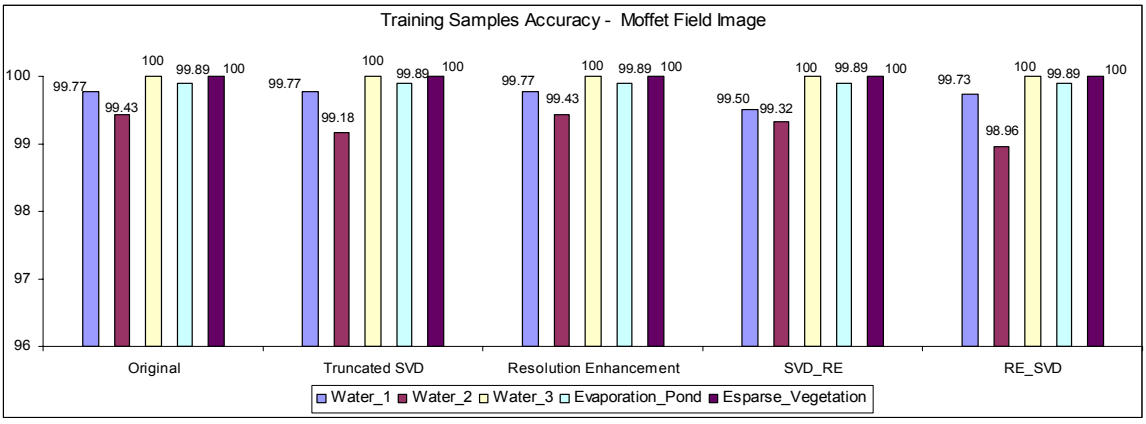

Figure 37 - Classification Accuracy of the training samples per class in the Moffet Image

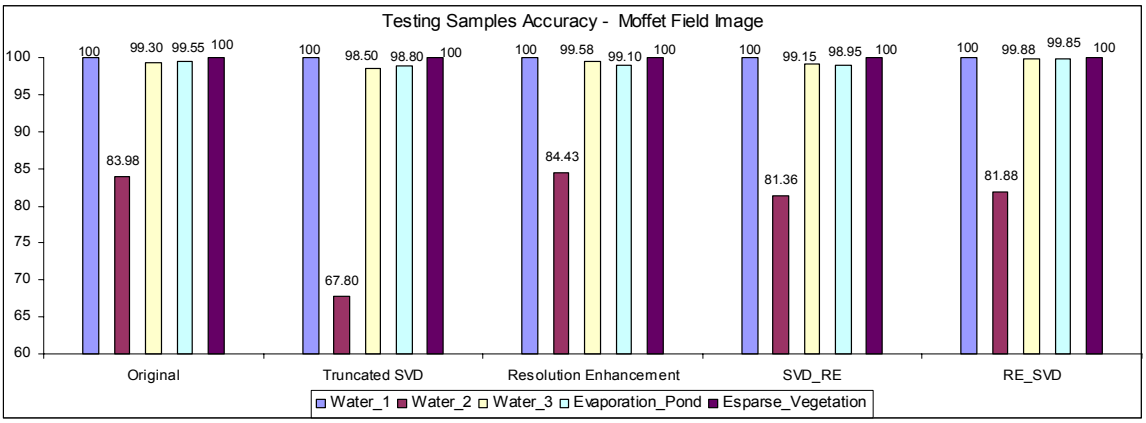

Figure 38 - Classification Accuracy of the testing samples per class in the Moffet Image

The overall classification accuracy and the improvement over classification of the image without pre-processing (None) are shown in Table 8 and Table 9. The frequency of the low pass filter used for resolution enhancement was 0.9π and the number of singular values taken was 8. As shown in Table 9, resolution enhancement increments the overall accuracy in 0.2078% in comparison with the accuracy on the image without preprocessing (None).

Table 8 - Overall Classification Accuracy per each Preprocessing Scheme of Moffet Field (Training Samples)

Image Preprocessing Scheme	Overall Classification Accuracy (%)	Increase in accuracy from None
None	99.8082	N/A
Truncated SVD	99.7498	-0.0584
Resolution Enhancement	99.8082	0
TSVD_RE	99.7248	-0.0834
RE_TSVD	99.6915	-0.1167

Table 9 - Overall Classification Accuracy per each Preprocessing Scheme of Moffet Field (Testing Samples)

Image Preprocessing Scheme	Overall Classification Accuracy (%)	Increase in accuracy from None
None	95.2312	N/A
Truncated SVD	89.7247	-5.5065
Resolution Enhancement	95.439	0.2078
TSVD_RE	94.4	-0.8312
RE_TSVD	94.9091	-0.3221

Figure 28 shows the minimum Bhattacharya distance among classes for each preprocessing scheme. As can be seen, Truncated SVD increase class separability in the majority of cases, meanwhile, amplitude resolution spectral enhancement based on oversampling decrement the minimum Bhattacharya distance for the Water_1, Water_2 and Water_3 classes, however resolution enhancement increment the minimum distance of Evaporation_Pond and Sparse_Vegetation classes.

Figure 40 shows the maximum Bhattacharya distance per class for each preprocessing scheme. In this case, resolution enhancement increment the distance of the Water_2, Water_3 and Sparse_Vegetation but decrement the distance of the Water_1 and Evaporation_Pond; meanwhile, truncated SVD reduces the maximum Bhattacharya distance of the Water_2 and Water_3 classes, but increase the distance of the Water_1, Evaporation_Pond, and Sparse_Vegetation classes.

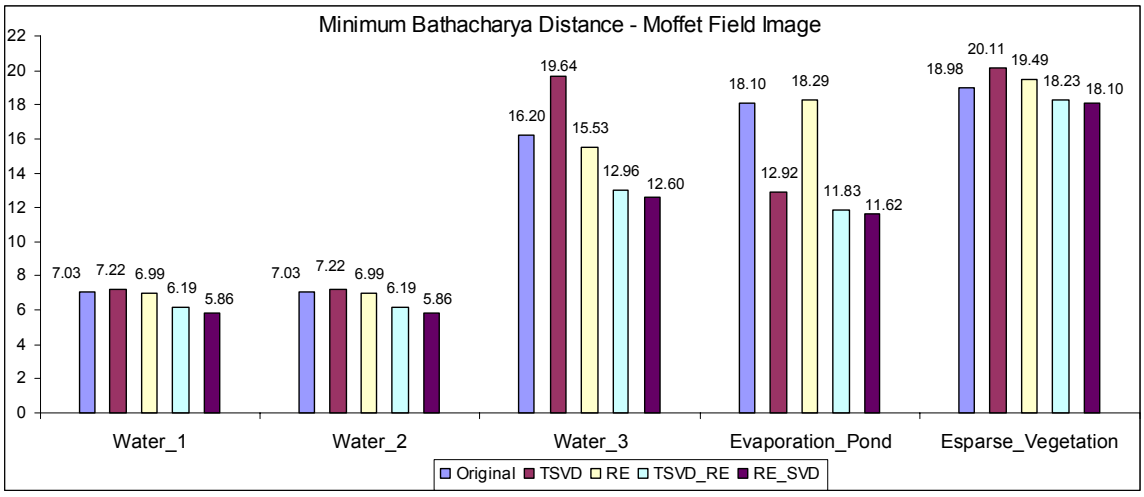

Figure 39 - Minimum Bhattacharya Distance of the Moffet Field Image

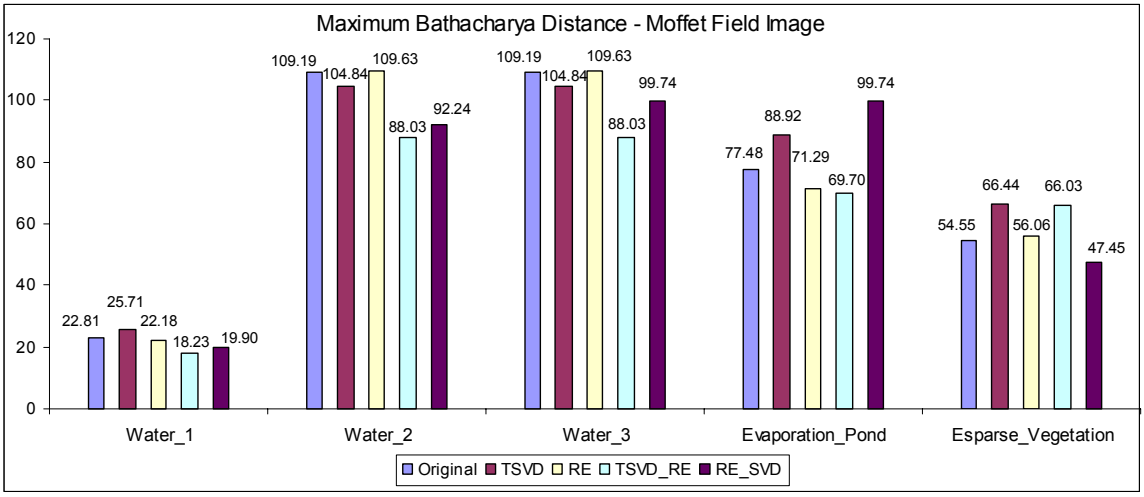

Figure 40 - Maximum Bhattacharya Distance of the Moffet Field Image

Noise Reduction Effect

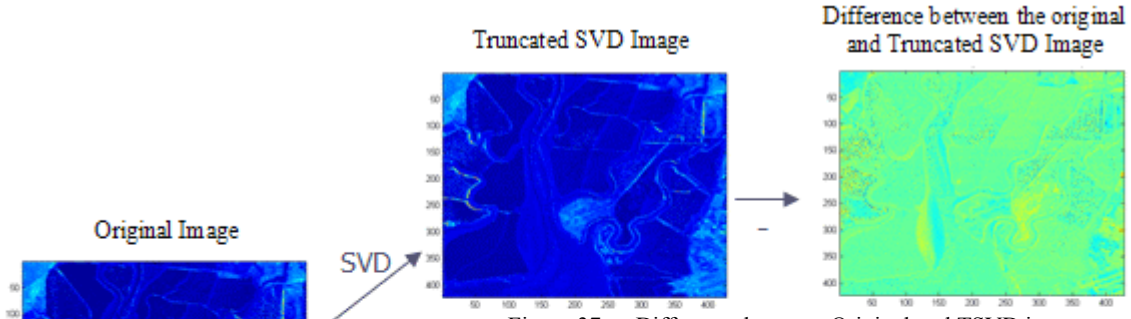

Figure 37a – Difference between Original and TSVD images

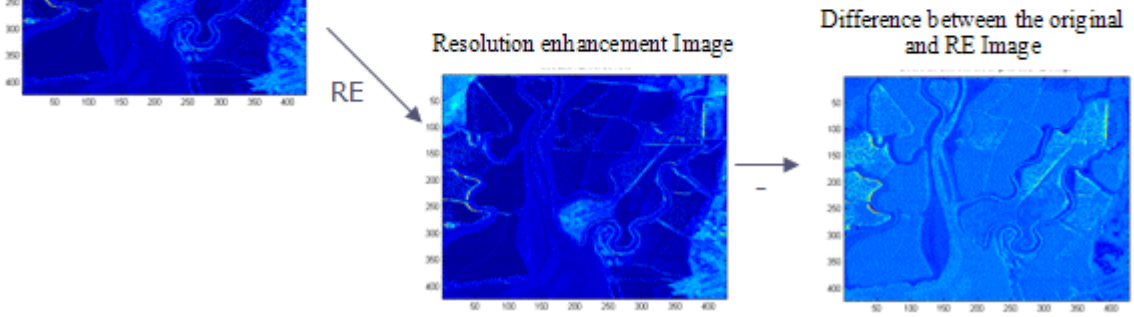

Figure 37b – Difference between Original and RE images

Figure 41 - Noise reduction effect on Moffet Field Image

Figure 41a shows the image difference between the original and truncated SVD images,

Figure 41b shows the image difference between the original and resolution enhancement images. In the two images it is clear that resolution enhancement and truncated SVD are removing some information as can be seen on the image difference. However, resolution enhancement clearly filters more features of the original image than truncated SVD.

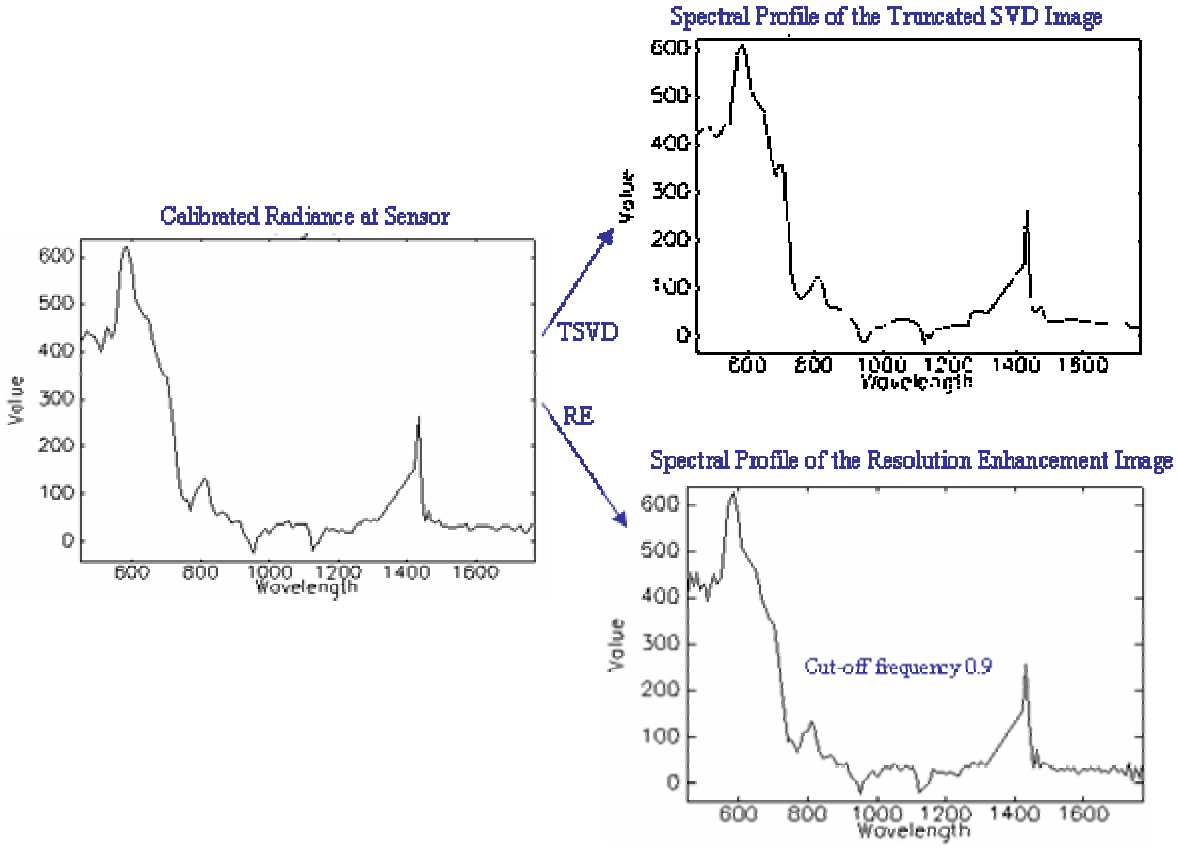

Figure 42 - Effect of Image Pre-Processing on the spectral signature (Moffet Field)

Figure 42 shows the effect of truncated SVD and resolution enhancement on the spectral signature of the Moffet Field image. It can be seen that truncated SVD does not affect sensibly the spectral signature of the original image, meanwhile resolution

enhancement extract only the low frequency components of the spectral signature and modifies it sensibly.

Although truncated SVD seems to increase class separability better than resolution enhancement, the classification accuracy is improved more by resolution enhancement.

4.1.3 GRS-S Data Set

Figure 43 and Figure 44 show the classification accuracy of the testing and training samples using the maximum likelihood classifier, per class of the each combination preprocessing scheme for the GRS-S Data Set. As can be seen in Figure 44 resolution enhancement and truncated SVD increment the classification accuracy in all the cases. However, it is important to point out that resolution enhancement increment the accuracy more than truncated SVD.

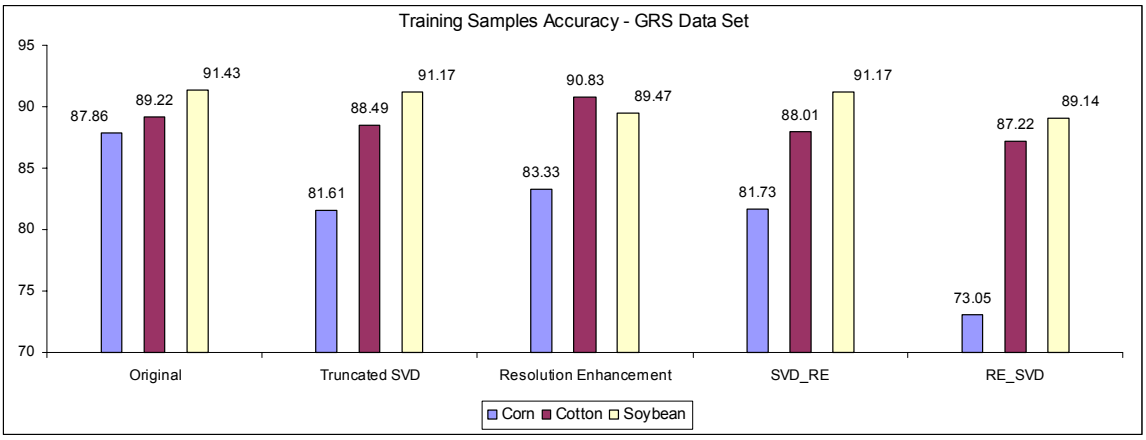

Figure 43 - Classification Accuracy of training samples per class in the GRS-S Data Set

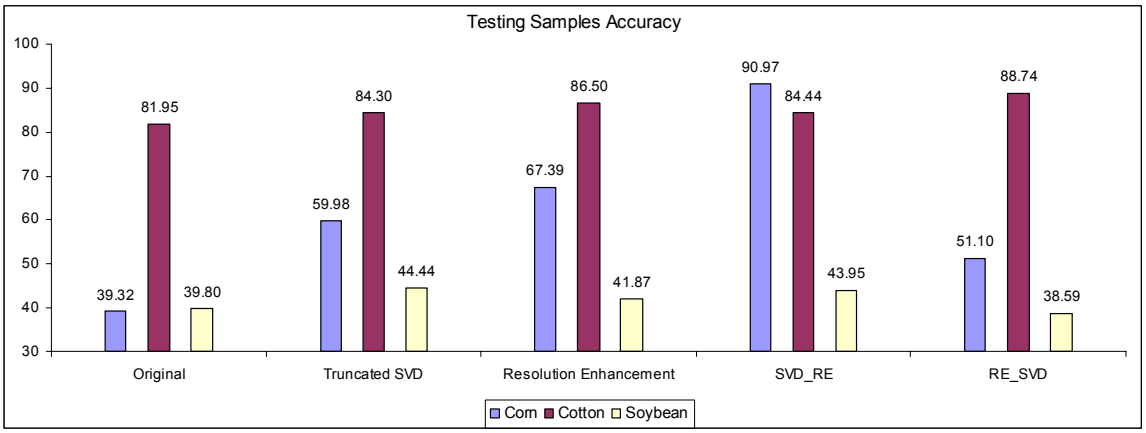

Figure 44 - Classification Accuracy of the testing samples per class in the GRS-S Data Set

The overall classification accuracy and the improvement over classification of the image without pre-processing (None) are shown in Table 10 and Table 11. The frequency of the low pass filter used for resolution enhancement was 0.1π and the number of singular values taken was 13. As shown in Table 11, resolution enhancement increments the overall accuracy in 10.3211% whereas truncated SVD increase the overall accuracy in 8.0682% in comparison with the accuracy on the image without preprocessing (None).

Table 10 - Overall Classification Accuracy per each Preprocessing Scheme of GRS-S Data Set (Training Samples)

Image Preprocessing Scheme	Overall Classification Accuracy (%)	Increase in accuracy from None
None	89.0483	N/A
Truncated SVD	85.9501	-3.0982
Resolution Enhancement	87.2208	-1.8275
TSVD_RE	85.8322	-3.2161
RE_TSVD	81.2864	-7.7619

Table 11 - Overall Classification Accuracy per each Preprocessing Scheme of GRS-S Data Set (Testing Samples)

Image Preprocessing Scheme	Overall Classification Accuracy (%)	Increase in accuracy from None
None	57.0258	N/A
Truncated SVD	65.094	8.0682
Resolution Enhancement	67.3469	10.3211
TSVD_RE	65.3573	8.3315
RE_TSVD	62.724	5.6982

Figure 45 shows the minimum Bhattacharya distance among classes for each preprocessing scheme. As can be seen, Truncated SVD and amplitude resolution enhancement increases class separability in all cases. It is noteworthy that truncated SVD increases the separability more than resolution enhancement.

Figure 46 shows the maximum Bhattacharya distance per class for each preprocessing scheme. In this case, resolution enhancement and truncated SVD decrement the distance in all cases.

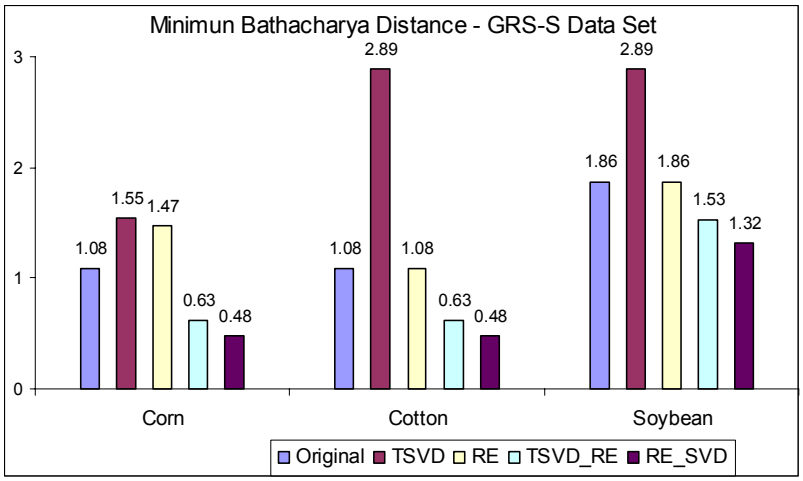

Figure 45 - Minimum Bhattacharya Distance of the GRS-S Data Set

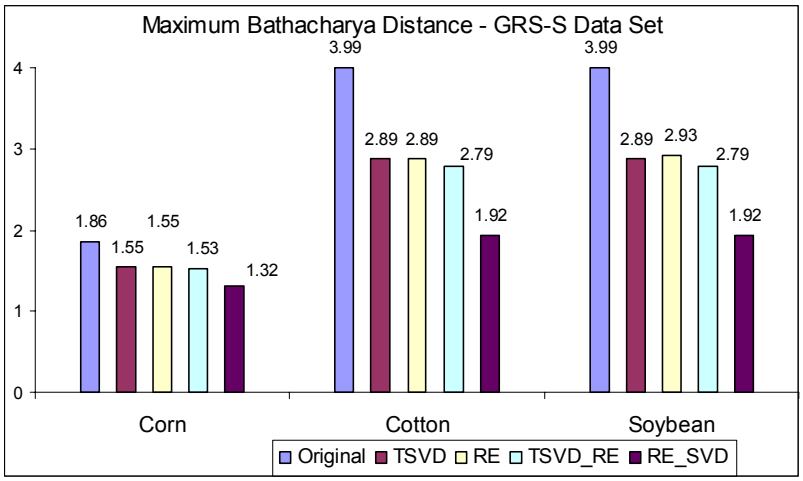

Figure 46 - Maximum Bhattacharya Distance of the GRS-S Data Set

Noise reduction effect

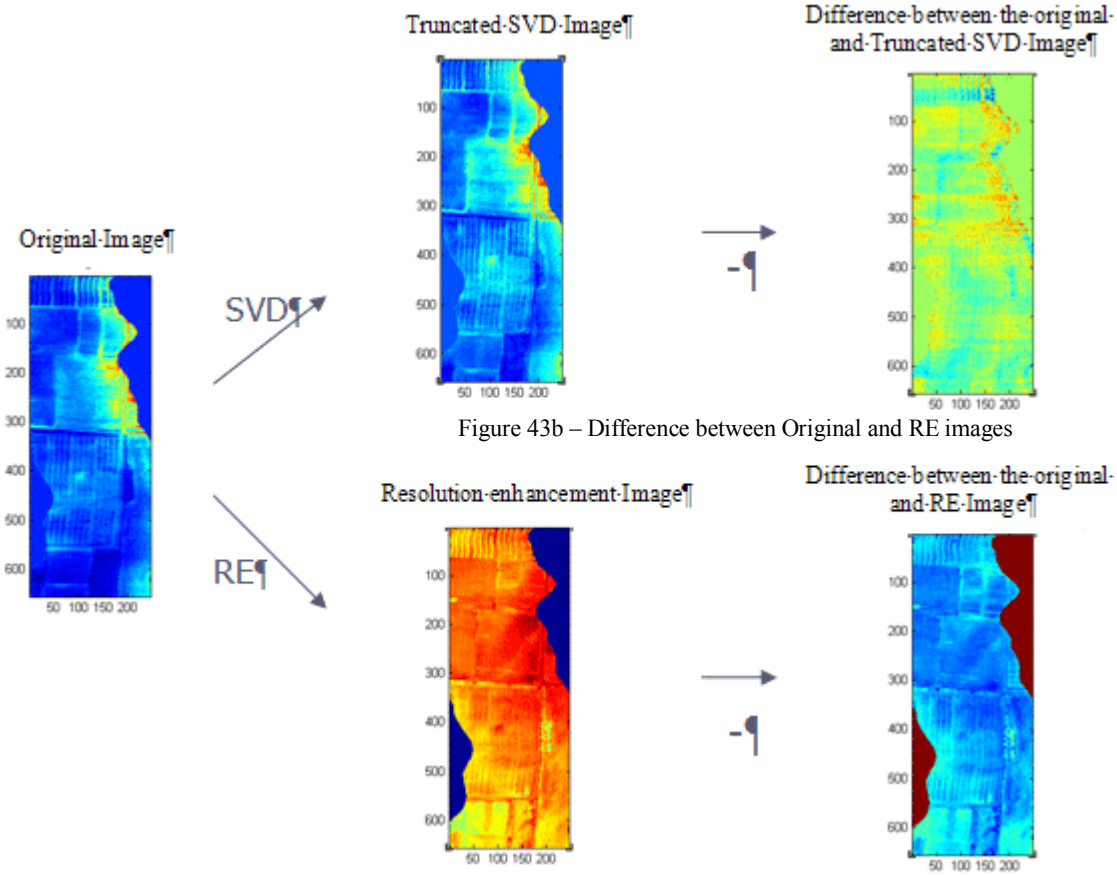

Figure 43b – Difference between Original and RE images

Figure 43a – Difference between Original and TSVD images

Figure 47 - Noise reduction effect on GRS-S Data Set

Figure 47a shows the image difference between the original and truncated SVD images, Figure 47b shows the image difference between the original and resolution enhancement images. In the two images resolution enhancement and truncated SVD are removing some information as can be seen on the image difference.

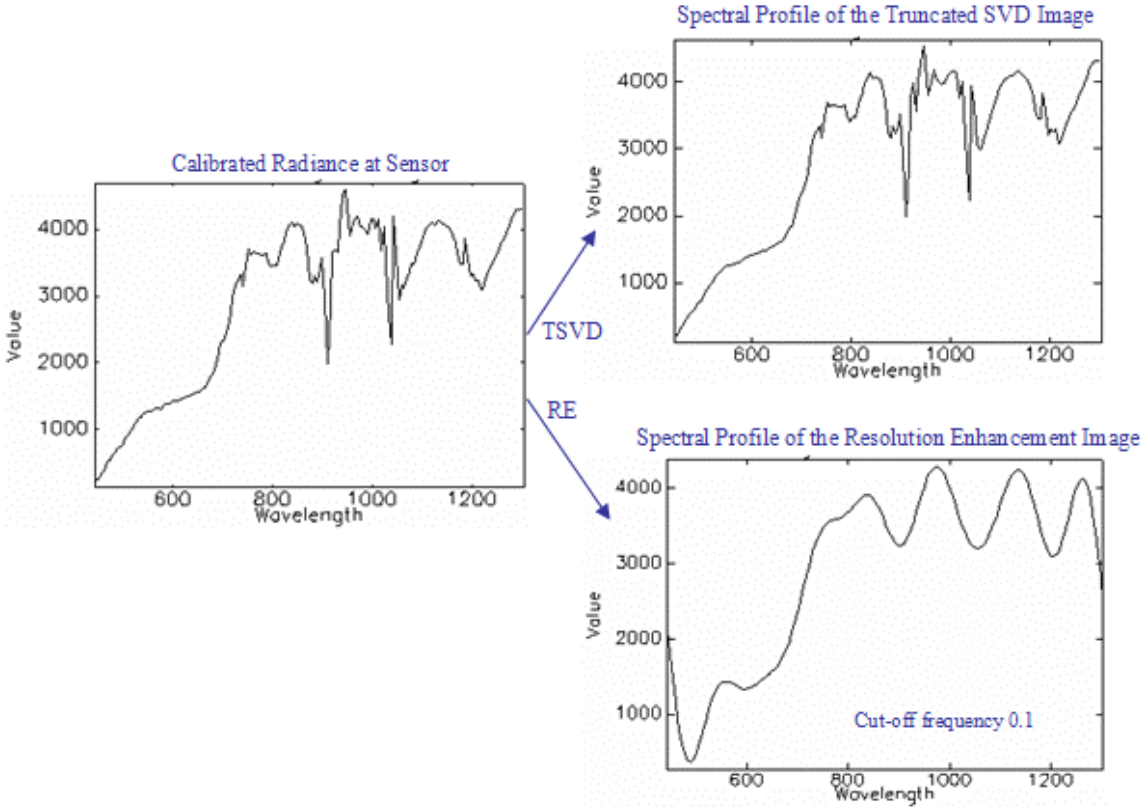

Figure 48 - Effect of Image Pre-Processing on the spectral signature (GRS-S Data Set)

Figure 48 shows the effect of truncated SVD and resolution enhancement on the spectral signature of the GRS-S data set. It can be seen that truncated SVD does not affect sensibly the spectral signature of the original image, meanwhile resolution enhancement extract only the low frequency components of the spectral signature and modifies it sensibly.

Even though truncated SVD seems to increase class separability better than resolution enhancement, however, the classification accuracy is improved more by resolution enhancement.

4.1.4 Benthic Habitat Classification of "La Parguera" in Puerto Rico

Figure 49 and Figure 50 show the classification accuracy of the testing and training samples using the maximum likelihood classifier, per class of the each combination preprocessing scheme for the "La Parguera" Image. As can be seen in Figure 50 resolution enhancement increments the accuracy in all cases. Whereas, truncated SVD decrements the accuracy of the Seagrass, Coral Community and SeaWater classes, meanwhile the Mangrove class remains with the same accuracy.

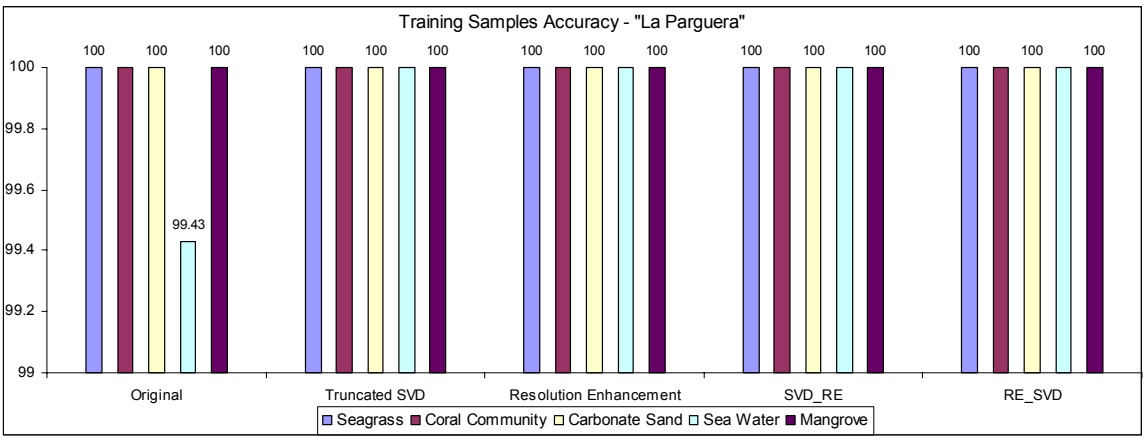

Figure 49 - Classification Accuracy of the training samples per class in "La Parguera"

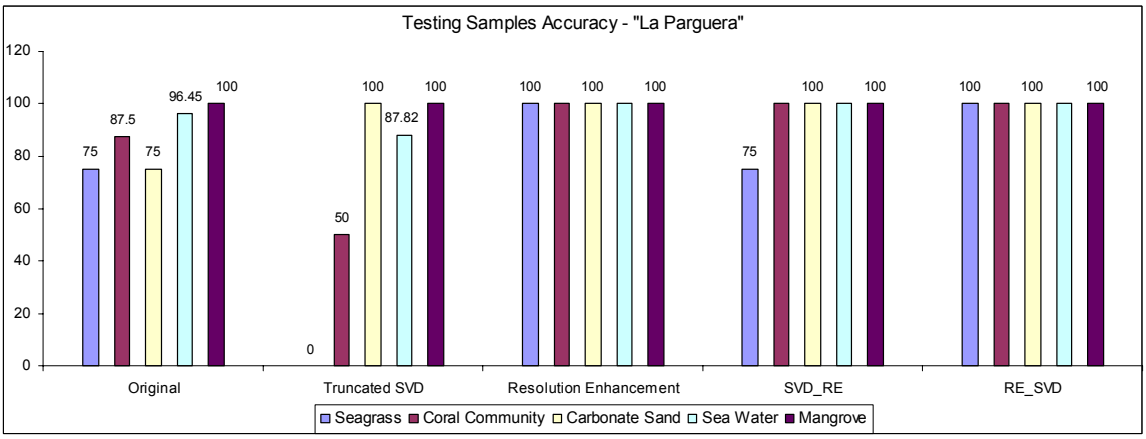

Figure 50 - Classification Accuracy of the testing samples per class in "La Parguera"

The overall classification accuracy and the improvement over classification of the image without pre-processing (None) are shown in Table 12 and Table 13. The

frequency of the low pass filter used for resolution enhancement was 0.2π and the number of singular values taken was 8. As shown in Table 13, resolution enhancement increments the overall accuracy in 4.4843% in comparison with the accuracy on the image without preprocessing (None).

Table 12 - Overall Classification Accuracy per each Preprocessing Scheme of "La Parguera" (Training Samples)

Image Preprocessing Scheme	Overall Classification Accuracy (%)	Increase in accuracy from None
None	99.5495	N/A
Truncated SVD	100	0.4505
Resolution Enhancement	100	0.4505
TSVD_RE	100	0.4505
RE_TSVD	100	0.4505

Table 13 - Overall Classification Accuracy per each Preprocessing Scheme of "La Parguera" (Testing Samples)

Image Preprocessing Scheme	Overall Classification Accuracy (%)	Increase in accuracy from None
None	95.5157	N/A
Truncated SVD	85.65	-9.8657
Resolution Enhancement	100	4.4843
TSVD_RE	95.5516	0.0359
RE_TSVD	100	4.4843

Figure 51 shows the minimum Bhattacharya distance among classes for each preprocessing scheme. As can be seen, truncated SVD and resolution enhancement increase the minimum Bhattacharya distance in all cases.

Figure 52 shows the maximum Bhattacharya distance per class for each preprocessing scheme. In this case, resolution enhancement increment the distance of the Seagrass, Coral_Community, Carbonate_Sand, and Mangrove but decrement the distance of the Sea_Water; meanwhile, truncated SVD reduces the maximum Bhattacharya distance of the Seagrass, Coral_Community and Sea_Water classes, but increase the distance of the Carbonate_Sand and Mangrove classes.

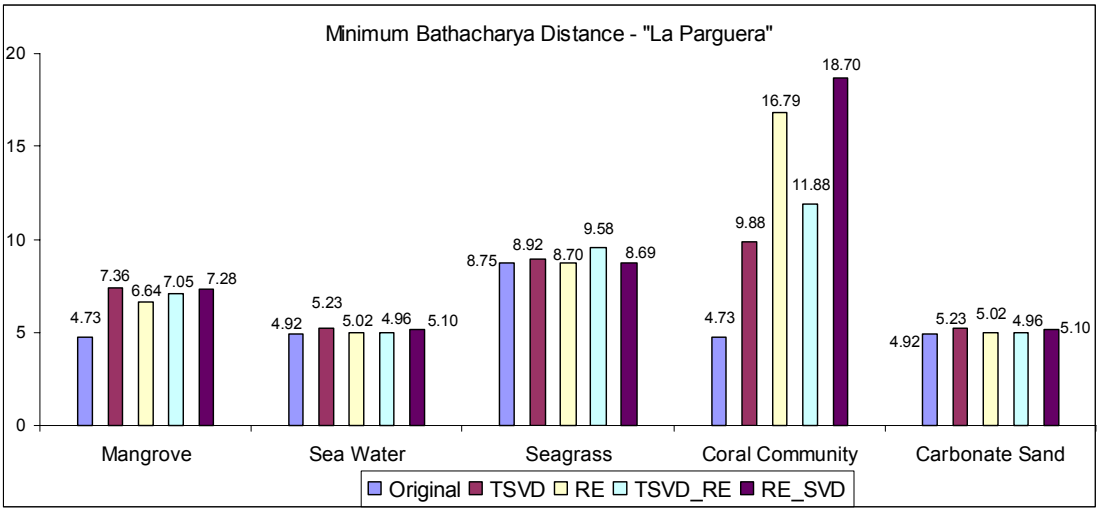

Figure 51- Minimum Bhattacharya Distance of "La Parguera"

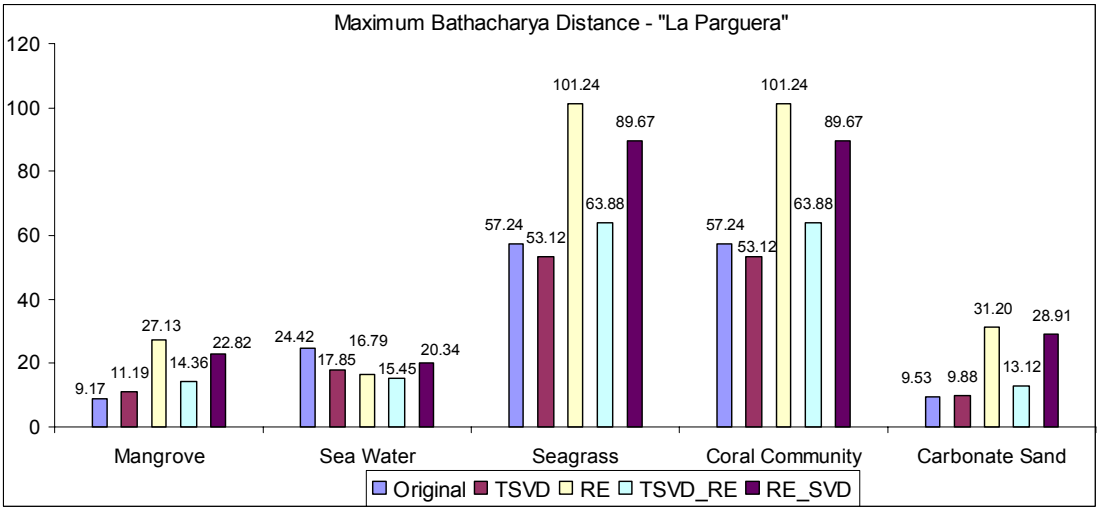

Figure 52 - Maximum Bhattacharya Distance of "La Parguera"

Noise reduction effect

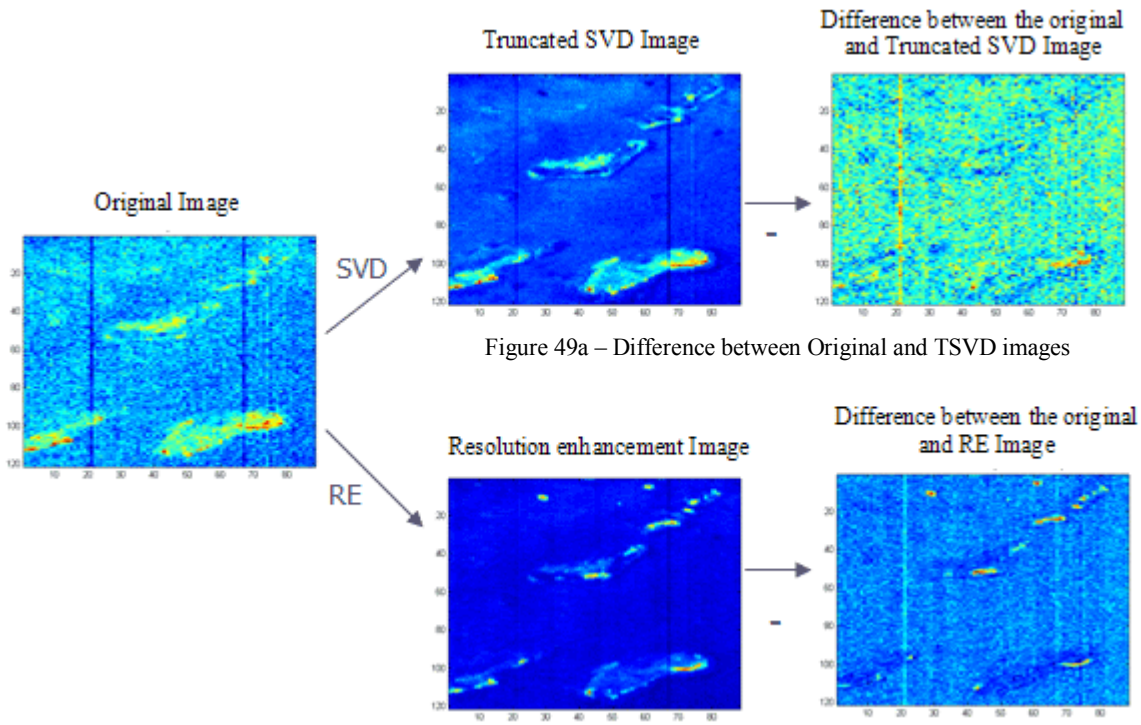

Figure 49a – Difference between Original and TSVD images

Figure 49b – Difference between Original and RE images

Figure 53 - Noise reduction effect on "La Parguera" Image

Figure 53a shows the image difference between the original and truncated SVD images, Figure 53b shows the image difference between the original and resolution enhancement images. In the two images it is clear that resolution enhancement and truncated SVD are removing some information as can be seen on the image difference. However, resolution enhancement clearly filters more features of the original image than truncated SVD.

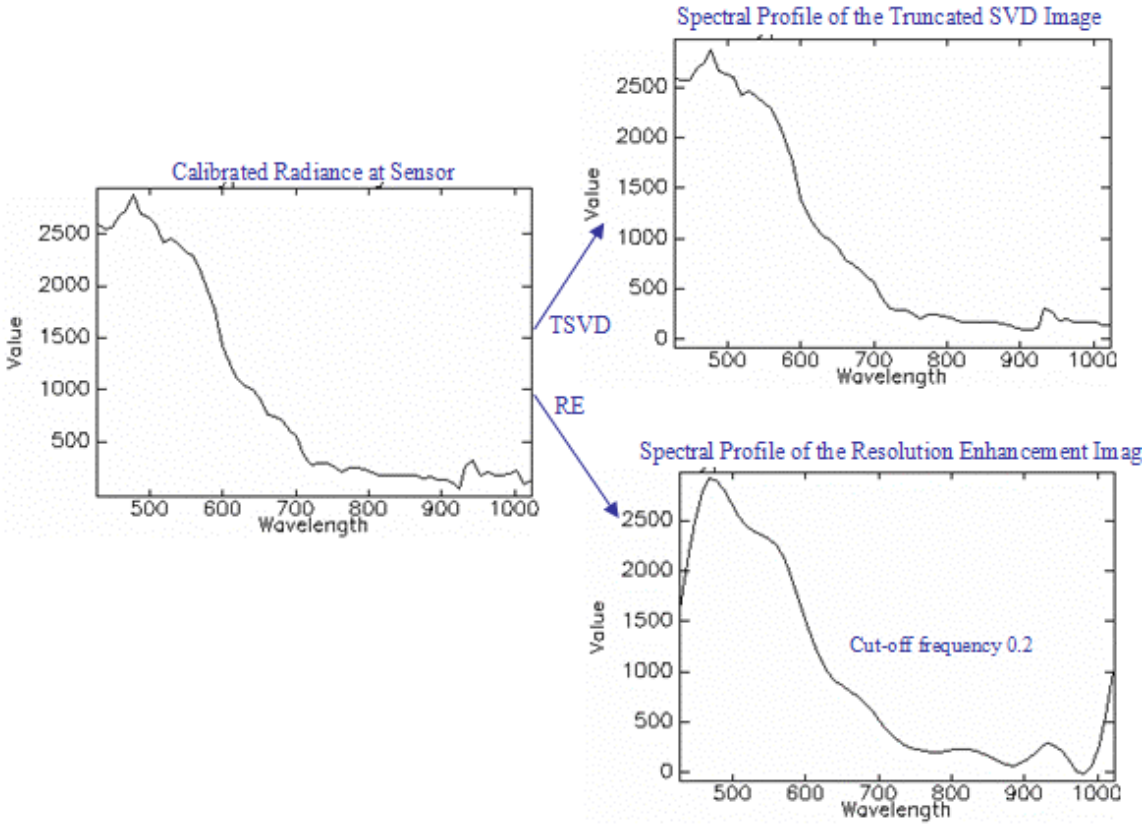

Figure 54 - Effect of Image Pre-Processing on the spectral signature ("La Parguera")

Figure 54 shows the effect of truncated SVD and resolution enhancement on the spectral signature of the "La Parguera" image. It can be seen that truncated SVD does not affect sensibly the spectral signature of the original image, meanwhile resolution enhancement extract only the low frequency components of the spectral signature and modifies it sensibly.

Notwithstanding truncated SVD seems to increase class separability better than resolution enhancement, but the classification accuracy is improved more by resolution enhancement.

4.1.4.1 Atmospheric correction on benthic habitat of "La Parguera"

Figure 55 and Figure 56 shows the classification accuracy of the testing and training samples using the maximum likelihood classifier, per class of the each combination preprocessing scheme including the atmospheric correction for "La Parguera" Image. As revealed by the Figure 56 resolution enhancement increments the accuracy in all cases. Whereas, truncated SVD decrements the accuracy in the majority of cases, in the same way atmospheric correction decrement the accuracy of Sea_Water Class, and increment the Coral_Community and Carbonate_Sand classes, besides the Seagrass and Mangrove remain the same value.

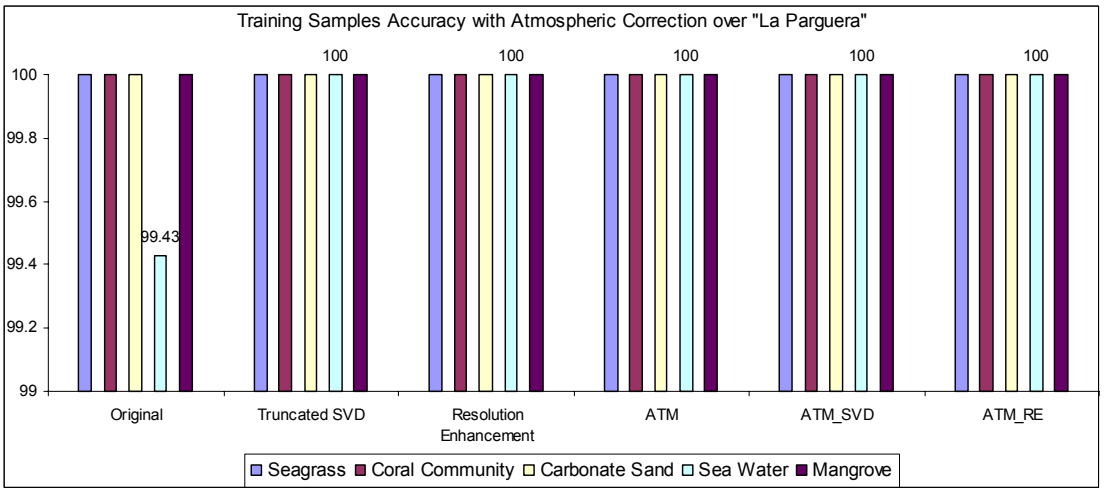

Figure 55 - Training Samples Accuracy with Atmospheric Correction over "La Parguera"

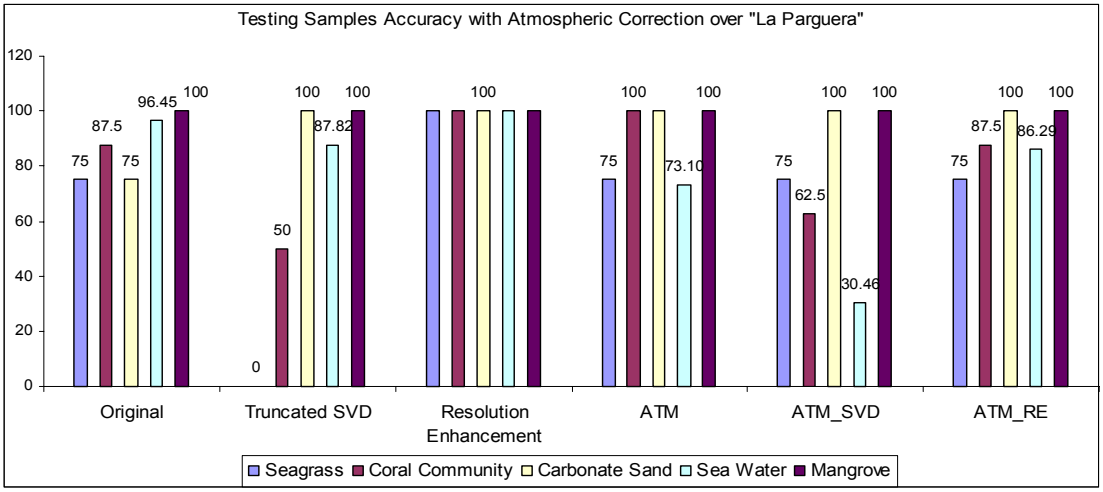

Figure 56 - Testing Samples Accuracy with Atmospheric Correction over "La Parguera"

The overall classification accuracy and the improvement over classification of the image without pre-processing (None) with atmospheric correction are shown in Table 14 and Table 15. As shown in Table 14, resolution enhancement increments the overall accuracy in 4.4843% in comparison with the accuracy on the image without preprocessing (None) and in comparison with the accuracy on the atmospheric corrected image the overall increase in 24.23%

Table 14 - Overall Classification Accuracy per each Preprocessing Scheme of "La Parguera" Corrected (Training Samples)

Image Preprocessing Scheme	Overall Classification Accuracy (%)	Increase in accuracy from None
None	99.5495	N/A
TSVD	100	0.4505
RE	100	0.4505
ATM	100	0.4505
ATM_SVD	100	0.4505
ATM_RE	100	0.4505

Table 15- Overall Classification Accuracy per each Preprocessing Scheme of "La Parguera" Corrected (Testing Samples)

Image Preprocessing Scheme	Overall Classification Accuracy (%)	Increase in accuracy from None
None	95.5157	N/A
TSVD	85.65	-9.8657
RE	100	4.4843
ATM	75.7648	-19.7509
ATM_SVD	36.7713	-58.7444
ATM_RE	86.9955	-8.5202

Figure 57 shows the minimum Bhattacharya distance among classes for each preprocessing scheme including atmospheric correction. As can be seen, truncated SVD and resolution enhancement increase the minimum Bhattacharya distance in all cases, whereas the atmospheric correction reduces the minimum distance in almost all cases.

Figure 58 shows the maximum Bhattacharya distance per class for each preprocessing scheme. In this case, resolution enhancement increment the distance in the majority of cases; meanwhile, truncated SVD and atmospheric correction reduces the maximum Bhattacharya distance in almost all cases.

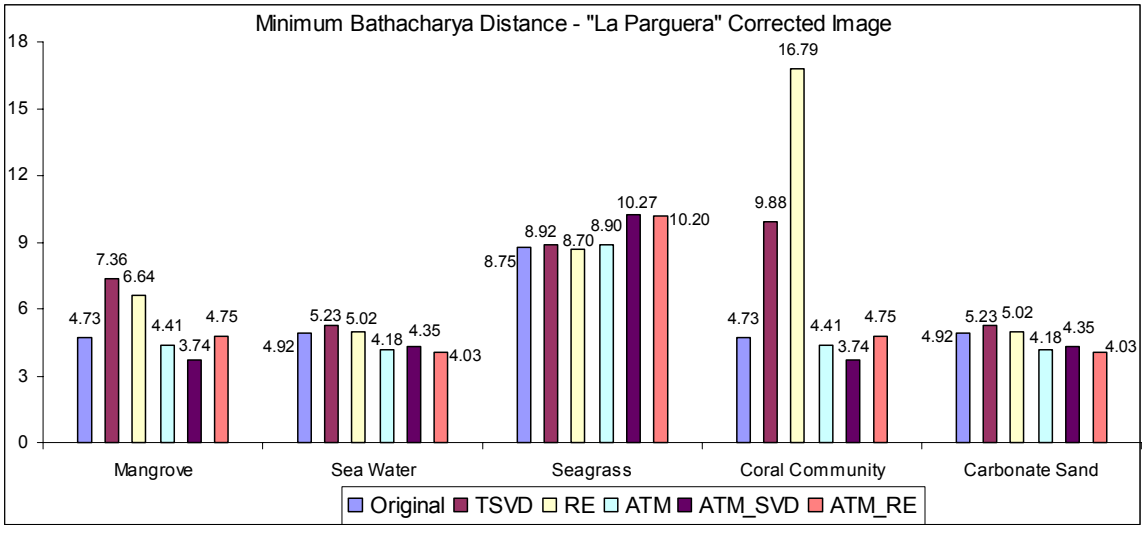

Figure 57 - Minimum Bhattacharya Distance of "La Parguera" Corrected Image

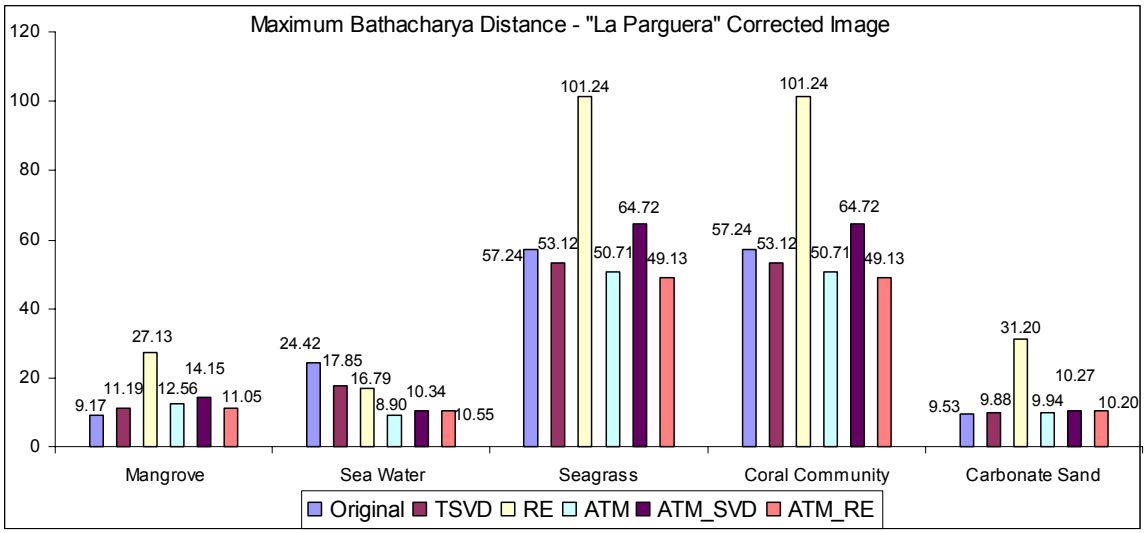

Figure 58 - Maximum Bhattacharya Distance of "La Parguera" Corrected Image

It is important to point out that in this example resolution enhancement results in higher class separability than atmospheric correction by itself. This support our thesis that atmospheric pre-processing might not be needed for HSI classification and use of the simple low pass filtering used in resolution enhancement can results in higher classification accuracy at a low computational cost.

4.1.5 Hyperspectral SOC700 Camera Test Image

Figure 59 and Figure 60 show the classification accuracy of the testing and training samples using the maximum likelihood classifier, per class of the each combination preprocessing scheme for the test image. As can be seen in Figure 60 resolution enhancement increments the classification accuracy in all cases, whereas truncated SVD decrement the accuracy in the Cein_Coint class. However, it is important to point out that resolution enhancement increment the accuracy more than truncated SVD.

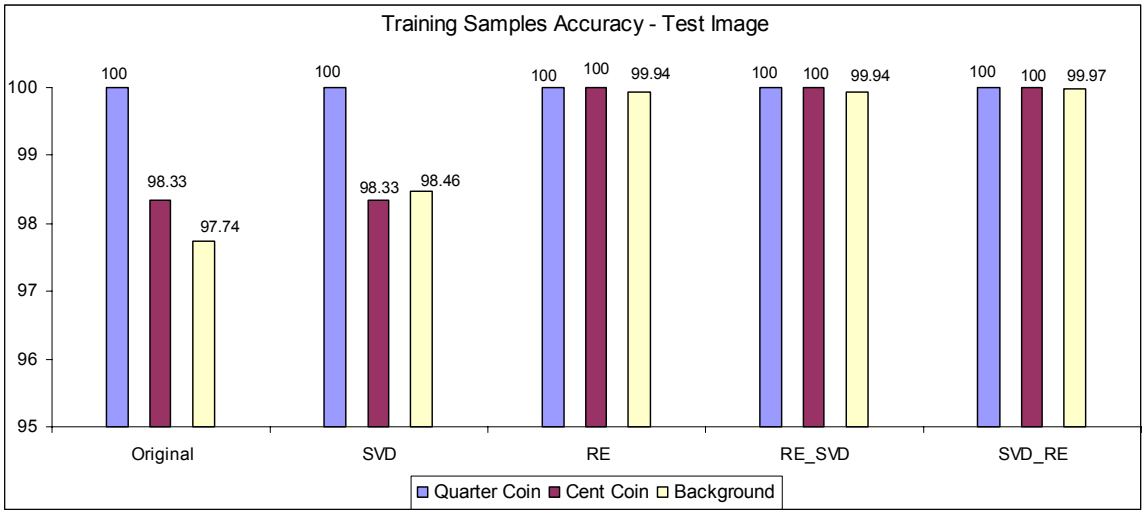

Figure 59 - Training Samples Accuracy - Test Image

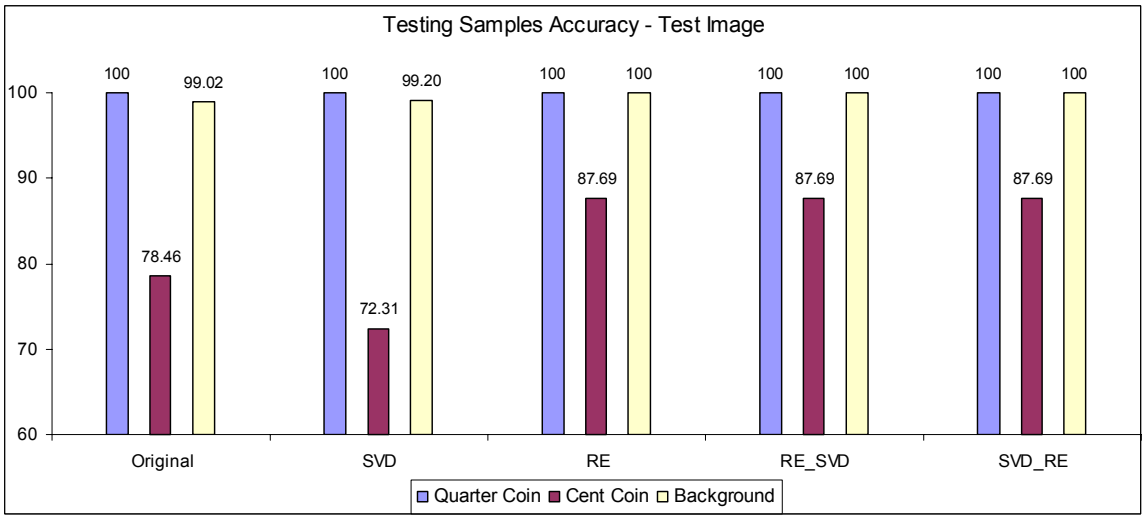

Figure 60 - Testing Samples Accuracy - Test Image

The overall classification accuracy and the improvement over classification of the image without pre-processing (None) are shown in Table 16 and Table 17. The frequency of the low pass filter used for resolution enhancement was 0.1π and the number of singular values taken was 13. As shown in Table 17, resolution enhancement increments the overall accuracy in 3.4048% in comparison with the accuracy on the image without preprocessing (None).

Table 16 - Overall Classification Accuracy per each Preprocessing Scheme of the Test Image (Testing Samples)

Image Preprocessing Scheme	Overall Classification Accuracy (%)	Increase in accuracy from None
Original	98.69126667	N/A
Truncated SVD	98.9319	0.240633333
Resolution Enhancement	99.9791	1.287833333
TSVD_RE	99.9691	1.277833333
RE_TSVD	99.9791	1.287833333

Table 17 - Overall Classification Accuracy per each Preprocessing Scheme of the Test Image (Training Samples)

Image Preprocessing Scheme	Overall Classification Accuracy (%)	Increase in accuracy from None
Original	92.4926	N/A
Truncated SVD	90.5042	-1.9884
Resolution Enhancement	95.8974	3.4048
TSVD_RE	99.8945	7.4019
RE_TSVD	95.8974	3.4048

Figure 61 shows the minimum Bhattacharya distance among classes for each preprocessing scheme. As can be seen, Truncated SVD and amplitude resolution enhancement increases class separability in all cases. It is noteworthy that resolution enhancement increases the separability more than truncated SVD.

Figure 62 shows the maximum Bhattacharya distance per class for each preprocessing scheme. In this case, resolution enhancement and truncated SVD increment the distance in all cases.

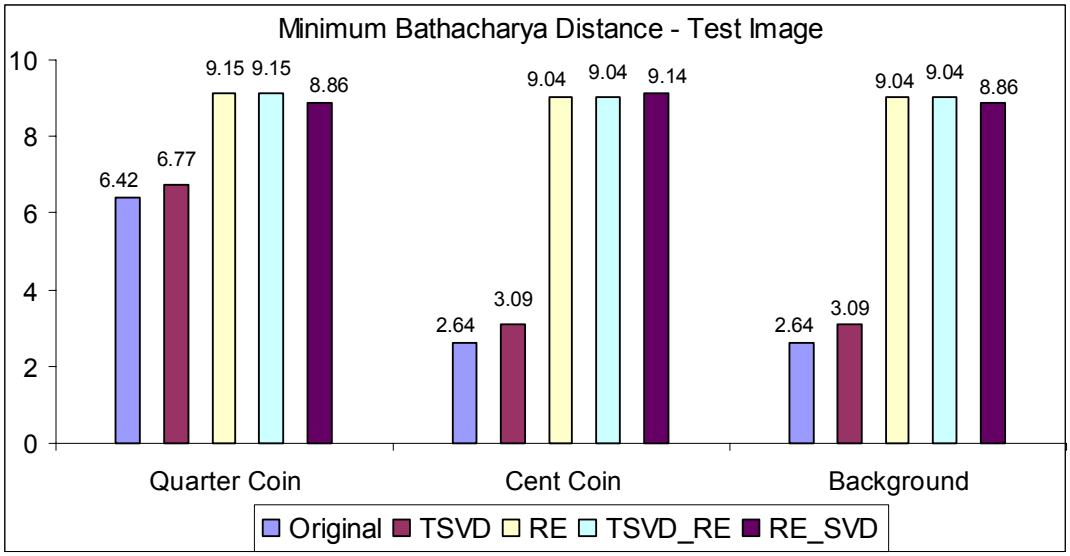

Figure 61 - Minimum Bhattacharya Distance of the Test Image

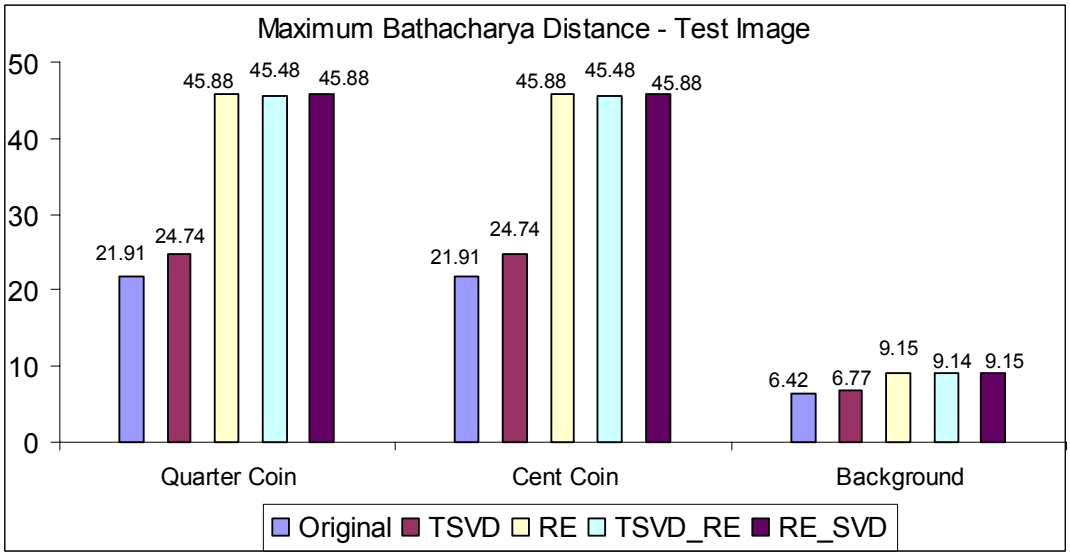

Figure 62 - Maximum Bhattacharya Distance of the Test Image

Noise reduction effect

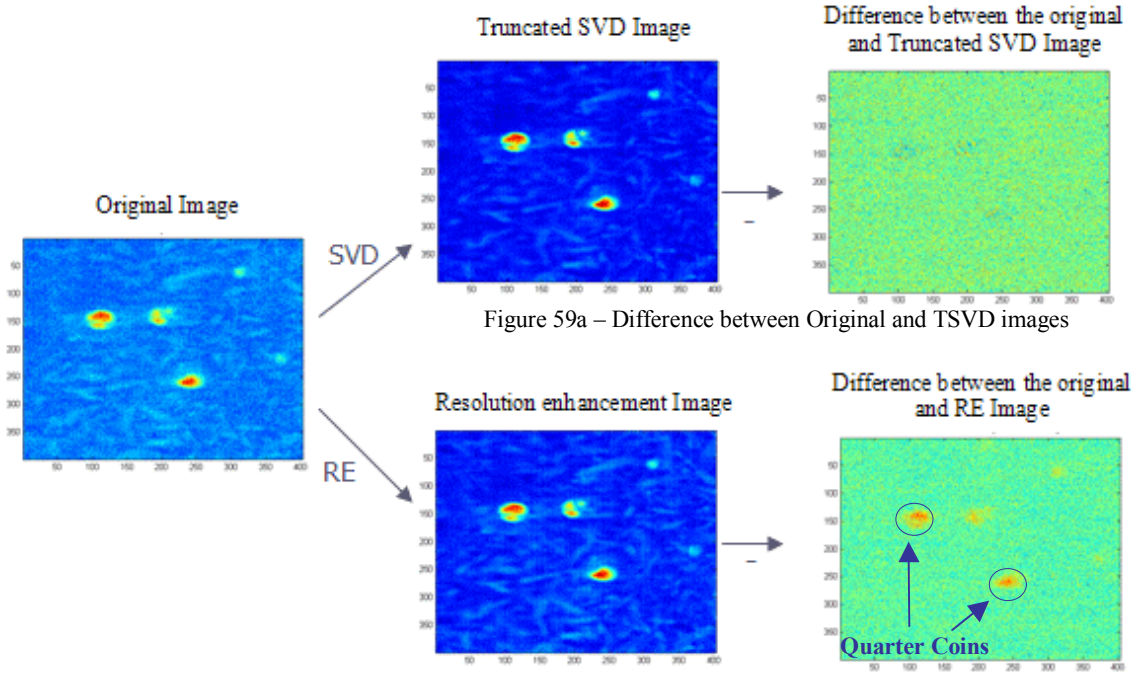

Figure 59a – Difference between Original and TSVD images

Figure 59b – Difference between Original and RE images

Figure 63 - Noise reduction effect on Camera Test Image

Figure 63a shows the image difference between the original and truncated SVD images, Figure 63b shows the image difference between the original and resolution enhancement images. It is clear from this figure that truncated SVD is removing noise meanwhile; resolution enhancement is removing some information as can be appreciated on the image difference that shows clearly some features of the original image: the Quarter Coins.

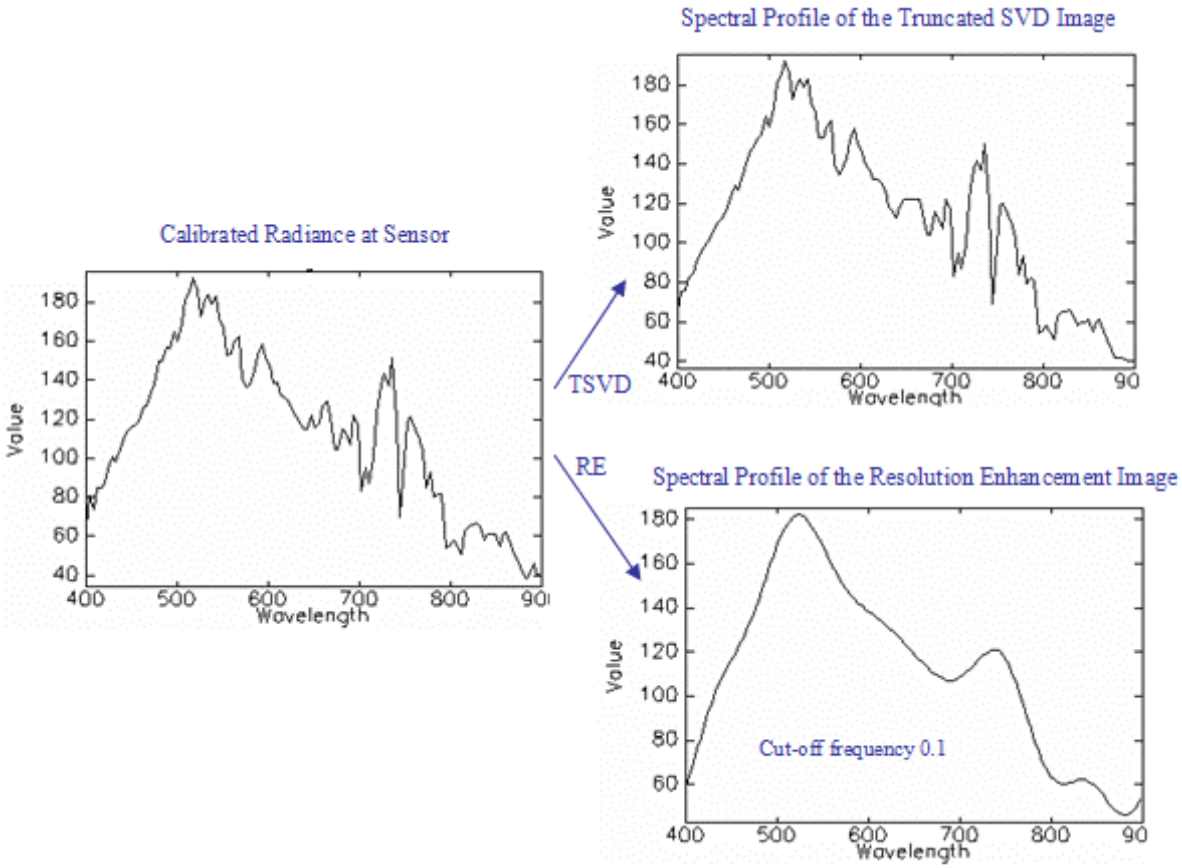

Figure 64 - Effect of Image Pre-Processing on the spectral signature (Test Image)

Figure 64 shows the effect of truncated SVD and resolution enhancement on the spectral signature of the "La Parguera" image. It can be seen that truncated SVD does not affect sensibly the spectral signature of the original image, meanwhile resolution enhancement extract only the low frequency components of the spectral signature and modifies it sensibly.

Classification Map

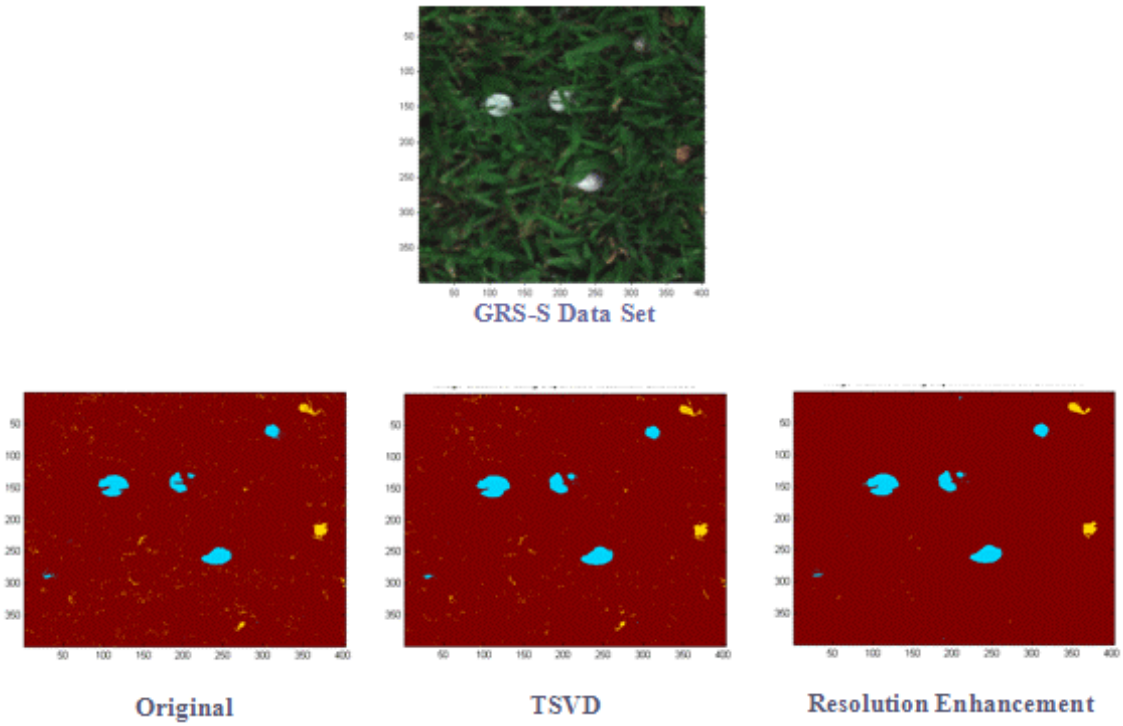

Figure 65 - Classification Maps of the GRS-S Data Set

Figure 65 shows the classification maps of the GRS-S data set for original, truncated SVD and resolution enhancement preprocessing. It is noteworthy that resolution enhancement improve the classification accuracy, because as we can see in Figure 65 the classification map of resolution enhancement is better that the classification map of truncated SVD.

4.2 Concluding remarks

The experiments presented in this chapter showed that Resolution enhancement based on oversampling theory increased the overall classification accuracy better than Truncated SVD, as can be seen in Table 18.

Table 18 - Increase in the Overall Classification Accuracy

Image Name	Resolution Enhancement %	Truncated SVD %
Indiana Pine	3.0822	0.0955
Moffett Field	0.2078	-5.5065
GRS Image	8.0682	10.3211
Test Image	3.4048	-1.9884
"La Parguera"	4.4843	-9.8657
Average	**3.84946**	**-1.3888**
Standard deviation	2.8	7.6

Spectral resolution enhancement based on oversampling is a technique with excellent noise reduction and in comparison with TSVD demonstrated the method as an effective technique for Hyperspectral data analysis.

Resolution enhancement runs, in average, at approximately a half (48%, δ=15%) of the time expended by truncated SVD in all experiments conducted in this work. These results validate the theoretical complexities of the algorithms TSVD, $O(mn^2)$, and resolution enhancement, O(mnlogn); being thus resolution enhancement asymptotically faster than TSVD and hence more cost-effective.

Atmospheric correction also improved classification accuracy with results comparable to resolution enhancement. However, spectral resolution enhancement is just a low pass filtering of the image while atmospheric correction is a significantly more complex computational process.

CHAPTER 5

5. CONCLUSIONS AND FUTURE WORK

This Chapter presents the conclusions of this research work and proposes further research activities.

5.1 Summary

This research work compares the use of amplitude resolution enhancement based on oversampling versus truncated singular value decomposition filtering as image enhancement preprocessors on classification accuracy and class separability of Hyperspectral imagery. Hyperspectral imagery from different sensors showing different scenarios were use for the study.

The improvements over classification of the images without pre-processing (None) are shown for each image as follow:

The results with the Indiana Pine image shows that resolution enhancement increments the overall accuracy in 3.082%, meanwhile truncated SVD increments the overall accuracy in. 0.0955%, these results are in comparison with the accuracy on the image without preprocessing (None). Amplitude resolution spectral enhancement based on oversampling and Truncated SVD increase class separability in the majority of cases.

- The results with the Moffet field image shows that resolution enhancement increments the overall accuracy in 0.2078%, meanwhile truncated SVD reduce the overall accuracy in. 5.5056%, these results are in comparison with the accuracy on the image without preprocessing (None). Amplitude resolution spectral enhancement based on oversampling and Truncated SVD increase class separability in all cases;

however truncated SVD seems to increase class separability better than resolution enhancement.

- The results with the GRS-S data set shows that resolution enhancement increments the overall accuracy in 10.3211%, meanwhile truncated SVD increments the overall accuracy in 8.0682%, these results are in comparison with the accuracy on the image without preprocessing (None). Amplitude resolution spectral enhancement based on oversampling and Truncated SVD increase class separability in all cases; however truncated SVD seems to increase class separability better than resolution enhancement.

- The results with the "La Parguera" image shows that resolution enhancement increments the overall accuracy in 4.4843%, meanwhile truncated SVD reduces the overall accuracy in 9.8657%, these results are in comparison with the accuracy on the image without preprocessing (None). Amplitude resolution spectral enhancement based on oversampling and Truncated SVD increase class separability in all cases; notwithstanding truncated SVD seems to increase class separability better than resolution enhancement.

- The results with the "La Parguera" corrected image shows that, atmospheric correction reduces the overall accuracy in 19.7509% resolution enhancement increments the overall accuracy in 4.4843% and truncated SVD reduces the overall accuracy in 9.8657%; these results are in comparison with the accuracy on the image without preprocessing (None). Amplitude resolution spectral enhancement based on oversampling and Truncated SVD increase class separability in all cases, meanwhile atmospheric correction reduces the minimum distance in almost all cases.

- The results with the Test Image shows that resolution enhancement increments the overall classification accuracy in 3.4048%, meanwhile truncated SVD reduces the overall classification accuracy in 1.9884%; these results are in comparison with the accuracy on the image without preprocessing (None). Amplitude resolution spectral

enhancement based on oversampling and Truncated SVD increase class separability in all cases; resolution enhancement increases the class separability more than truncated SVD. It is important to point out that resolution enhancement improve the classification accuracy.

5.2 Conclusions

Resolution enhancement increases the overall classification accuracy by approximately 3.9% (δ=2.8%) in average, with respect to the classification without image pre-processing. Otherwise, TSVD decreases the overall classification accuracy by approximately 1.4% (δ=7.6%) in average.

Resolution enhancement runs, in average, at approximately a half (48%, δ=15%) of the time expended by truncated SVD in all experiments conducted in this work. These results validate the theoretical complexities of TSVD and resolution enhancement algorithms, being thus resolution enhancement more cost-effective than TSVD.

Atmospheric correction improves the classification accuracy with results comparable to resolution enhancement, in land areas and shallow water benthic habitats as coral, sea grass and sand; but degrades the classification accuracy over deep waters as it should be expected of algorithms that were not designed for sea water.

Resolution enhancement increases classification accuracy in HSI processing. Furthermore, we can see that the combination of atmospheric and resolution enhancement pre-processing does not add significant accuracy improvement over resolution enhancement by itself. This result points out at the possibility that resolution enhancement can be used as the only pre-processing stage in classification systems for hyperspectral imagery. The little effect of the atmospheric correction could be due to the fact that the image visibility was high, but in general it is convenient to reduce sources of variability that may degrade the performance of the classifier. It is important, to conduct

similar studies with images of lower visibility where atmospheric effects are mode significant.

In general we can conclude that spectral resolution enhancement preprocessing does a better job improving the classification accuracy than truncated singular value decomposition and at a much lower computational cost.

5.3 Future Work

Spectral resolution enhancement might be improved by adding a convenient window (Hamming, Hann, Bartlett, among others) to reduce the oscillations introduced on both extremes of the spectral signature after filtering.

Further work could be to apply these algorithms to images affected by a more optically challenging media (turbid atmosphere, skin, water with high sedimentation)

It is necessary to develop an algorithm that automatically determines the cut off frequency of spectral resolution enhancement low pass filter from the image data.

BIBLIOGRAPHY

Adler-Golden, S., Berk, A., Bernstein, L.S., Ritchtmeier, S., Acharya, P.K., Mattew, M.W., Anderson, G.P., Allred, C.L., Jeong, L.S., and Chetwynd, J.H. 1998. "FLAASH, A Modtran4 Atmospheric Correction Package for Hyperspectral Data Retrievals and simulations". AVIRIS Earth Science and Applications Workshop Proceedings.

Arzuaga, E., Jimenez-Rodriguez, LO., and Vélez-Reyes, M. 2003. "Unsupervised Feature Extraction and Band Subset Selection techniques based on Relative Entropy Criteria for Hyperspectral data Analysis". Algorithms and Technologies for Multispectral, Hyperspectral, and Ultraspectral Imagery IX. SPIE Proceedings 5093:462-473.

Arzuaga-Cruz, A., Jimenez-Rodriguez, LO., Velez-Reyes, M., Kaeli, D., Rodriguez-Diaz, E Velazquez-Santana, HT., Castrodad-Carrau, A., Santos-Campis, LE., and Santiago, C., 2004. "A MATLAB Toolbox for Hyperspectral Image Analysis". IEEE Internacional Geoscience and Remote Sensing Symposium.

CSIRO Commonwealth Scientific & Industrial Research Organization. "An Overview of Hyperspectral Remote sensing". http://www.eoc.csiro.au/hswww/Overview.htm

CCRS Canada Center for Remote Sensing. 2004. "Fundamentals of Remote Sensing Tutorial". http://www.ccrs.nrcan.gc.ca/ccrs/learn/tutorials/fundam/fundam_e.html

Chang, C. I., 2003. *Hyperspectral Imaging, Techniques for Spectral Detection and Classification*. Kluwer Academic/Plenum Publishers, New York.

Cormen, T., Leiserson, C., Rivest, R., Stein, C., 2001. *Introduction to Algorithms*. McGraw-Hill. 2nd edition.

EarthSat, 2004. Earth Satellite Corporation Webpage. "Commercial Sensors: Features & Comparison". http://www.earthsat.com/ip/production/comm_sensors.html

Earth Observing-1 - EO-1 Webpage. http://eo1.gsfc.nasa.gov/Technology/Hyperion.html

Fukunaga, K., and Hayes, R. R., 1989. "Effects of sample size in classifier design". IEEE Trans. Pattern Anal. Machine Intell., vol. PAMI-11, No. 8, pp. 873-885.

Gao, BC., Montes, MJ., Ahmad, Ziauddin and Davis, CO., 2000. "Atmospheric correction algorithm for Hyperspectral remote sensing of ocean color from space". Applied Optics, Vol. 39, No. 6.

Hansen, PC., and Jensen, SH., 1998. "FIR Filter Representations of Reduced-Rank Noise Reduction". IEEE Trans. On Signal Processing. 46:1737-1741.

Hansen, PC., 1987. "The truncated SVD as a method for regularization". BIT, 27:534-553.

Herries, G., Selige, T., and Danaher, S. 1996. "Singular Value Decomposition in applied Remote Sensing". IEE, Savoy Place, London WC2R OBL, UK

Hsieh, P, F., Landgrebe, D., 1998. "Lowpass Filter for Increasing Class Separability". IEEE, International Geoscience and Remote Sensing Symposium, Seattle, Washington.

Hunt, S., and Sierra, H., 2003. "Spectral Oversampling in Hyperspectral Imagery". In Algorithms and Technologies for Multispectral, Hyperspectral, and Ultraspectral Imagery IX, Proceedings of SPIE 5093:643-650.

Hunt, S., and Laracuente, J., 2004. "Determining noise in Hyperspectral Imagery for the application of Oversampling to Supervised Classification". Algorithms and Technologies for Multispectral, Hyperspectral, and Ultraspectral Imagery X, Proceedings of SPIE Vol. 5425.

ImSpec LLC, 2002. "ACORN™ User's Guide", ACORN Version 3.12. ImSpec LLC

Kappus, M. E., Davis, C. O., and Rhea, W. J., "HYDICE data from Lake Tahoe: Comparison to coincident AVIRIS and in-situ measurements". Proceedings of the SPIE, Volume 2819, Denver, Colorado, August 1996.

Keeling, J., and Mauger A., 1998. "The HyMAP™ Airborne Hyperspectral Sensor: the System, Calibration and Performance". 1st EARSEL Workshop on Imaging Spectroscopy, Zurich.

Landgrebe, D. A., 2003. *Signal Theory Methods in Multispectral Remote Sensing.* A John Wiley & Sons Publication. Hoboken, New Jersey.

Landgrebe, D. A., Swain, P. H., and S. M. Davis, 1978. *Remote Sensing: The Quantitative Approach*. McGraw-Hill, New York.

Migliaco, M., and Gambardella, A., 2003. "TSVD Spatial Resolution Enhancement of Microwave Radiometer Data: a Sensitivity Study". IEEE, pp 3854-3856.

Moigne, J. Le., Yeh, P.-S., Joiner, J., Donohoe, G., El-Ghazawi, T.. Agarwal, A., Xia, W., 2004. "Dimension Reduction of Hyperspectral Data on Reconfigurable Computers". NASA's Earth Science Technology Office (ESTO)'s fourth annual Earth Science Technology Conference (ESTC), Palo Alto CA.

Pearlman, J.S., Marmo, J., Folkman, M., Sandor, S., Davis, B., Stone, D., Jennings, D., Dozier, Jeff. 1999. "Lewis Satellite Hyperspectral Payloads and applications demonstrations". http://ltpwww.gsfc.nasa.gov/ISSSR-95/lewissat.htm

Pettis, K.W., Bailey, A. K., and Dubes, R. C., 1979. "An intrinsic dimensionality estimator from near–neighbor information". IEEE Trans. Patt. Anal. Machine Intell, PAMI–1 pp 25–37.

Research Systems, 2001. "FLAASH User Guide". ENVI FLAASH version 1.0. Research Systems, Inc.

Sandor-Leahy, S.R., Beiso, D., 2000. "Analysis of agricultural imagery acquired by the TRWIS III hyperspectral sensor. Signals, Systems and Computers". Conference Record of the Thirty-Fourth Asilomar Conference, IEEE. 177-181 vol.1

Subramanian, S., Gat, N., Sheffield, M., Barhen, J., and Toomarian, N., 1997. "Methodology for hyperspectral image classification using novel neural network". Algorithms for Multispectral and hypespectral Imagery II, SPIE Vol. 3071.

Surface Optics Corporation (SOC), "Hyperspectral Imager and Imaging Spectrometer System". http://www.surfaceoptics.com/Products/Hyperspectral.htm

Tadjudin, S., Landgrebe, D., 1998. *Classification of High Dimensional Data with Limited Training Samples*, Purdue University, West Lafayette, IN, TR-ECE 98-8.

Te-Ming Tu., Ching-Hai Lee., Chung-Shi Chiang., and Chien-Ping Chang. 2001. "A visual disk approach for determining data dimensionality in hyperspectral imagery". Proc. Natl. Sci. Counc. ROC(A), 25(4):219–231.

Trefethen, L. N., Bau, D, 1997. *Numerical Linear Algebra*. Siam, Philadelphia, PA.

Umaña, A., and Vélez-Reyes, M., 2003. "Determining the dimensionality of hyperspectral imagery for unsupervised band selection". In Algorithms and Technologies for Multispectral, Hyperspectral, and Ultraspectral Imagery IX, Proceedings of SPIE Vol. 5093.

Van Loan, C., Golub G., 1997. *Matrix Computations*, 3rd Edition, John Hopkins University Press, Baltimore, MD.

Vélez-Reyes, M., Hunt, S. D., Morillo, S., and Sierra-Gil, H., 2004. "Effects of resolution enhancement pre-processing in atmospheric correction of hyperspectral imagery", Algorithms and Technologies for Multispectral, Hyperspectral, and Ultraspectral Imagery X, Proceedings of SPIE Vol. 5425.

Vélez M. and Jiménez L. 1998. "Subset Selection Analysis for the Reduction of Hyperspectral Imagery". Geoscience and Remote Sensing Symposium Proceedings, 1998. IGARSS '98. IEEE International 3:1577 -1581.

Wei, JJ., Chang, CJ., Chou, NK and Jan, GJ., 2001. "ECG Data Compression Using Truncated Singular Value Decomposition". IEEE Trans. On Information Technology in Biomedicine. 5:290-299

Winter, M., and Winter, E., 2002. "Physics-based Resolution Enhancement of Hyperspectral data". Algorithms and Technologies for Multispectral, Hyperspectral, and Ultraspectral Imagery VIII, Proceedings of SPIE 4725:580-587.

APPENDICES

A. Data Files for Atmospheric Correction over HYPERION using ACORN

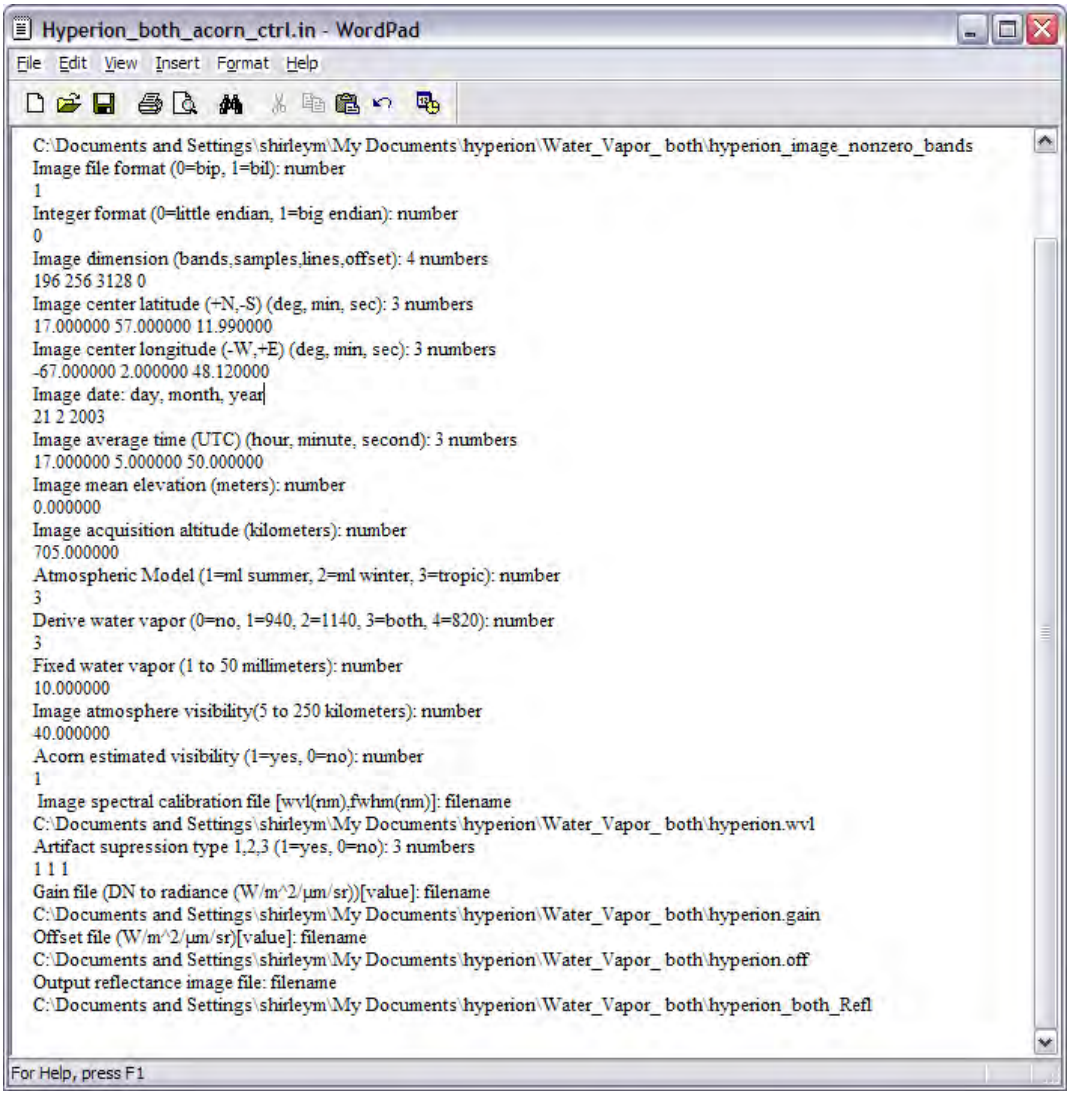

Figure 1 - Control File

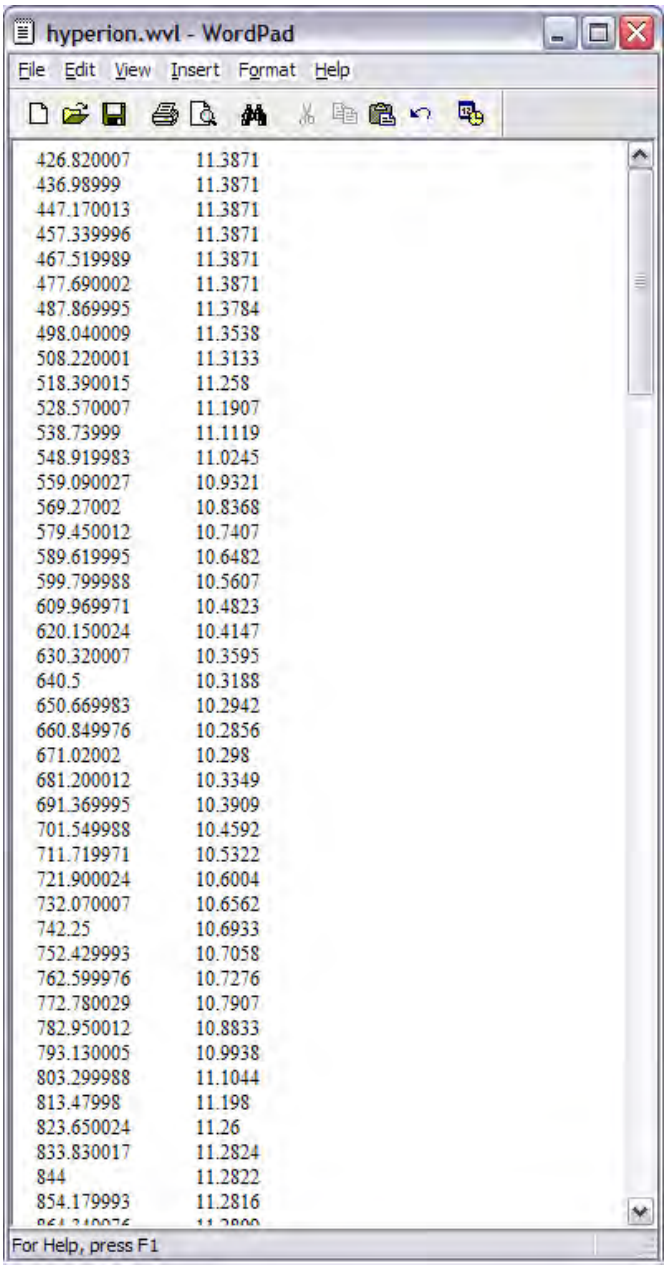

Figure 2 - Spectral Calibration file

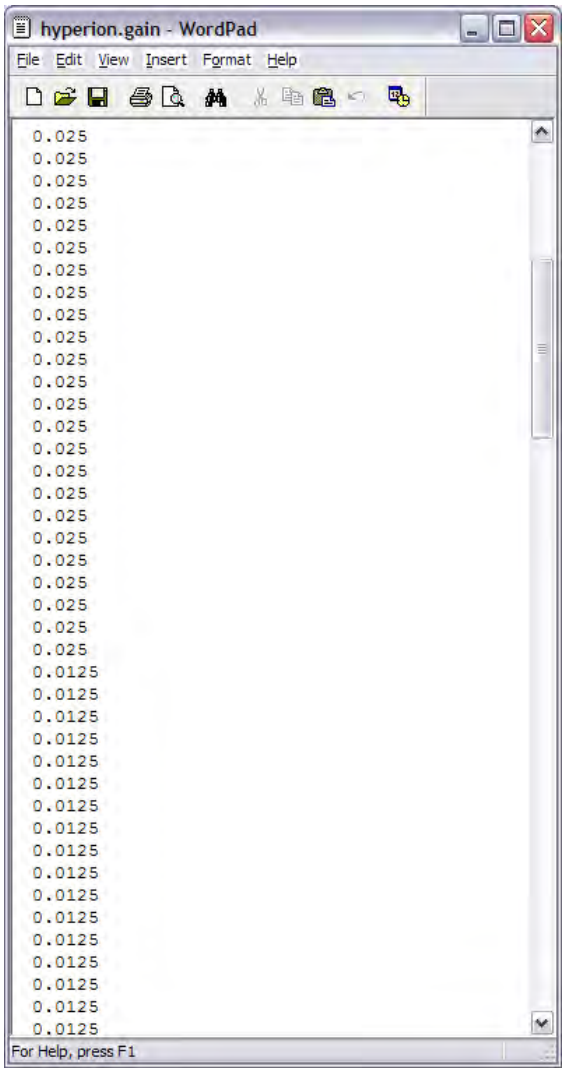

Figure 3 - Gain File

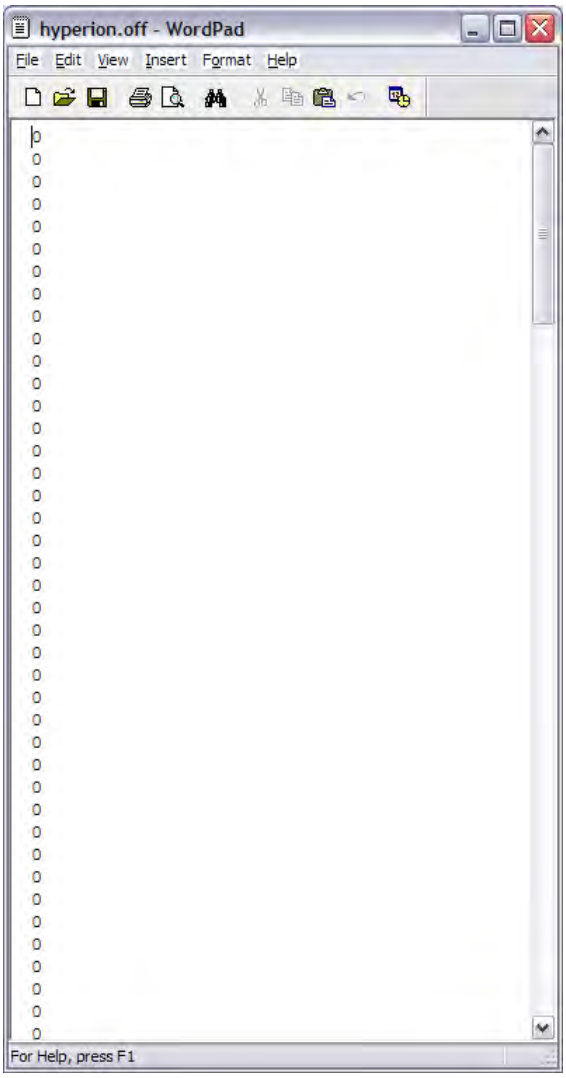

Figure 4 - Offset File

B. Truncated Singular Value Decomposition Algorithm

```
%Loading the Image
load ('Image_Name');
[U, S, V] = svd(pixels',0);
Diagonal= diag(S);
figure; plot(log(Diagonal),'.');
Total   = sum(Diagonal);
x    = (0.995 * Total);
r       = 0;
acum    = 0;
while acum<x
    r   = r+1;
   acum = acum+Diagonal(r);
end
% r is the number of singular values
r;
S2 = S(1:r,1:r);
V2 = V(:,1:r);
U2 = U(:,1:r);
pixels = V2*S2*U2';

%Saving the Filter Image
save('Image_Name_TSVD',
'pixels','number_of_bands','number_of_columns','number_of_rows');
```

C. Amplitude Resolution Spectral Enhancement Based on Oversampling Algorithm

```
%Do the loads
filename = 'Image_Name';
load(filename);
pixels2  = pixels;
w        = [0.1:0.1:1];
wk       = w.*pi;
L     = length(wk);
[rows , cols] = size(pixels);
%Outer Loop (This loops acquires a new cutoff frequency)
for m = 1:L
    %empty matrix
    pixels = zeros(rows, cols);
    %selects the appropriate number of bands to be filtered
    k      = fix ((wk (m)*rows) / (2*pi));
    %two-dimensional discrete filter, composed of ones and zeros
    h      = [ones (k, 1); zeros (rows-2*k, 1); ones (k, 1)];
    for counter = 1:cols
        %obtain the fft of every column vector (column vector is a pixel)
        fpixels  = fft(pixels2(:,counter));
        %obtain absolute value (magnitude)
        fapixels = abs(fpixels);
        %phase angle
        theta    = angle(fpixels);
     %multiply the image with the filter
        temp     = fapixels.*h;
     %reconstructs the signal
        X        = temp.*exp (i*theta);
        %obtain the inverse fft
        ifpixels = ifft(X);
        %keep the real part, remember: original data was real
        pixels(:,counter) = real(ifpixels);
    end
    %Save the image in the frecuency wk
    save(['Image_Name_RE_' num2str(w(m)*10)], ...
   'pixels','number_of_bands','number_of_columns','number_of_rows');
end
```